Dynamics of Resident Memory B Cell Responses in the Lung

By
Andrew J. MacLean

Supervisor: Dr. Tal I. Arnon
Co-supervisor: Prof. Michael L. Dustin

DPhil in Molecular and Cellular Medicine

University of Oxford
St. Edmund Hall

Abstract

Immunological memory is the central mechanism supporting the protective effects of vaccination. This phenomenon is mediated primarily by antigen-specific memory B and T lymphocytes, which enforce accelerated clearance of infectious agents and rapid return to health. Memory B cells can be found in the circulation, where they are thought to migrate between secondary lymphoid organs surveying the body for secondary infection. Following pulmonary viral infections, such as influenza, memory B cells can also be found in the lung. Recent findings have shown that these resident cells can persist for prolonged periods of time and may confer enhanced protection from secondary infection. However, the microanatomical site of retention of this population, their dynamic responses to infection and the cues guiding their positioning and responses are poorly understood.

Here, two-photon and confocal microscopy coupled with flow cytometry and RNA sequencing is used to study the positioning, migration patterns and expression profiles of memory B lymphocytes before and after rechallenge with influenza infection. Following primary infection with influenza, resident memory B cells are found distributed across the lung where they appear to continuously scan alveoli. Shortly after rechallenge, Bmem cells increase their migration speeds in response to innate stimuli and, guided by an as-yet unknown G-protein-coupled receptor, move towards sites of infection where they undergo local proliferation. Reinfection also leads to the later appearance of plasma cells within these infected sites, in a manner independent of recirculating Bmem. Plasma cell distribution into infected alveoli was also dependent on innate stimulation by viral RNA in an antigen-independent manner, and may permit local antibody secretion at the site of pathogen exposure. The finding of plasma cell establishment within sites of infection after virus rechallenge may indicate an early protective role of local humoral immune mechanisms.

Contents

Abstract 2
Contents 3
List of figures 5
List of abbreviations 7
1. Introduction 9
1.1 Humoral immunity 9
1.2 Spatiotemporal regulation of humoral immune responses 10
1.2.1 Antigen encounter and early activation events 10
1.2.2 T cell-B cell interaction 11
1.2.3 The early plasmablast response 13
1.2.4 The germinal center reaction 14
1.3 Humoral memory responses 15
1.4 Long-lived plasma cells 15
1.5 Memory B cells 17
1.5.1 Memory B cell characteristics 17
1.5.2 Origin of canonical Bmem 18
1.5.3 Longevity and maintenance of circulating Bmem 19
1.5.4 Microanatomical positioning of memory B cells 20
1.5.5 Reactivation of memory B cells 21
1.6 Tissue-resident memory lymphocytes 24
1.6.1 Lymphocyte recirculation 24
1.6.2 Resident memory T cells 25
1.6.3 B cell responses in mucosal tissues 28
1.6.4 Resident humoral memory lymphocytes 31
1.7 Influenza virus 33
1.8 Hypothesis 35
1.9 Aims 35
2. Materials and methods 36
2.1 *In vivo* methods 36
2.2 *In vitro* methods 41
3. Validation of a mouse model to track memory B cells and long-lived plasma cells in the lungs of influenza-infected animals 48
Chapter 3: Background 48
3.1 Tracking influenza-specific memory B cells with recombinant viral antigens 51

3.2 Kinetics of humoral immune responses in the lung and secondary lymphoid organs. 53
3.3 Transcriptional characterisation of lung-resident memory B cells 56
3.4 Chapter 3: Summary and discussion 57
4. Microanatomical positioning and migratory behaviour of humoral memory populations in the lung in steady state and after rechallenge 61
Chapter 4: Background 61
4.1 Microanatomical localisation of humoral memory populations in the lung 64
4.2 Mobilisation of memory B cells following influenza rechallenge 67
4.3 Transitional behaviour in migratory Bmem following influenza rechallenge 71
4.4 Molecular mechanisms underlying memory B cell reactivation in the lung. 72
4.5 Mononuclear phagocytes are involved in early Bmem mobilisation following rechallenge 74
4.6 Microanatomical distribution of Bmem is altered following reinfection 76
4.7 Bmem colocalise with infected cells early after reinfection 78
4.8 Chapter 4: Summary and discussion 81
5. Distribution and activation of plasma cells in the lung during recall responses. 86
Chapter 5: Background 86
5.1 Plasma cells redistribute into the alveoli following reinfection 88
5.2 Plasma cell redistribution into alveoli is antigen-independent 89
5.3 Plasma cells redistribute into infected alveoli after rechallenge 90
5.4 Plasma cell redistribution is independent of recruitment of systemic memory or newly activated naïve B cells 91
5.5 Plasma cell entry into the alveoli occurs independently of the GC 95
5.6 Memory B cells and plasma cells are generated locally during secondary responses 96
5.7 Chapter 5: Summary and discussion 98
6. Conclusions 103
6.1 Conclusion 103
Model for humoral memory in the lung 106
6.2 Future work 109
6.3 Acknowledgements 112
6.4 References 113

List of figures

Figure 1. 1 The roles and importance of microanatomical segregation of primary B cell responses…….. 12

Figure 1. 2 Memory B cells are major contributors to reactive humoral immunity.…16

Figure 1. 3 Functional responses of memory B cells …..……22

Figure 1. 4 Phenotypic and functional adaptations of tissue-resident memory lymphocytes…….27

Figure 3. 1. Optimisation of antigen-specific B cell labelling with recombinant X31 haemagglutinin…….51

Figure 3. 2. 1. Utilisation of a fate-mapping reporter mouse to track humoral memory populations……...53

Figure 3. 2. 2. Gating strategy to define lung-resident and SLO Bmem following infection with X31 influenza……54

Figure 3. 2. 3. Quantitation of humoral memory populations post-infection……55

Figure 3. 3 RNA sequencing analysis of lung-resident memory, splenic circulatory memory and splenic naïve B cells……56

Figure 4. 1. 1 Microanatomical localisation of humoral memory populations in the lung……...65

Figure 4. 1. 2 Quantitative PCR analysis of total AID-Tomato^{+} lung Bmem..……66

Figure 4. 2. 1 Mobilisation of memory B cells following influenza rechallenge……...68

Figure 4. 2. 2. Validation of Bmem sequestration in SLO following treatment with FTY720……69

Figure 4. 3. Transitional behaviour in migratory Bmem following influenza rechallenge……...71

Figure 4. 4. Memory B cell mobilisation is induced by an antigen-independent RNAse-sensitive element……..72

Figure 4. 5. Depletion of mononuclear phagocytes disrupts early Bmem mobilisation following rechallenge……...75

Figure 4. 6. 1 Using Ripley's K statistic to track spatial patterning……...76

Figure 4. 6. 2. Microanatomical distribution of lung Bmem becomes altered following reinfection…….77

Figure 4. 7. 1. Description of infected and uninfected sites in the lungs of mice rechallenged with X31-CFP-s-flu…….79

Figure 4. 7. 2. Bmem colocalise with infected cells at early timepoints after reinfection…….80

Figure 5. 1. Plasma cells redistribute into the alveoli following reinfection…….88

Figure 5. 2. Plasma cell redistribution into alveoli is antigen-independent and induced by viral RNA…….89

Figure 5. 3. Plasma cells redistribute out of airway niches into infected alveoli…….91

Figure 5. 4. 1. Establishment of a system to isolate input from naive B cells during secondary responses…….93

Figure 5. 4. 2. Plasma cell redistribution occurs independently of input from the naïve B cell pool…….94

Figure 5. 5. Plasma cell entry into the alveoli occurs independently of the GC…….95

Figure 5. 6. Memory B cells and plasma cells are newly generated locally during secondary responses…….97

Figure 6. 1 Proposed model for humoral immunological memory in the lung…….106

List of abbreviations

AID Activation-induced deaminase

AM Alveolar macrophage

APRIL A proliferation-inducing ligand

BCR B cell receptor

Bmem Memory B cell

BSA Bovine serum albumin

CFP Cyan fluorescent protein

CSR Class-switch recombination

FACS Fluorescence-activated cell sorting

FBS Foetal bovine serum

FDC Follicular dendritic cell

GC Germinal center

GFP Green fluorescent protein

GPCR G-protein coupled receptor

HA Haemagglutinin

i.n. Intranasal

i.p. Intraperitoneal

i.v. Intravenous

IAV Influenza A virus

Ig Immunoglobulin

IL Interleukin

LLPC Long-lived plasma cell

LN Lymph node

MHC Major histocompatibility complex

MZ Marginal zone

NA Neuraminidase

PC Plasma cell

PD-L1 Programmed-death ligand 1

PD-L2 Programmed-death ligand 2

PFA Paraformaldehyde

PLC Phospholipase C

rHA Recombinant haemagglutinin

SCS Subcapsular sinus

SHM Somatic hypermutation

SLO Secondary lymphoid organ

SLPC Short-lived plasma cell

Tcm Central memory T cell

TCR T cell receptor

TLR Toll-like receptor

TNF Tumour necrosis factor

TPLSM Two-photon laser scanning microscopy

Trm Resident memory T cell

VLP Virus-like particle

YFP Yellow fluorescent protein

Chapter 1

1. Introduction

1.1 Humoral immunity

The humoral arm of the immune system represents one of the most effective methods of immune protection from viral infection. Indeed, the majority of vaccines produced to date exploit the protective capacity of the humoral immune system (1, 2). The central effector mechanism mediating these protective effects is the secretion of antigen-specific antibodies, the soluble form of the B cell receptor (BCR). These antibodies bind to the surfaces of pathogens, opsonising them to promote their destruction by innate immune mechanisms, promoting their processing and presentation to T cells and formation of immune complexes to enhance B cell responses (3). Antibodies can also directly neutralise pathogens and thereby inhibit critical processes such as viral fusion with host cells or the function of pathogenic toxins. Whilst the cellular immune arm is essential for the induction of primary antibody responses, antiviral humoral immunity has been shown to be functional in the absence of T cells, and can protect mice from lethal infection (4, 5). Depletion of B cells drastically increases susceptibility to lethal viral infections (6), and the capacity of B cells to provide protection is highlighted by the observation that transfer of antibody to naïve animals results in complete protection from acute viral infections (7). While cytotoxic T lymphocytes can eliminate infected cells, the neutralisation function of antibodies can bypass this potentially immunopathological defence mechanism. Thus, antibodies act as an early and essential barrier to pathogen infection. Antibodies are produced by plasmablasts and mature plasma cells, highly specialised lymphocytes that develop from activated B cells during the course of an immune response. The initial

activation events of naïve B cell can be seen as the first step towards development into fully-fledged antibody-secreting plasma cells and long-term immunity.

1.2 Spatiotemporal regulation of humoral immune responses

B cell activation is tightly controlled, in part by regulated expression of unique activation-regulated transcription factors, costimulatory molecules and other mediators. Cellular positioning in spatially restricted niches where these signals are available is essential for mature germinal center (GC) formation and the establishment of an effective antibody response (8-10). The molecular and cellular interactions that occur in these specialised niches to control B cell transitions between activation states will be briefly outlined here, 1) to establish how the spatial positioning of B cells is linked to their functional responses and 2) to describe the cellular events leading to memory B cell establishment (10).

1.2.1 Antigen encounter and early activation events

The spatiotemporal regulation of humoral immune activation has been particularly well characterised in the lymph nodes and spleen (Fig.1.1). Naïve B cells migrate through organised follicles, scanning the surface of local populations for antigens. Lymph-borne antigens derived from peripheral tissues enter lymph nodes via the afferent lymphatics and can be captured by specialised macrophage populations that line the subcapsular sinus (SCS) of the lymph node. These macrophage capture and present intact antigens on their surface by a variety of receptors including complement receptors and immunoglobulin Fc receptors (11). Antigens encountered on the surface of macrophage at the follicle perimeter are acquired by naïve B cells at the subcapsular sinus. Here, encounter of cognate antigen leads to a reduction of B cell migration and transient retention in the vicinity of the macrophage (11). Non-cognate antigen is acquired from SCS macrophage by binding complement receptors (CR)1 and 2 on naïve

B cells that subsequently transport this antigen to follicular dendritic cells (FDC) in the follicle center (12). FDCs can present antigens for prolonged periods, and are thought to retain antigens on CR1 and CR2, which are very highly expressed by FDCs, among other receptors (11). Cognate interaction with antigen on the surface of FDCs likely represents the principal route of antigen encounter for naïve B cells. Other routes of antigen distribution through the lymph node have been described, such as the conduit system that permits the distribution of small molecules and in some cases intact virions (13-17).

1.2.2 T cell-B cell interaction

After cognate interaction with antigen, either on the surface of FDC or SCS macrophage, stimulated B cells upregulate the chemokine receptor CCR7, which facilitates migration towards the CCL19/CCL21-rich T cell zone. EBI2, a G-protein coupled receptor (GPCR) which directs migration towards oxysterol ligands, is also upregulated, and directs activated B cells to migrate to the outer follicle (18-20). By this time, B cells have bound and internalised antigens via the BCR, processed them and now present peptide epitopes in the context of class II MHC (pMHCII). These early activation-induced repositioning events prime B cells for antigen acquisition and processing, to allow interactions with T cells to receive enhanced activation signals.

Due to the continued expression of CXCR5 and upregulation of CCR7 and EBI2, activated B cells home to the T cell-B cell border (21-23). Meanwhile, a subset

of $CD4^+$ T cells known as T follicular helper cells (Tfh) begin to develop after

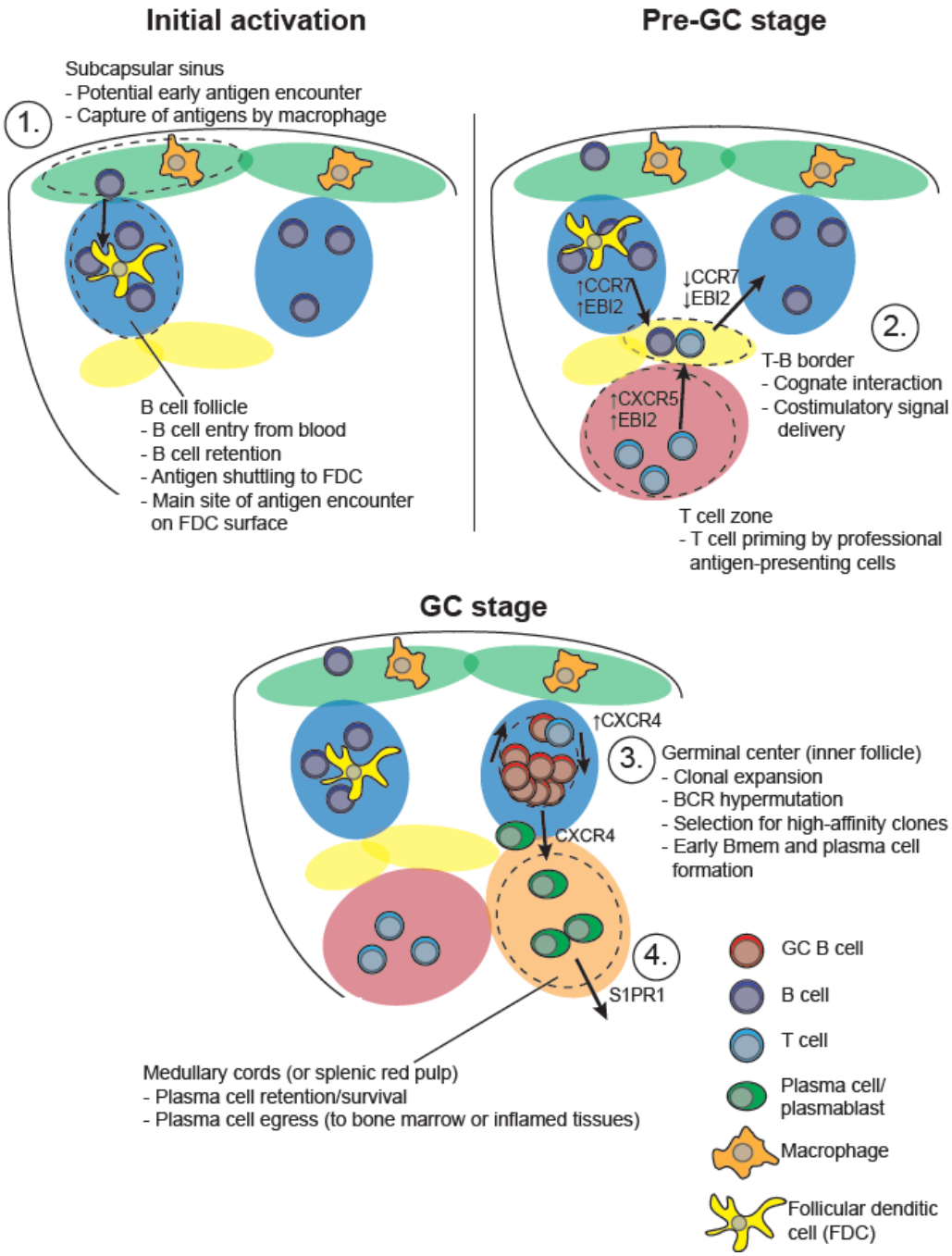


Figure 1. 1 The roles and importance of microanatomical segregation of primary B cell responses. Naïve B cell activation occurs through the sequential migration through select microanatomical niches of secondary lymphoid tissues. Early activation stages include antigen encounter, primarily on the surface of FDC in the B cell follicle, and perhaps on the surface of subcapsular sinus macrophage [1]. Activated B cells then progress to the pre-GC stage, characterised by CCR7 upregulation driving migration to the T-B border, permitting extensive interactions with antigen-specific T cells [2]. Finally, the mature GC is formed, characterised by the presence of light and dark zones. Migration between these regions is regulated by CXCR5 and CXCR4, in a manner that permits B cell BCR mutation, BCR turnover, antigen acquisition and selection by a limiting number of T cells [3]. Plasma cells have been shown to egress the GC area and localise in the medullary cords. CXCR4 is known to be important for this process. At later timepoints, a fraction of plasma cells will enter the blood via a S1PR1-dependent process, and eventually establish a niche in the bone marrow, where they can provide long-term serological protection [4].

stimulation by dendritic cells (DCs) in the T cell zone, and are directed to migrate towards the T-B border by upregulation of CXCR5 and downregulation of CCR7 (24). These early phases of the initial immune response bring together antigen specific lymphocytes in a manner that allows interaction of pMHC on the B cell surface and TCR on the Tfh cell. A number of costimulatory molecules expressed by $CD4^+$ T cells including CD40L, SLAM-associated protein (SAP) and inducible costimulator (ICOS) interact with ligands on the surface of activated B cells, and successful ligation and signal transduction through these molecules is crucial at this stage and throughout the GC response (25). Interaction of molecules such as ICOS further enhance Tfh differentiation, and promote maturation of GC B cells (24). ICOS also has roles in Tfh migration, cytokine production and prolonging T-B interactions (26). Human immunodeficiency syndromes or murine knockout models that lack these costimulatory molecules fail to establish mature GC reactions and exhibit impaired humoral immunity (26). Thus, through the coordinated up- and down-regulation of chemotactic receptors, B cells migrate through distinct cellular niches that provide signals that result in B cell activation and productive interaction with activated, pathogen-reactive T lymphocytes. These interactions with T cells promote the establishment of the early GC.

1.2.3 The early plasmablast response

Upon first exposure to antigen, naïve B cells must undergo a number of crucial differentiation steps to allow 1) early control of pathogens through secretion of low-affinity antibody, and 2) induction of long-term responses that allow enhanced elimination of pathogens later in the response and establishment of long-lived protective immunity. B cells interacting with cognate antigen in a high-affinity manner preferentially enter the extrafollicular plasmablast response (27, 28). This can occur in a T cell-dependent or independent manner, depending on the type of antigenic

stimulation (29). B cells undergoing this pathway migrate to the medullary cords of the lymph node or the splenic red pulp, where they undergo plasmablast differentiation (27, 29). Here, plasmablasts generate early, typically low-affinity antibody that may promote antigen acquisition through complement activation and opsonisation. Enhanced antigen presentation by DCs to $CD4^+$ and $CD8^+$ T cells, and the display of antigen on the surface of FDCs in the B cell follicle via Fc receptors may promote the induction of adaptive immunity (3), and in addition to potential pathogen clearance, highlight important protective function of early plasmablast-derived antibody.

1.2.4 The germinal center reaction

B cells that do not enter the early plasmablast pathway can enter the GC reaction where they undergo prolonged interactions with T cells. As this cognate T-B cell interaction proceeds, these cells downregulate EBI2 and migrate into the follicle center to form the nascent GC. These structures, which form ~6 days after immunisation facilitate extensive proliferation of activated B cells (8).Within these sites, B cells undergo repetitive cycles of somatic hypermutation (SHM) and low levels of class-switch recombination (CSR). Both of these processes are dependent on the expression and function of activation-induced deaminase (AID) in activated B cells. This protein catalyses the deamination of cytosines to uracils preferentially in VDJ and switch regions of the immunoglobulin genes, an important step in initiating base mutations, single- and double-strand DNA breaks, promoting the genetic recombination or mutational events required for CSR and SHM (8, 30). Repeated rounds of SHM and selection for antigen uptake, processing and presentation for limiting amounts of T cell help results in the gradual increase of B cell affinity for antigen. Arising from the GC are two main populations of lymphocytes: both long- and short-lived populations of antibody-secreting plasma cells (PC), and memory B cells (Bmem). As such, SHM and

CSR processes carried out in the GC influence the effector function and efficacy of PC-derived antibodies and the sensitivity of cell-surface BCR on Bmem.

The above findings have been elucidated from a considerable number of studies, highlighting the appreciation of the close link between the positioning of humoral lymphocytes and their biological function in immunity. Thus, the primary lymphocyte response can be viewed as a highly-orchestrated sequence of discrete cell activation stages, with particular dedicated events occurring in distinct microanatomical niches.

1.3 Humoral memory responses

The vast majority of successful vaccination strategies to date exploit the protective capacity of the systems outlined above to target and neutralise virus particles and bacterial toxins. Enhanced secondary responses to pathogen challenge are thought to be mediated primarily by humoral memory populations induced during the primary response (31). Humoral memory consists of the two main populations mentioned above; memory B cells (Bmem) and long-lived plasma cells (LLPC), both of which are primarily derived from GC reactions induced after initial encounter with a pathogen (Fig.1.2).

1.4 Long-lived plasma cells

LLPCs constitutively secrete antibody into the serum or mucus in the absence of antigen stimulation. These antibodies provide a constant level of protection if the concentration is sufficiently high at the site of pathogen exposure (32). Due to alternative splicing, these plasma cells do not express BCR on their surface and so are thought to be incapable of reactivation upon re-exposure to the eliciting antigen. Thus, LLPCs represent a constitutively active humoral memory population, capable of pathogen neutralisation in the absence of any cellular infection.

In contrast to GC B cells and Bmem, that exhibit variable affinity for antigen, LLPCs that successfully enter the bone marrow niche bear immunoglobulin genes with typically high levels of mutation, which promotes high-affinity antibody-antigen interactions (8, 33). It has been proposed that throughout the course of the primary immune response bone marrow plasma cells are gradually replaced by recent emigrants of the GC, leading to this high mutation load (34). This is supported by recent EdU pulse-labelling studies that showed LLPC typically arise from the mature GC later than 14d post-immunisation, and any PC generated early either fail to enter the niche or are outcompeted (35). LLPC primarily localise within niches in bone marrow or some

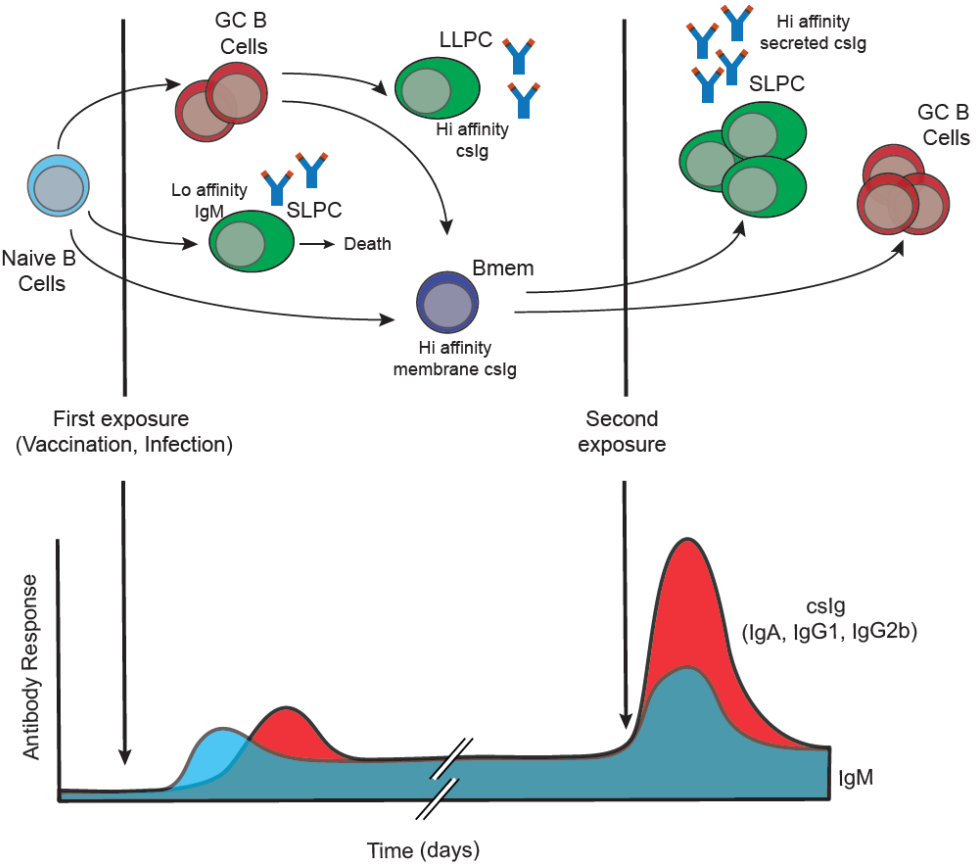


Figure 1. 2 Memory B cells are major contributors to reactive humoral immunity. Humoral memory populations are primarily generated from GC established upon primary exposure to an antigen or pathogen. Although a GC-independent route of Bmem formation has been identified, little is known about the activation/selection events involved. After the resolution of primary infection, LLPC provide constitutive protection through continual secretion of high-affinity, primarily class-switched (cs) antibody into serum or mucus. In contrast, after secondary exposure, Bmem are able to respond with rapid development into secondary GC and newly generated plasma cells. These events occur with enhanced kinetics relative to the primary response, and result in antibody production that is an order of magnitude greater than the primary response.

mucosal tissues. Studies performed by the Radbruch lab and others revealed that the bone marrow niche supports the long-term survival of antigen-specific plasma cells for >120d (36, 37), and human evidence indicates that antiviral serum antibody responses persist for >75 years following vaccinia vaccination (38). Current cellular, molecular and spatial descriptions of the bone marrow niche occupied by LLPC are incomplete, but stroma-derived CXCL12, APRIL and CD44 ligands such as hyaluronic acid, as well as the cytokines IL-6 and TNF have been implicated in PC maintenance at these sites (32, 39-41).

1.5 Memory B cells

In contrast to plasma cells, memory B cells retain their BCR on the cell surface, and represent a reactive immune memory component capable of responding after rechallenge with either doses of pathogen that overcome, or pathogen variants that bypass, constitutive protection by LLPC-derived antibody. Thus, a greater understanding of the mechanisms regulating Bmem generation, maintenance and function may aid rational vaccine design, particularly against variant viral pathogens.

1.5.1 Memory B cell characteristics

Secondary humoral responses to antigen rechallenge have long been associated with 1) rapid kinetics of antibody titre elevation and 2) a predisposition for production of class-switched antibodies. As LLPCs are largely thought to be a non-responsive element of humoral memory, a population of clonally expanded memory B cells are thought to mediate these effects through rapid differentiation into PC and GC (31).

Relative to naïve B cells, antigen-specific memory lymphocytes have increased frequencies, lower activation thresholds and enhanced effector functions and kinetics. Bmem are known to bear surface marker expression profiles remarkably similar to naïve B cells, a feature that has historically made Bmem difficult to selectively isolate

and analyse (42). Reliable identification of this population of lymphocytes in experimental systems has been achieved through surface staining with labelled model or pathogen-derived antigens (31, 42, 43). In humans, CD27 is commonly used as a cell-surface marker to identify antigen-experienced Bmem because it was found to correlate with isotype switched-BCRs and V region mutations (42, 44, 45), but reports indicate that identical Bmem clones are commonly composed of $CD27^+$ and $CD27^-$ subsets (46), highlighting the potential problem of using this marker alone to identify Bmem.

1.5.2 Origin of canonical Bmem

Current prevailing hypotheses postulate that canonical Bmem typically possess IgV regions with intermediate to high mutation loads and bear surface BCRs with class-switched antibody isotypes, indicative of a potential GC origin of these cells. However, the kinetics and molecular regulation of selection into the Bmem pool is not well characterised. Cells with Bmem phenotypes can be found in the blood as early as one week after immunisation, indicating that Bmem may be generated in the nascent GC (47). More recent studies using EdU pulse-labelling to track when activated B cells cease proliferation revealed a striking tendency of Bmem to derive from the early GC, where mutation load is low and specificities more broad, and for the output of late GC to shift towards LLPC formation, where mutation loads were high and BCR specificities presumably more 'committed' (35). Indeed, class-switched Bmem induced by immunisation with the antigen NP-KLH bear a similar number of mutations and antigen affinity levels to GC B cells, but of lower affinity than plasma cells (33, 48). These data have led to the proposal that Bmem may stochastically develop from the pool of activated GC B cells (8). These observations suggest a system where a somewhat broader repertoire of Bmem remain responsiveness to antigens and the

capacity to re-enter the GC or form SLPC in response to reactivation, but where the highest affinity GC B cells develop into active, antibody-secreting LLPC (Fig.1.3).

Whilst it appears that the majority of Bmem induced in an immune response are generated from the GC reaction, a number of studies have confirmed that in mice and humans incapable of forming GC, Bmem are still formed, albeit with reduced mutational loads and class-switching (49-52). In addition, Bmem have been observed to form in the absence of T cell help in responses to T-independent antigens (53). Advances in memory B cell identification using genetic reporter systems have also revealed a putative IgM^+ Bmem subset with variable levels of SHM (45, 54, 55). These observations have given rise to the concept of the GC-independent pathway of memory B cell formation, which may arise from weak or transient interactions with Th cells at the T-B border (31). The relative contribution of GC-independent and -dependent pathways in establishing the Bmem pool are still not fully understood.

1.5.3 Longevity and maintenance of circulating Bmem

Studies have shown that, in humans, pathogen-specific Bmem can represent a substantial portion of the $IgG1^+$ Bmem pool and persist for several months post-infection. After an initial phase of decline, numbers of Bmem begin to stabilise and in this form persist for many years. Indeed, human studies revealed the remarkable survival potential of these cells, lasting for more than 50 years (56). Quiescent Bmem have even been isolated from the peripheral blood of survivors from the 1918 influenza pandemic over 90 years after exposure (57). In animal models, Bmem have been shown to be maintained for >120d following immunization or infection (55, 58). It is unknown whether discrepancies between mouse and human memory longevity represent the difference in lifespans of the organisms, the semi-sterile environment in which experimental animals exist, or other factors yet unknown.

The factors that regulate the long-term maintenance of circulatory Bmem are not well defined. Multiple studies have been performed to assess the role for antigen in this process. Early studies in which cells were intravenously transferred into naïve recipients indicated that Bmem failed to survive when antigen was absent (59). However, a later study utilised inducible genetic recombination of the BCR of mature Bmem in the same animal to modify the antigen specificity of these cells after memory formation. Their findings revealed that Bmem expressing a recombined BCR responsive to irrelevant antigens survived for >100 days, providing strong evidence that Bmem survival is independent of persistent antigen-driven BCR signalling (60). However, Bmem are lost in mice with conditional deletion of PLC-γ2 in post-GC B cells, supporting a possible role for tonic signalling through the BCR in ensuring Bmem maintenance (61).

T cell help, whilst involved in establishing primary humoral immunity, has been shown to be dispensable for Bmem survival (62, 63). T cell depletion 3 weeks post-immunization led to no detectable difference in secondary antibody responses of Bmem (62). In addition, Bmem transfer into naïve hosts in the absence of T cell memory were found to survive for >90d (64). Lastly, multiple other lines of evidence from murine studies indicate no clear correlation between $CD4^+$ T cell memory and antibody titers (38, 65, 66).

1.5.4 Microanatomical positioning of memory B cells

Bmem can be found in secondary lymphoid tissues of immunised animals, as well as peripheral blood in low frequencies, where they undergo recirculation through lymph nodes, spleen and blood. In support of this, transcriptional analyses have confirmed that Bmem express the basic circulatory machinery such as S1PR1 and CD62L (67, 68). A number of potential sites of Bmem maintenance in secondary

lymphoid organs (SLO) have been proposed. Over 30 years ago, antigen labelling of the spleens of immunised rats revealed Bmem residence in a marginal zone niche of the spleen (69). In other studies, pulse-labelling of proliferating cells using BrdU at the peak of the response revealed labelled quiescent Bmem populations 12 weeks later evenly distributed within the marginal zone and B cell follicle (67). In support of this observation, the use of Cγ1-Cre to fate-map class-switched B cells, Bmem positioning in splenic follicles was observed (70). This latter study noted that genetic ablation of CCR6 abrogated Bmem distribution, secondary plasma cell formation and serum antibody responses to systemic antigen challenge. Mixed bone-marrow chimeras, restricting CCR6 knockout to the B cell lineage, showed that functional CCR6 on B cells was responsible for these effects (70). Histological staining of $IgG1^+$ $CD38^+$ B cells further identified sites of collapsing GCs as potential Bmem maintenance sites (71).

1.5.5 Reactivation of memory B cells

The function of memory B cells is to rapidly induce secondary humoral immunity. This is thought to include both the rapid generation of high-affinity secondary plasma cells and re-induction of the GC response (42). As Bmem retain the capacity to re-enter the GC, at least in certain settings, they have been proposed to possess the ability to target viral escape mutants. Indeed, whilst PC-derived antibodies are typically high-affinity and neutralising for immunodominant epitopes, Bmem can express BCRs with greater affinity for escape mutants than the initiating virus, perhaps further supporting the notion that low-affinity interactions in the primary response can induce Bmem (72)(Fig.1.3). As a note, whilst both PC and GC pathways appear available to Bmem subsets (54, 55), the events and molecular signals directing the fate

decision between secondary plasma cell generation and secondary GC induction remain elusive.

Previous studies attempting to address this issue have found phenotypic subsets of Bmem that have different tendencies to develop into GC or PC following rechallenge. For example, the antibody isotype expressed by Bmem has been proposed to be linked to differentiation potential. Bmem transfer into naïve hosts followed by rechallenge has revealed that Bmem expressing surface IgG primarily develop into plasma cells. In contrast, IgM^+ Bmem were found to preferentially establish or enter secondary GCs following restimulation (54, 55). However, this has been challenged by

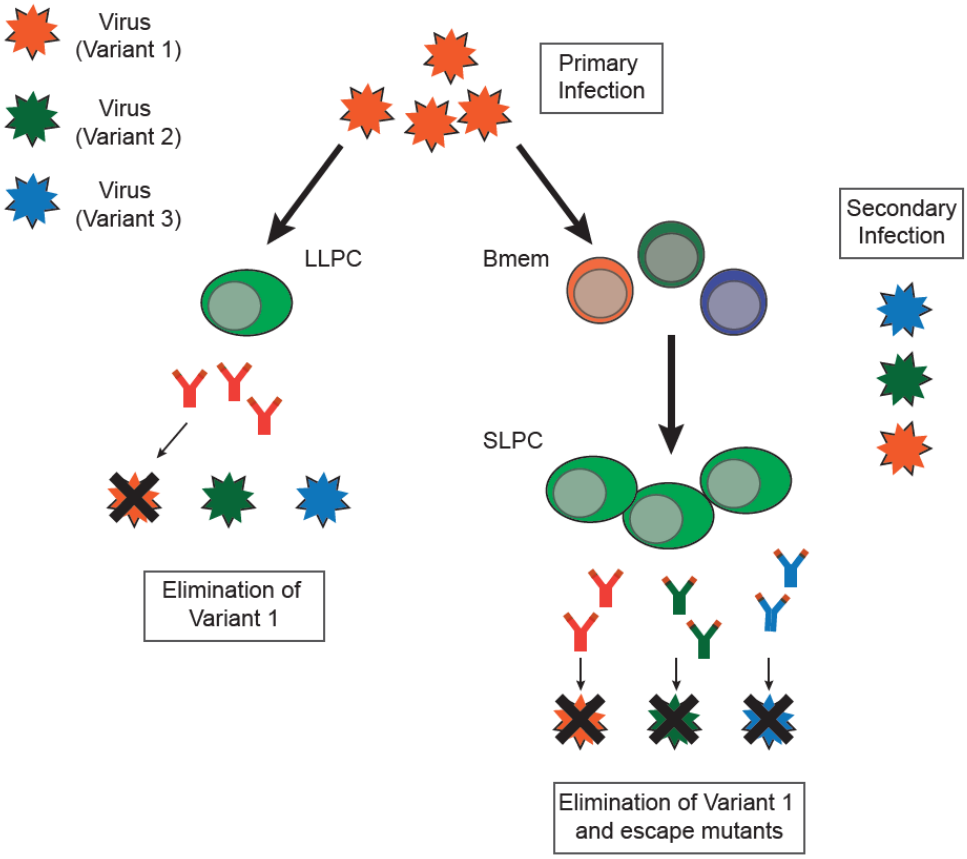


Figure 1. 3 Functional responses of memory B cells. Memory B cells generally arise early in the events of the GC response, before the BCR has been subjected to mutative pressure, whereas long-lived plasma cells (LLPC) arise from heavily mutated GC B cells. Thus, upon viral rechallenge, whilst antibodies produced by LLPC can immediately provide stringent protection from the initial virus isolate, these specific antibodies may be rendered non-functional by the mutation or inter-strain recombination of viral antigens. Meanwhile, a broader range of antigens may be able to reactivate lower affinity B_{mem}, and the rapid reformation of the GC response allows generation of an immediate pool of protective effector plasmablasts. The relative proportion of Bmem entering GC versus immediate plasma cell development remains unknown.

findings by Shlomchik and colleagues, who provide data indicating that Bmem populations expressing PD-L2 and CD80 have increased propensity to develop into antibody-secreting plasmablasts or plasma cells, whereas PD-L2$^-$ CD80$^-$ Bmem preferentially enter GC response following reactivation, seemingly independently of BCR isotype (73). Importantly, these are not necessarily mutually exclusive theories, and the majority of IgG$^+$ Bmem express PD-L2 and CD80, whereas most IgM$^+$ Bmem fail to express these markers (73, 74). Whilst a consensus has not yet been reached, it appears that a subset of Bmem are specialised for rapid development into functional antibody-secreting cells. Whether these observations hold true for memory B cell populations outside of secondary lymphoid organs remains unknown.

The mechanisms controlling accelerated Bmem reactivation kinetics are not fully elucidated. One common theory is that Bmem antigen-detection events are fundamentally distinct from that of naïve B cells. The interaction of IgG1 with antigen has been proposed to trigger distinct signalling events from the longer cytoplasmic tail of IgG1, compared to that of IgM (31). The recruitment of signalling adaptors to IgG1 has also been shown to enhance early Bmem proliferation (75). Additionally, isotype-independent adaptations to downstream signalling pathways have been proposed to enhance Bmem responsiveness. Nuclear transfer experiments in which 'naïve' B cells were generated that expressed surface IgG1 BCR demonstrated that enhanced development into plasma cells was a feature of antigen-experienced IgG1$^+$ Bmem, and not naïve IgG1$^+$ cells (76).

Given the unique responses of these cells, considerable effort has been invested in uncovering a core gene expression profile of B cell memory. A number of groups have made efforts in developing gene expression profiles of circulating or splenic memory B cells (68, 77-81). To date, no unique transcriptional regulator of Bmem has

been identified, and these studies reveal that similar to Bmem phenotype, their transcription profiles largely resemble that of naïve B cells, with a number of differences in activation-induced signalling and apoptosis pathways.

In contrast to primary responses, very little is known about the spatiotemporal orchestration of secondary humoral immune responses. Only recently it has been revealed that memory B cell reactivation may occur in a unique region of the LN. Moran et al utilised two-photon laser scanning microscopy (TPLSM) to track memory B cell responses in the lymph nodes of live mice (82). Transfer of fluorescently-tagged HEL-specific SW_{HEL} B cells prior to immunisation with HEL permitted tracking of fluorescently labelled memory populations. This approach revealed that Bmem undergo a phase of rapid proliferation and PC development shortly after restimulation, and that these stages occur selectively in the subcapsular sinus of the lymph node.

Memory B cell and long-lived plasma cell responses to pathogens are thus highly distinct, despite sharing an effector mechanism, as they are maintained by distinct molecular pathways, in different anatomical locations. Recirculating antigen-responsive Bmem, together with antibody-secreting LLPC in the bone marrow or mucosa, permit effective humoral protection from pathogen reinfection. However, in the last 20 years, a number of studies have identified a population of specialised memory lymphocytes with potent effector function and very early protective capacity – tissue-resident memory lymphocytes.

1.6 Tissue-resident memory lymphocytes

1.6.1 Lymphocyte recirculation

The vast majority of what is known about Bmem is derived from studies assessing splenic or lymph node populations, which are known to undergo recirculation through SLOs and blood. This process permits efficient surveillance and exposure to

antigens derived from peripheral tissues. B cells migrate through the follicles of secondary lymphoid tissues at a constant rate of ~6μm/min. In the absence of antigen stimulation or inflammation, B cells will exit lymph nodes after ~24h of residence by migrating to egress sites where the lipid sphingosine-1-phosphate (S1P) promotes lymphocyte access to the lymph via cortical and medullary sinuses (in the lymph node) (83-85). In this way, S1PR1 acts to overcome chemokine-directed retention signals (86). In the blood and lymph, ligand-induced downregulation of S1PR1 due to high ligand bioavailability results in a shift in potential of B cells, allowing cells to rapidly reverse the direction of their migration and move against S1P gradients as they enter back into lymphoid tissues (87). The process of cell entry into lymphoid organs has been extensively studied in lymph nodes. In these organs, T and B lymphocytes arrive from the blood, entering the tissue by crossing high endothelial venules (HEVs). This process requires the expression of CD62L (encoded by *Sell*), which binds sialylated ligands on the HEVs, allowing cells to roll on the blood vessel. Chemokines presented on the HEVs activate homing GPCRs, including CCR7 and CXCR5 and to some extent CXCR4, which rapidly trigger integrin activation (most notably LFA-1 and VLA-4) to mediate firm adhesion and transmigration (88). Thus, cells that continuously recirculate via lymph nodes are expected to express a minimal set of receptors to allow their entry (CD62L, CCR7, CXCR5, LFA-1 and VLA-4) and egress (S1PR1) from these structures.

1.6.2 Resident memory T cells

A population of memory lymphocytes that has been observed to reside long-term in peripheral tissues does not recirculate in the above manner, and instead remains lodged in previously-infected tissues. This class of memory lymphocytes has been particularly well-described when studying T cells in various settings including lungs,

skin and other sites following infections such as lymphocytic choriomeningitis virus or influenza virus (89). This population is unique to memory and appears primarily after induction by local inflammatory or infectious challenge (89, 90). The true extent of segregation of secondary response components was found to be significant once the tissue-resident memory (Trm) lymphocytes were compared to circulating memory T cell (Tcm) populations. It was revealed that tissue Trm have higher expression of effector molecules such as perforin and granzyme B and/or effector cytokines (90). Trm lymphocytes were also found to exhibit reduced proliferative capacity relative to recirculating Tcm subsets (Fig.1.4). Thus, adaptive immunity appears to be segregated in a way that allows a strong, rapid response at the site of secondary pathogen encounter whilst a central, circulating population known as Tcm proliferate extensively to produce classical short-lived effector cells.

Initially identified as memory T cells found in nonlymphoid tissues, Trm were defined by the expression of CD69 (a molecule which blocks the egress-promoting function of S1PR1, thus proposed to facilitate residence(91, 92)) and CD103 (an integrin alpha-E chain implicated in binding E-cadherin), although it is now appreciated that not all Trm cells exhibit this phenotype. Resident memory T cells also transcriptionally downregulate the S1PR1 surface receptor, which promotes cell egress from tissues (93, 94). In fact, enforced expression of S1PR1 blocks the establishment of resident memory T cells after viral infection (93). Thus, the localisation of Trm in peripheral tissues is tightly linked to their establishment and survival.

Techniques such as *in vivo* labelling and parabiosis have been used to more elaborately investigate the residence of these populations. '*In vivo* labelling' is the intravenous administration of a fluorescently labelled antibody shortly before

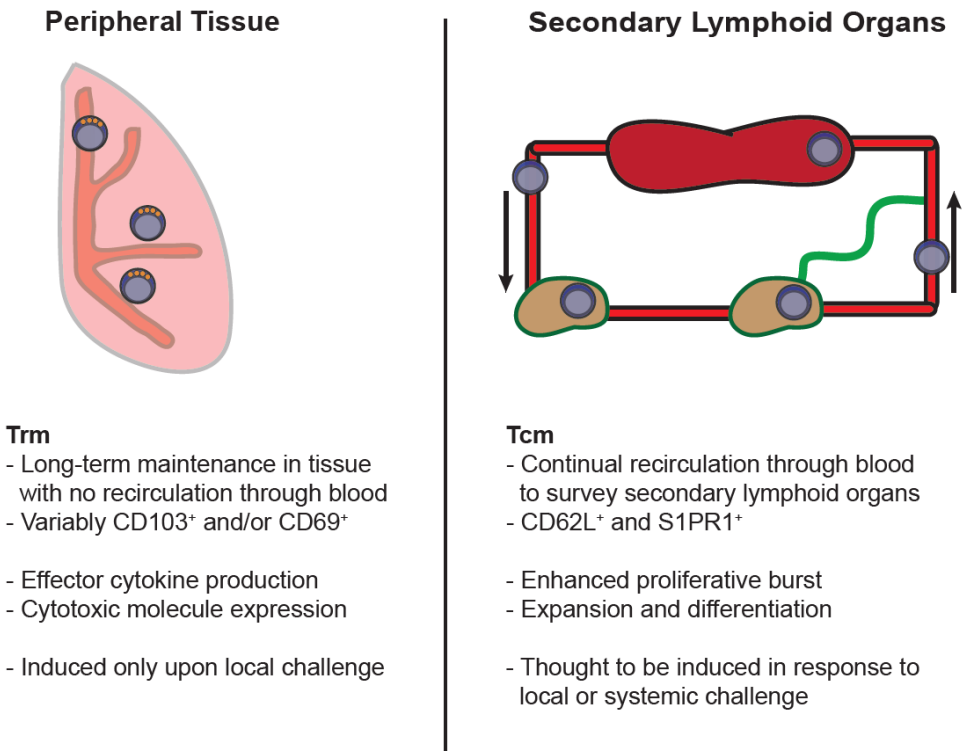


Figure 1. 4 Phenotypic and functional adaptations of tissue-resident memory lymphocytes. Memory T cells positioned in peripheral tissues (Trm) do not enter the blood or secondary lymphoid organs, and after reactivation rapidly secrete cytokines and exert cytotoxic function, to provide an early wave of protection. In contrast, circulatory central memory T cells (Tcm) survey secondary lymphoid organs, where after activation they undergo extensive rounds of proliferation and differentiation into effector lymphocytes.

sacrificing the mouse, in a way that selectively labels blood-exposed lymphocytes. Using this technique in combination with flow cytometry, it is possible to identify whether the cells of interest are within the tissue parenchyma or in the bloodstream. Parabiosis studies, wherein the circulatory systems of two animals are conjoined, have further clarified the tissue-anchored nature of resident-memory lymphocytes (89). These studies highlight the segregation that exists between resident lymphocytes and their circulatory counterparts, and show the long-lived nature of these populations.

1.6.3 B cell responses in mucosal tissues

Whilst humoral immune responses have been mostly characterised by studying secondary lymphoid organs, humoral immunity at barrier sites represents a major element of functional immunological protection, as these tissues are often the primary sites of pathogen encounter. Plasma cells have been known to enter inflamed mucosa including the nasal mucosa (95, 96), salivary glands (97, 98), and the lung airways (99). A smaller population of long-lived plasma cells has also been identified in the tonsils (100). The largest pool of antibody-secreting cells, in terms of total numbers, is the small intestinal mucosa. Plasma cells here are thought to derive from local lymphoid tissues known as Peyer's patches that support GC structures and local BCR mutation and diversification (101, 102). Plasma cells in mucosal tissues are mostly class-switched to IgA isotype. Secretory IgA can be transcytosed to mucosal surfaces by the poly-Ig receptor (103), where it can regulate barrier function and bacterial growth (104, 105).

Similar to bone marrow plasma cells, PC in the intestinal mucosa have been shown to be highly mutated, within both class-switched and non-switched populations, indicating historic passage through the GC (106, 107). Shared BCR clones were also identified in the IgA^+ Bmem pool in the local lymphoid tissues and the IgA^+ plasma

cell pool in the lamina propria, indicating that local humoral immunity may be induced in mucosal lymphoid structures (108). It has been suggested that the appearance of shared B cell clones between different mucosal compartments may indicate that in mice Bmem are capable of recirculation through mucosal sites (108). Interestingly, B cells have been proposed to locally expand and form plasma cells in the gut after indirect stimulation with bacterial products (109, 110). This concept is supported by further comparisons of clonal relationships between Bmem and PC in mucosal sites, revealing that Bmem and PC may be linked in steady state and disease conditions (109, 111).

Interestingly, human B cells in the gut have been proposed to have distinct thresholds for activation regarding immunogenic and inflammatory stimuli. Expression of FCRL4 by human Bmem has been proposed to dampen BCR-derived signalling events and to enhance innate signalling such as that from TLRs (112). Whether this applies to mucosal B cell populations in other mucosa has not been determined, and FCRL4 is not expressed by murine B cells.

Within the lung, our understanding of B cell immunity is largely confined to a number of pathological disease states. This is primarily due to the absence of naïve B cells in non-inflamed pulmonary tissue parenchyma. In contrast, after the induction of excessive or chronic local inflammation, by stimuli such as influenza infection, B cells are known to enter the lung and organise within structures known as inducible bronchо-alveolar lymphoid tissue (iBALT). Here, responding B cells develop a number of characteristics similar to GC B cells, such as expression of the GL7 antigen, the initiation of GC B cell transcriptional profiles and the induction of somatic hypermutation (113). This local lymphoid structure also houses a number of cell types that have established roles in supporting primary humoral responses. T cells with Tfh-like phenotypes, follicular dendritic cells and B cells exhibiting GC phenotype

(expression of the GL7 antigen) can be found in these sites (114). $CD11c^+$ DCs are also present, and may have roles in cytokine and chemokine liberation as well as maintaining the iBALT GC itself (115).

Histological analysis has revealed that iBALT have a tendency to form at the branching points of airways and bronchovascular bundles (116). The underlying biological explanation for this positioning remains unknown, but may relate to the deposition of antigen at airway branch points where air turbulence promotes particle interaction with the respiratory mucosa, or to the vicinity of blood vasculature and relative efficiency of the recruitment of leukocytes involved in iBALT establishment. Mechanistically, these sites are formed following the induction of inflammatory signals, such as type I interferon, that drive the development of specialised stromal populations (117). Pulmonary dendritic cells are essential for iBALT maintenance, and DC-derived lymphotoxin-beta has been suggested to have a role in iBALT formation, indicating that perhaps the sentinel activity of mononuclear phagocytes in the lung may shape local B cell responses (115). Interestingly, localised pulmonary expression of chemokines with principal roles in lymphoid tissue organisation, such as CCL19, CCL21 and to some extent CXCL13, has been shown to correlate with the induction of iBALT and local humoral immunity (118). IL-17 derived from $CD4^+$ T cells also promotes local expression of CXCL13, and is essential for the development of iBALT (119). Recent studies suggest that pulmonary CXCL13 may have a role in the establishment, although not necessarily the maintenance, of iBALT and pulmonary GC's (117), perhaps through the initial recruitment of naive B cells to the local tissue. Blood vessels within iBALTs also express a variety of adhesion molecules that have known roles in lymphocyte entry to the local niche, including VCAM-1 and PNAd (120).

Thus, the recruitment of B cells to peripheral mucosal sites and their maintenance there appears to be closely related to the level of inflammatory or pathogenic stimuli present within the tissue.

Functionally, iBALTs are involved in protection from respiratory virus infection. In mice that fail to develop lymph nodes or spleen, but that retain the capacity to establish iBALT, influenza infection is efficiently cleared, and these mice can survive high doses of viral infection, displaying the potential of these tertiary lymphoid structures to support local immunity and antiviral protection (121, 122). In addition, somatic hypermutation of B cells within iBALT has been proposed to confer altered selection pressures, relative to SLO GCs, and potentially promote the development of cross-reactive antibodies (123).

Recently, Oh et al. have provided evidence that circulating Bmem have the potential to enter infected mucosa of the female reproductive tract and provide early protection from viral reinfection (124). One potential defence strategy that may allow yet more rapid and effective antiviral immunity may be through the action of tissue-resident Bmem. However, at this point much less is known about the induction and regulation of this population.

1.6.4 Resident humoral memory lymphocytes

Whilst tissue-resident memory cells have been primarily studied in the context of T cell biology, recently a number of studies have shown that an analogous population exists within the humoral arm of the immune system. This may not be entirely unexpected, as plasma cells have been known to enter inflamed peripheral tissues, and long-lived plasma cell populations may be established in select mucosal sites. Whilst any unique functional responses related to residence in these sites remain unknown, tissue-resident PC have been shown to produce microbe-specific antibodies that are

translocated into the gut lumen to regulate bacterial populations (104, 105). $CD27^+$ and $CD27^-$ B cell populations that bear somatically hypermutated IgA and IgG BCRs have also been reported in the human tonsils and gingival mucosa in the steady state (80, 125, 126). Given the exposure of these sites to microbiota populations and food antigens, Bmem in the mucosa may be reactive to these antigens as well as infectious agents.

Most recently, pathogen-reactive memory B cells have been found in the lungs of mice after resolution of influenza virus infection. The initial observation that influenza-specific Bmem can be found in the lung for prolonged periods following infection was performed by Onodera et al (127). This study identified influenza-specific IgM^- IgD^- $CD38^+$ B cells that persisted in lung tissue for >150 days after infection. Whilst this group did not use *in vivo* labelling to prevent potential contamination from blood Bmem, they did demonstrate that transfer of these lung Bmem into naïve recipients conferred more effective protection from virus rechallenge than transfer of spleen-derived Bmem. Subsequent work identified enhanced cross-reactivity of lung Bmem relative to splenic Bmem populations (123). This was detected by labelling with recombinant influenza antigens from different strains of virus, and was attributed to high mutational loads in BCR V-region sequences, presumably acquired from local GC in the lung. Interestingly, when lung or splenic Bmem induced by X31 influenza were separately transferred into mice that were then rechallenged with a different strain of influenza, Bmem derived from lung were found to generate more antibody-secreting cells responsive to the different strain of IAV, suggesting that the cross-reactive repertoire of lung Bmem may be functionally significant (123).

More recently, parabiosis studies have provided firm evidence that lung Bmem represent a truly tissue-resident population that fails to equilibrate between mice with

linked circulatory systems (128). Through the use of anti-CD40L antibody to collapse established GCs, this group also provided evidence that while GC are required to establish lung Bmem cells, they are not essential for their maintenance. Indeed, Allie et al have provided the first detailed phenotypic description of lung-resident Bmem in comparison to splenic Bmem. Using a flow cytometric approach, they revealed that the majority of these cells are $CXCR3^{high}$, $CD73^{low}$, $PD\text{-}L2^{high}$, $CD62L^{low}$, $CD69^{+}$ and $CD103^{-}$ (128). As such, this paper provides a valuable initial characterisation of the phenotypic and developmental requirements of resident Bmem in the lung of influenza-infected mice. However, much remains unknown of the biology regarding the maintenance, activation and functional responses of this population.

1.7 Influenza virus

Influenza virus represents a major contributor to disease-associated mortality and also economic cost. Seasonal influenza infections are responsible for up to 650,000 deaths worldwide annually, and viral gene reassortment can lead to the development of pandemic strains that can cause the death of millions (129, 130).

Influenza is an encapsulated negative strand RNA virus, with a genome carried on 7/8 gene segments (99). Due to gene duplication and divergent mutation, various strains of influenza A viruses recirculate, each with distinct haemagglutinin (HA) and neuraminidase (NA) variants. HA permits virus entry into host cells by interacting with sialic acids on host cell membranes, whilst NA is thought to be involved in virion release from infected cells (129). Low-fidelity replication and viral genome reassortment cause these two main protective antigens to undergo extensive mutation, allowing evasion of antibody neutralisation function.

Adaptive immunity plays a key role in maintaining robust protection from influenza reinfection. T cells possess the capacity to target internal peptide epitopes that

tend to be more conserved between strains, due to critical virological function (131-133). The activation of antigen-reactive B cell clones allows B cells to enter GCs and re-diversify their antigen receptors (134), thus increasing the odds of generating B lymphocytes and antibodies that can target viral escape mutants (123). Naïve and memory B cells also remain able to develop into antibody-secreting cells with the potential to generate broadly neutralising antibodies. These broadly neutralising or cross-reactive antibodies are able to neutralise or bind multiple strains of virus by targeting of conserved regions on the viral surface, and antibodies capable of binding all known influenza virus strains have been identified in human blood (135-138).

Influenza virus only infects lung cell populations such as alveolar epithelial cells, and in some cases alveolar macrophages. Thus, local immunity is of crucial importance in effectively targeting and overcoming infection. Influenza infection of the lung is known to cause the formation of inducible lymphoid tissues known as inducible-bronchoalveolar lymphoid tissue (iBALT) (139). Influenza-induced iBALT GC B cells interestingly have transcriptional profiles very similar to secondary lymphoid organ GC B cells, however little sharing of BCR clones between these sites has been observed (113). These findings suggest that the peripheral tissue iBALT represents a distinct and separate site of B cell selection during the primary response to respiratory pathogens. These observations highlight the importance of such local tissues to the developing humoral response to respiratory pathogens such as influenza.

1.8 Hypothesis

As outlined above, the microanatomical positioning of lymphocytes is vital to the regulation of their function, and memory B cells represent a population exquisitely adapted for reactivation.

Thus, this study was conceived with the hypothesis that the microanatomical positioning of lung-resident memory B cells in peripheral tissues is involved in their role in maintaining robust and rapid humoral responses to viral rechallenge. To investigate the positioning, migration and cellular dynamics of B_{mem}, we developed two-photon live imaging and histological analysis approaches combined with mouse models based on cell fate mapping. We hope that these studies will provide potential clues for the function of these cells.

1.9 Aims

The specific aims I will address in this thesis are:

1. To characterise the transcriptional profile of influenza-specific lung Bmem, and compare this signature to circulating Bmem

2. To define the positioning and migration patterns of resident memory B cells in the lungs, and explore interactions with other cell types

3. To describe the early response dynamics of resident memory B cells after rechallenge with influenza virus

Chapter 2

2. Materials and methods

2.1 *In vivo* methods

Animals

Male and female mice at 8-12 weeks of age were used in this project. All mice were housed in the Biological Services Unit at the Kennedy Institute of Rheumatology, University of Oxford or the Biomedical Services Facility, John Radcliffe Hospital, University of Oxford. Aicda-cre (Aicda$^{tm1(Cre)Mnz}$, Stock No: 007770) and Rosa26-stop-dTomato mice (Stock No: 007909) were obtained from JAX. CD19ko mice on a B6 background were generated by intercrossing CD19$^{Cre/+}$ mice to obtain CD19$^{Cre/Cre}$(140). BLIMP1-Venus mice on a B6 background were obtained from Mitinori Saitou (141). All procedures carried out on animals are approved by the Home Office under the United Kingdom Animals (Scientific Procedures) Act 1986. Project licences 40/3629, 30/3343 and P1F0EF2FE.

Influenza infection

The primary strain of influenza used in this project was the mouse-adapted H3N2 X31 strain, kindly provided by Dr. Oliver Bannard. Recombinant strains were kindly provided by Prof. Alain Townsend or produced in collaboration with the Townsend lab. For more details on recombinant virus production see Chapter 2.2 *In vitro* methods. For infection with X31 and recombinant strains of influenza, mice weighing ≥20g were anaesthetised and intranasally administered 2x10^4 PFU of X31, PR8 S-flu or CFP-S-flu in sterile PBS (Sigma-Aldrich). Mouse weight and behaviour were monitored every day for 14d following infection. For rechallenge experiments, high-dose challenge was

performed using $1x10^6$ PFU of X31 influenza, or for localisation studies $1x10^6$ PFU of CFP-S-flu strains.

Bone Marrow Chimeras

Mice were lethally irradiated (11Gy) in two dosages, separated by 4 hours. Long bones of the lower limbs of BLIMP1-Venus AID-dTomato mice were collected into DMEM collection medium (10% FBS, 1% penicillin/streptomycin, 1% HEPES). Bones were cleaned and bone marrow removed by dissecting the ends of the femur or tibia and flushing clean sterile DMEM through the bones. Cells were resuspended at ~$1x10^7$ cells/ml and each recipient mouse received i.v. ~$2.5x10^6$ total cells.

Clodronated liposome (CLL) treatment

Mice were anaesthetised, and 45µl of Clodrosome® (Encapsula NanoSciences LLC) was administered intranasally, twice on d-6 and twice on d-3. For experiments assessing Bmem reactivation in the context of macrophage depletion, CLL-treated mice were rechallenged with influenza on d0 and analysed 18-24h later.

Cell purification and transfers

Spleens were harvested from donor mice into sterile RPMI (Gibco) containing 2%FBS and strained through a 40µm filter. Red blood cells were lysed by 3min incubation in red blood cell lysis buffer at room temperature and B cell isolation was performed using MagniSort B Cell Enrichment kit (Affymetrix eBioscience) as per manufacturer's instructions. Cells were resuspended in RPMI before i.v transfer into recipients. For B cell transfer experiments ~$10x10^6$ cells were adoptively transferred into $CD19^{-/-}$ recipients.

In vivo labelling

Mice were intravenously administered 2.5µg phycoerythrin (PE)/Pacific Blue-conjugated anti-CD45 in PBS. After four minutes mice were euthanized and lungs perfused with cold PBS through the right ventricle of the heart. Immediately, lungs were harvested and oesophagus, trachea, thymus and heart removed, and mediastinal lymph node collected separately.

Flow cytometry and cell sorting

Lungs were removed and individual lobes were collected. Lungs were digested in 1mg/ml collagenase D (Roche) and 10µg/ml DNAse I in RPMI for 30 minutes at 37°C. Following digestion, tissue was homogenised through a 70µm filter and lymphocytes were enriched by Ficoll-Paque (GE Healthcare) density centrifugation. Cell suspensions were incubated with FC block in FACS buffer (2% FBS, 0.1% Sodium Azide, 1mM EDTA in sterile PBS) for 15min, and were then stained in FACS buffer using predetermined optimal antibody concentrations for 30min. Cell suspensions were washed, labelled with secondary labelling agents for 20min and resuspended in FACS buffer for data acquisition on Fortessa X20 or LSRII analysers (BD Biosciences). For cell sorting, samples were prepared as above and sorted on a FACSAria III (BD Biosciences). For RNA sequencing approximately 100 cells were sorted directly into 4µl lysis buffer (0.2% Triton X, U RNAse Inhibitor 2.5mM OligoDT and 2.5µM dNTP), immediately snap-frozen on dry ice and stored at -80°C.

Multiphoton imaging of live lung explants

Mice were euthanised with a single dose of i.p. pentobarbitone, the trachea exposed, and 1-1.5ml of 1% low-melt agarose was injected into the lungs before solidifying by rinsing in cold sterile PBS. Individual lung lobes were dissected, stored in RT RPMI and sectioned at 450µm on a vibratome (Campden Instruments Ltd.) immersed in RT PBS. Sections were mounted on plastic coverslips using Vetbond Tissue Glue (3M), placed in RT RPMI and immediately imaged. For two-photon imaging an explant setup was established, which maintained the tissue sample at 37°C under a continuous flow of RPMI perfused with 95% oxygen, 5% carbon dioxide. Sections were imaged by TPLSM on an upright Zeiss LSM880 microscope, with an Apochromat 20x1.0 DIC VIS-IR D=0.0 (UV) objective lens, equipped with two Mai Tai lasers (690-849nm, 850-990nm), using a laser excitation wavelength of 930nm.

Immunofluorescence staining and confocal microscopy

Preparation of lung samples for fluorescence staining was performed as for multiphoton imaging, with a number of modifications. Optimal cutting temperature compound (OCT, TissueTek) was used to inflate the lung, individual lobes were dissected and fixed in 1% PFA in PLP buffer (1mM Sodium periodate, 0.2M L-lysine, pH7.4) for 24h. After washing, lungs were incubated in 30% sucrose at 4°C for 24h for cryoprotection. Individual lobes were immersed in OCT and frozen in a methanol - dry-ice bath. 16-20µm tissue sections were taken on a cryostat at -23°C (Lecia Biosystems). Sections were blocked with mouse/rat serum and FC block in staining solution (5% normal mouse/rat serum, 0.3% Triton-X100 (Sigma), 0.2% FBS, 0.1% sodium azide) for 30min. Primary stains were carried out at predetermined optimal concentrations for 3h in staining solution. Secondary antibodies were applied for 2h and slides were

washed in PBS and mounted using fluoromount-G (Cambridge Bioscience Ltd.). Confocal microscopy was performed on an upright Zeiss LSM880.

Determination of infection foci in CFP-Flu-infected lungs

The 'Spots' function of the Imaris software was utilised to generate points, based on the fluorescent signal from CFP-S-flu-infected cells. Surface coordinates and image border parameters were exported and used with the Spatstat package in R. The quadratcount function of the Spatstat package was used to assess the density of infected cells across the tiled fluorescent image. Areas with infected cells at a density of >225cells/mm^3 (Approx. 9 cells per sample grid) were classified as infected, and the density of plasma cells or Bmem within these regions was quantified.

Data and Image analysis

Image files obtained from confocal or two-photon microscopes were analysed using Imaris software (Bitplane, version 8.3.1) or – for cell shape analysis ImageJ software. Flow cytometric data was analysed on FlowJo v9.9 (TreeStar Inc.). For calculation of Ripley's K statistic, data exported from Imaris' Spots or surfaces function was used with image metadata to supply an R script with cell event coordinates and image boundaries that allowed the generation of spatial point patterns. The spatstat package in R was used to calculate Ripley's K and L values using Kest and Lest functions. The raw data from these plots was used as input to Prism (Version 9) for graphical representation.

FTY720, EdU administration and tracking proliferating cells

FTY720 was administered intravenously at 1mg/kg in PBS 2d prior to rechallenge. For experiments requiring analysis at d4 after rechallenge timepoints treatment was also administered 2d after rechallenge. For experiments tracking cell proliferation 1mg EdU was administered intraperitoneally to synchronise labelling and animals were maintained on 0.3mg/ml EdU in drinking water, with 2.5% sucrose to prevent taste aversion. Lung sections were prepared for confocal imaging as described above, and stained for EdU using Click-iT Plus Alexa Fluor 647 imaging kit (Thermofisher). Analysis of images was performed using the 'colocalisation' function of Imaris software to identify EdU+ Tomato+ cells, and plasma cells and Bmem were segregated based on expression of BLIMP1-Venus. 'Spots' were generated on EdU^+ or EdU^- PC and Bmem, which were then quantified.

Pertussis toxin (PtX) treatment

In experiments using pertussis toxin (PTx, Quadratech Diagnostics Ltd.), influenza-immune mice (5w postinfection) were rechallenged with CFP-s-Flu. 3h later, PTx was administered intravenously to the rechallenged mice at a dose of 400µg/kg. This dosage has been previously reported to impact the *in vivo* migration of B cells in secondary lymphoid tissues (142).

2.2 *In vitro* methods

Cell Culture

293T and GP-293 cells were grown in DMEM with 4mM L-glutamine, 25mM glucose, 1mM sodium pyruvate (Life Technologies) and added 1%Penicillin-Streptomycin, 1% HEPES and 10% FBS. Cultures were split at 85-95% confluence, typically every 2-3d.

Cells were maintained in a sterile, humidified environment of 5% carbon dioxide at 37^{o}C. Culture flasks and plastics were obtained from Sarsedt Ltd.

Influenza X31 HA production

cDNA encoding the entire HA protein from influenza X31 was generated by high-fidelity RT-PCR of lysed virions. After sequencing (GATC Biotech), the HA-coding region - with some modifications - was inserted into a construct (Geneart) . The construct was inserted into the pQCXIX vector (Clontech, 631515) containing an IRES-eGFP cassette. Amplification was carried out in competent DH5α cells (Invitrogen). Retroviral particles containing HA-pQCXIX were packaged according to Clontech guidelines in GP-293 cells by co-transfection with the pVSVg vector (Clontech; PT3343-5), and 293T cells were then transduced using lipofectamine 2000 (Invitrogen). GFP^{+} cells were then sorted by FACS to establish a stably-expressing cell line, 293-HA.

Protein purification and biotinylation

Briefly, supernatant from 293-HA cultures was diluted 1:1 in binding buffer (PBS, 0.05% sodium azide, pH8), incubated with Ni-NTA agarose beads (Qiagen) overnight and applied to an equilibrated centrifuge column (Pierce). After the application of wash buffers containing increasing concentrations of imidazole(10mM, 20mM in PBS pH8), elution buffer (250mM imidazole, PBS) was added and eluant were collected in 0.5ml fractions. After western blot analysis, fractions were pooled and dialysed for 3d in PBS using a 10kDa dialysis cassette (Bio-Rad). HA was biotinylated at a 1:4.5 molar ratio of HA:Biotin with 0.5M EDTA and 0.1M sodium bicarbonate. Biotinylation reaction was carried out for 2h and excess biotin was removed by dialysis. For labelling of

influenza-specific Bmem, staining concentrations were optimised for each preparation of rHA, by assessing PR8/X31-infected animals lung-draining LN. Optimal labelling being within the range of 30-50ng rHA per 10^6 lymphocytes.

Western blot

293-HA culture supernatant was added to denaturing/loading buffer (250mM TrisHCL, 10% SDS, 30% glycerol, 5% β-ME, 0.02% bromophenol blue, pH=6.8) at 100°C for 5min, then loaded onto a SDS-PAGE gel (Bio-Rad) and subjected to electrophoresis before being transferred onto nitrocellulose membrane. Membrane was blocked using 5% milk in Tris-buffered saline and tween-20 (TBST; TBS, 0.01% Tween-20), washed in TBST and stained overnight at 4°C with primary rabbit anti-His antibody in TBST 5% BSA. Secondary staining with labelled anti-rabbit antibody was used to determine the presence of His-tagged protein. Images were acquired on the Odyssey CLx Imaging System (Li-Cor) and analysed using ImageStudioLite software.

Generation of CFP-S-Flu

Single-cycle fluorescent reporter strain of influenza A virus was prepared as previously published (143, 144). Briefly, plasmids encoding or eCFP with SapI restriction sites were synthesised by GeneArt and cloned into the pPoll vector. 293T cells were transfected with Lipofectamine 2000 (Invitrogen), in the presence of expression plasmid pCDNA3.1, which contained expression of full-length HA. This permits viral coating of HA and secretion from the 293T. The resulting viral particles were used as seed to infect a stable H3-expressing MDCK-SIAT1 cell line, thus generating viral particles which carry the genes for all IAV proteins except HA, and in its place eCFP, but that are coated with H3 HA to allow sialic acid-binding and

single cycle infection. Stocks of this CFP-S-Flu were produced by infecting HA-expressing SIAT1 cells in DMEM(0.1%BSA, 1%P/S) and 2h later adding 1µg/ml TPCK-treated trypsin (Sigma T-1426). The virus supernatant was collected after 48h of incubation at 37°C. The production of CFP-S-flu was performed with guidance from A. Townsend.

Production and RNAse treatment of VLPs

Qβ-VLPs were produced in *E. coli* and purified by chromatography by A. Cruz-Gomes from the Bachmann lab as previously described (145-147). Briefly, the bacteriophage Qβ coat protein pQβ10 was expressed in *E.coli* JM109 cells (Sigma-Aldritch) with the pGEM expression vector. After incubation, cells were harvested and lysed in 20 mM Tris pH 8.0, 0.1% (v/v) Triton X-100 buffer with Lysonase™ (Merck) at 20 µL/g pellet weight, and incubated for 1h at room temperature, followed by sonication on ice, (3 cycles; 30s on, 30s off), at 40% power amplitude. Lysates were clarified by centrifugation at 15,000 x g for 30 min at 4°C, and the soluble fraction diluted and concentrated by tangential flow filtration using a 750kDa cut-off hollow-fibre ultrafiltration unit. Subsequent selective purification by ion exchange chromatography separated charged VLPs from the majority of host cell proteins (~90% purity) followed by size exclusion chromatography using Sephacryl S500HR, yielding purified homogenous particles. For RNA removal, Qβ-VLPs were buffer-exchanged by diafiltration to 20mM HEPES, pH7. VLPs were concentrated to 2mg/ml and incubated with 1mg/ml RNAse A at 37°C for 3h. After diafiltration, RNA removal was confirmed by running a native 0.8% agarose gel with nucleic acid stain, followed by coomassie stain to confirm RNA degradation. Degraded RNA and RNase was removed by diafiltration against 20mM HEPES followed by PBS.

RNA sequencing analysis

After sorting ~100 cells directly into lysis buffer, libraries were prepared using a Smart-Seq2 protocol with a few modifications (148, 149). 19 cycles of preamplification were used for Bmem populations. Subsequent cDNA library preparation was performed by N. Ashley at the Weatherall Institute for Molecular Medicine Single Cell Genomics Facility. Ampure XP beads (Beckman Coulter) were used for cDNA purification. Libraries were analysed with a High Sensitivity Analyser (Agilent) and cDNA tagmentation was performed with the Nextera XT DNA Sample Preparation kit (Illumina).

Sequencing was performed using an Illumina NextSeq 500 System. Analysis of the RNAseq dataset was performed by E. Repapi and N. Gray at the Weatherall Institute for Molecular Medicine Computational Biology Research Group.

Quantitative PCR (qPCR)

For qPCR analysis of sorted Bmem (~200 cells/sample), an adapted protocol for single-cell qPCR was used. Cells were collected by direct sorting into lysis buffer (0.1% Triton X, 4U RNAse Inhibitor, 25µM OligoDT and 2.5µM dNTP), snap-frozen on dry ice and stored at -80°C until RT. Reverse transcription was performed using the Superscript III polymerase, after which 13x cycles of preamplification were performed using TATAA Preamplification kit (TATAA Biocenter). qPCR was performed using PrecisionFAST qPCR master mix+SYBR-green (Primerdesign). Data acquisition was performed on an ABI Viia7 system in 384-well format. Arbitrary units are displayed, corresponding to GAPDH-normalised CT values.

Statistical tests and analyses

Monte Carlo simulation tests for Ripley's K. 1000 simulations of random distribution were performed, and the range of these simulations was taken to generate confidence envelopes (plotted in gray in clustering plots). Experimental data lying outside and above of this envelope are significantly clustered, and data below the envelope are dispersed. For analysis of Bmem and plasma cell positioning, infected and uninfected areas in each mouse were used, and as such Paired t tests were utilised. GraphPad Prism 7.0b (GraphPad software, Inc.) was used to perform statistical analysis.

2.3 List of reagents

Collagenase D (Roche, 11088858001)

DNase I (Sigma, DN25)

RNase A (Sigma, R4875)

Biotin-X-NHS (Merck Millipore, 203188)

Fixable viability dye eFluor® 780 (Life Technologies, 65-0865-14)

Click-IT plus EdU A647 labelling kit (Life Technologies, C10640)

Pertussis toxin, salt-free (PtX; Quadratech Diagnostics Ltd., #181)

TPCK-treated Trypsin (Sigma, T1426)

Clodronated liposomes (CLL; Encapsula NanoSciences LLC)

MagniSort Mouse B Cell Enrichment Kit (Affymetrix eBioscience, 8804-6827-74)

QIAPrep Spin Miniprep Kit, HiSpeed Plasmid Midi Kit ,QIAquick Gel Extraction kit, MinElute PCR Purification Kit (All obtained from Qiagen)

PrecisionFAST qPCR master mix with SYBR Green (Primerdesign, PFASTBLUE-LR-SY-10ml)

TATAA Preamplification kit (TATAA Biocenter, TA05-100)

FTY720 (Fingolimod; Stratech, S5002)

Antibodies:

CD69 (H1.2F3), B220 (RA3-6B2), CD45 (104), GL7 (GL7), IgD (11-26c.2a), CD11b (M1/70) , F4/80 (BM8),CD11c (N418), all obtained from Biolegend and CD95 (Fas; Jo2, BD Pharmingen).

Blocking anti-CD40L (MR1; BioXcell)

Chapter 3

3. Validation of a mouse model to track memory B cells and long-lived plasma cells in the lungs of influenza-infected animals

Chapter 3: Background

Memory B cells exhibit unique properties including expression of unique immunoglobulin heavy chains and extended longevity, as well as the capability to very rapidly develop into germinal centre B cells and plasma cells following restimulation (31). These observations have led to investigation into transcriptional adaptations of B_{mem} that may facilitate such enhanced effector functions.

In contrast, no information is yet known about the expression profiles of tissue-resident memory B cells. Some phenotypic markers have recently been confirmed to faithfully report lung-resident Bmem. These include expression of CD69, CXCR3 and downregulation of CD62L (128). Long-term localisation within the lung is perhaps the most striking feature of this population, which may be enhanced by this altered phenotype, marked by the loss of molecules associated with recirculation (CD62L) and upregulation of CD69 – a molecule associated with tissue residence.

One of the defining features of canonical Bmem is their longevity. Splenic memory cells have been proposed to be induced early in immune responses (35), and studies in mice tracking the survival of Bmem suggest maintenance of this population for >120d after initial challenge, and in some cases up to 400d (55, 58). Indeed, influenza-reactive circulating memory B cells have been isolated from peripheral blood

of human survivors of the 1918 influenza pandemic over 90 years later (57). However, the longevity of lung-resident Bmem has not yet been fully resolved. To begin to address these gaps in understanding, a robust system of tracking memory B cells is required.

Defining memory B cells is technically difficult primarily due to the low number of these cells after the resolution of inflammation and because, post-activation, memory B cells in mice assume a phenotype similar to naïve B cells and lack specific molecular markers. Recently, genetic animal models have allowed more selective labelling of post-activation B cells by using fate-mapping to label all post-activation B cell subsets (54). This system has been shown to selectively identify memory B cells in the spleen and has provided insight into the sites of Bmem retention in SLO.

Recombinant antigens have been also used to label antigen-specific B cells by binding cell-surface BCR to track memory B cells (123, 127). Influenza HA represents the immunodominant antigen in natural infection, and as such allows tracking of a fraction of influenza-induced Bmem (129). The majority of memory B cells are class-switched and/or affinity-matured cells which arise from the germinal centre. Both of these processes are dependent upon the enzymatic activity of activation-induced deaminase (AID)(150). Fate-mapping B cells after expression of AID will highlight all B cells after early activation stages in the primary response, which can occur prior to entry into the GC (151). This AID-based monitoring will efficiently label historically activated B cell subsets but not specifically Bmem, as this population will include both Bmem and plasma cells, as well as GC B cells during the acute response. We therefore utilised a mouse strain that combines fate mapping of AID-expressing B cells with the ability to track plasma cells via the inducible expression of a yellow fluorescent protein under control of the BLIMP1 promoter. We hypothesised that the combination of this

reporter system with recombinant antigen staining would allow the tracking of influenza-reactive Bmem and plasma cells in infected animals over time.

Aims:

1. Establish a system to track robustly defined influenza-specific memory B cell populations
2. Use this system to describe the kinetics of humoral immunity in the lung following influenza infection
3. Define a transcriptional profile of lung-resident memory B cells in comparison to Bmem in the spleen

3.1 Tracking influenza-specific memory B cells with recombinant viral antigens

Protective antibody responses to influenza are thought to be predominantly targeted towards influenza haemagglutinin (HA)(129). Identification of antigen-specific B cells forms the basis of memory lymphocyte tracking, and one effective way to do this is to synthesise labelled recombinant antigens that highlight antigen-reactive B cells after BCR-binding (152, 153). To label influenza-specific Bmem we produced recombinant HA (rHA) derived from X31 influenza (H3N2) with an introduced Y114F mutation known to reduce the sialic acid-binding property of HA, thereby reducing signal noise when staining primary cells (152-154) (Fig 3.1A). Addition of a 6xHis tag allowed purification of the HA, and a T4 fibritin foldon domain permitted HA trimerization. Bir A biotinylation and TCS thrombin cleavage sites were also included (Fig.3.1A). The vector used contained an IRES-GFP cassette, which allowed FACS-based detection and purification of successfully transduced 293T cells. Recombinant HA was collected from cell supernatants and purified over an Ni-NTA column before

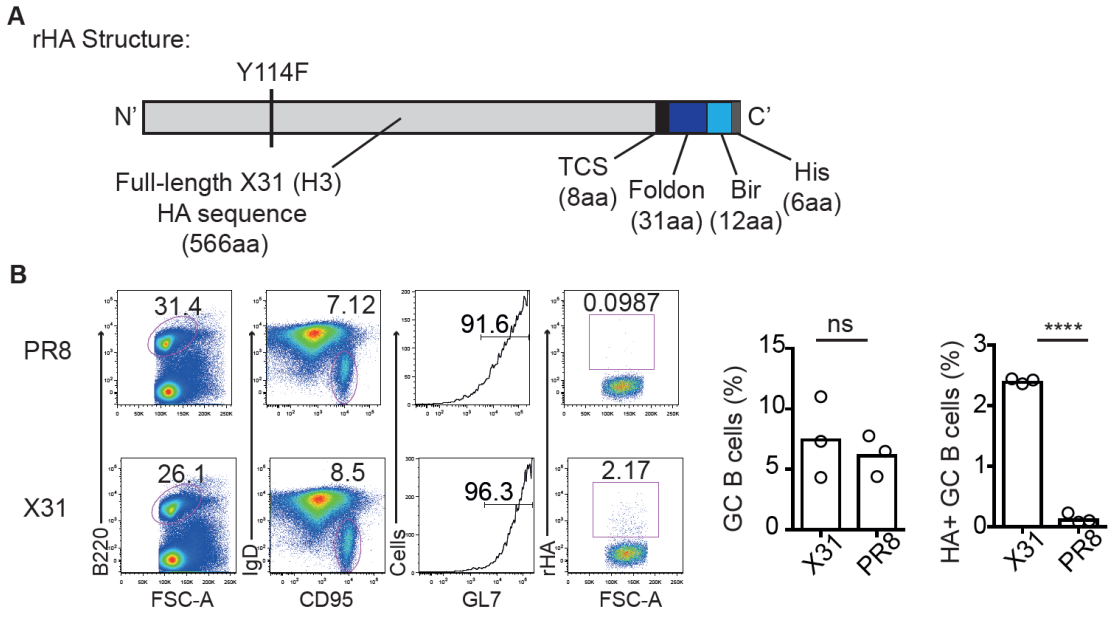


Figure 3. 1. Optimisation of antigen-specific B cell labelling with recombinant X31 haemagglutinin. A. Schematic structure of rHA. B. Mice were infected with X31 (H3N2) or PR8 (H1N1) influenza virus, and at d8 postinfection mediastinal LN GC were assessed for rHA-binding potential. Middle, total GC frequencies (of $B220^+$) in lung-draining LN. Right, HA^+ GC B cell frequencies of total GC B cells. (ns, not significant; ****, $p<0.0001$, Student's unpaired t test). Data are representative of 2 independent experiments, n=3, and was repeated for different preparations of rHA.

biotinylation. Specific labelling of X31-induced GC B cells ($B220^{+}$ IgD^{lo} $CD95(Fas)^{+}$ $GL7^{+}$) in lung-draining lymph nodes was confirmed by FACS analysis, a proportion of which bear a H3-reactive BCR (Fig.3.1B). In contrast, PR8(H1N1)-induced GC B cells failed to bind rH3. This assay confirmed the specificity of labelling influenza-specific B cells with rHA.

3.2 Kinetics of humoral immune responses in the lung and secondary lymphoid organs

To selectively label memory B cells in peripheral tissues, we utilised an activation-induced fate-mapping approach. AID-Cre Rosa26-stop-tdTomato mice were crossed to mice expressing the fluorescent protein Venus under the Prdm1 (BLIMP1) promoter. In these mice, the majority of post-activation B cells are permanently labelled with tdTomato, and all mature plasma cells are labelled with Venus (Fig.3.2.1).

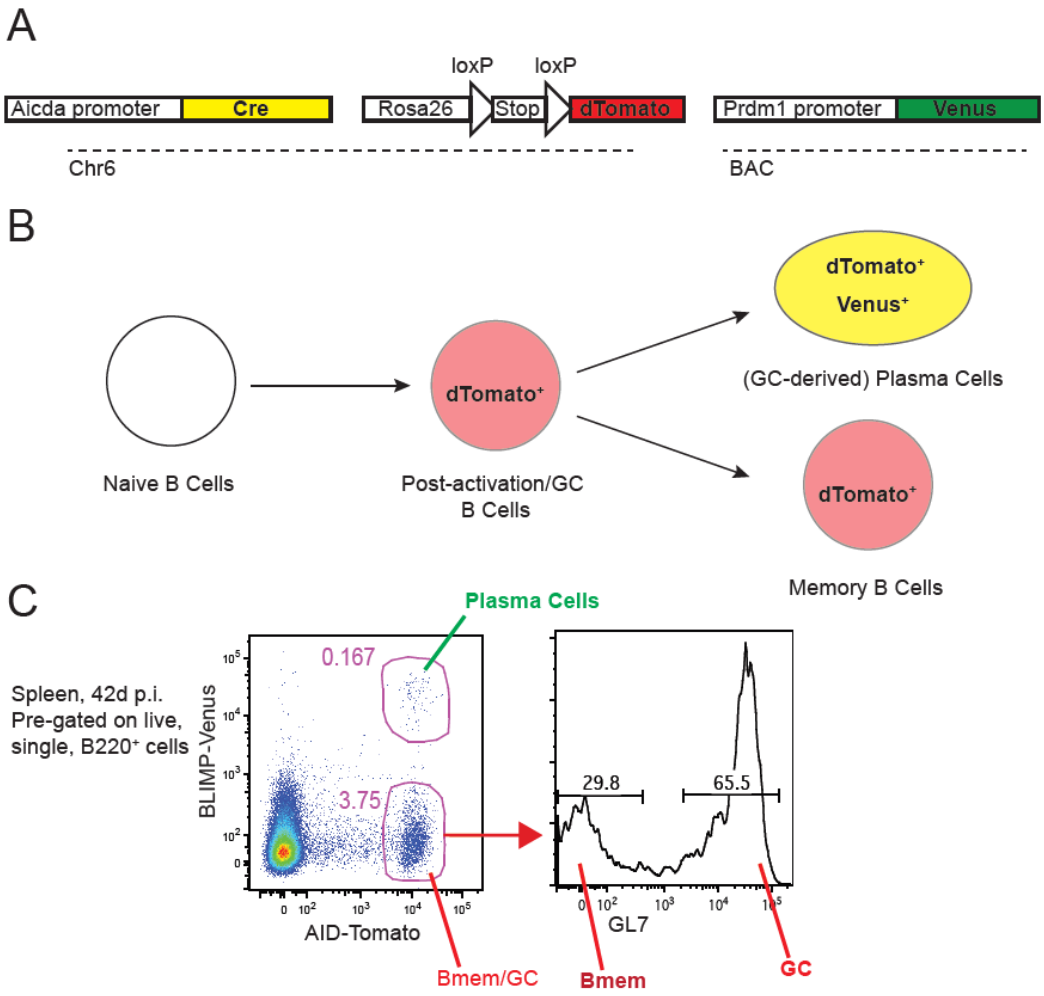


Figure 3. 2. 1. Utilisation of a fate-mapping reporter mouse to track humoral memory populations. A. Schematic layout of the genetic approach used to distinguish memory B cell populations. B. After activation, AID upregulation results in Cre-mediated elimination of the stop codon. This induces permanent expression of dTomato under the promoter of the ubiquitously expressed Rosa26 locus. Independently, upon induction of Prdm1 expression, the fluorescent protein Venus is induced, highlighting (within the humoral immune system) plasma cells. C. Representative flow cytometry plots displaying how this system can be used to distinguish PC, Bmem and persistent GC B cells in the spleens of mice 6w postinfection with influenza virus.

It has been shown that the lung harbours a substantial fraction of vascular lymphocytes, and that these circulating cells are not completely removed from the tissue even by perfusion (155). To remove potential contamination from the blood pool *in vivo* labelling was performed. This technique has been shown to selectively highlight blood-exposed lymphocytes in the bone marrow (156), lung (123, 157, 158), spleen (159), lymph nodes, small intestine and liver (155).

Given the potential sources of lymphocyte contamination, we stringently defined memory B cells as cells with historic activation and expression of AID (dTomato^{+}), found in the lung >35d postinfection that failed to be stained by *in vivo* labelling, were GL7^{-} non-GC B cells and bound X31 rHA on their surface. CD69 was additionally used as a phenotypic identifier of tissue-resident Bmem. In a similar manner (whilst PC bear no surface BCR and do not bind rHA) plasma cells were

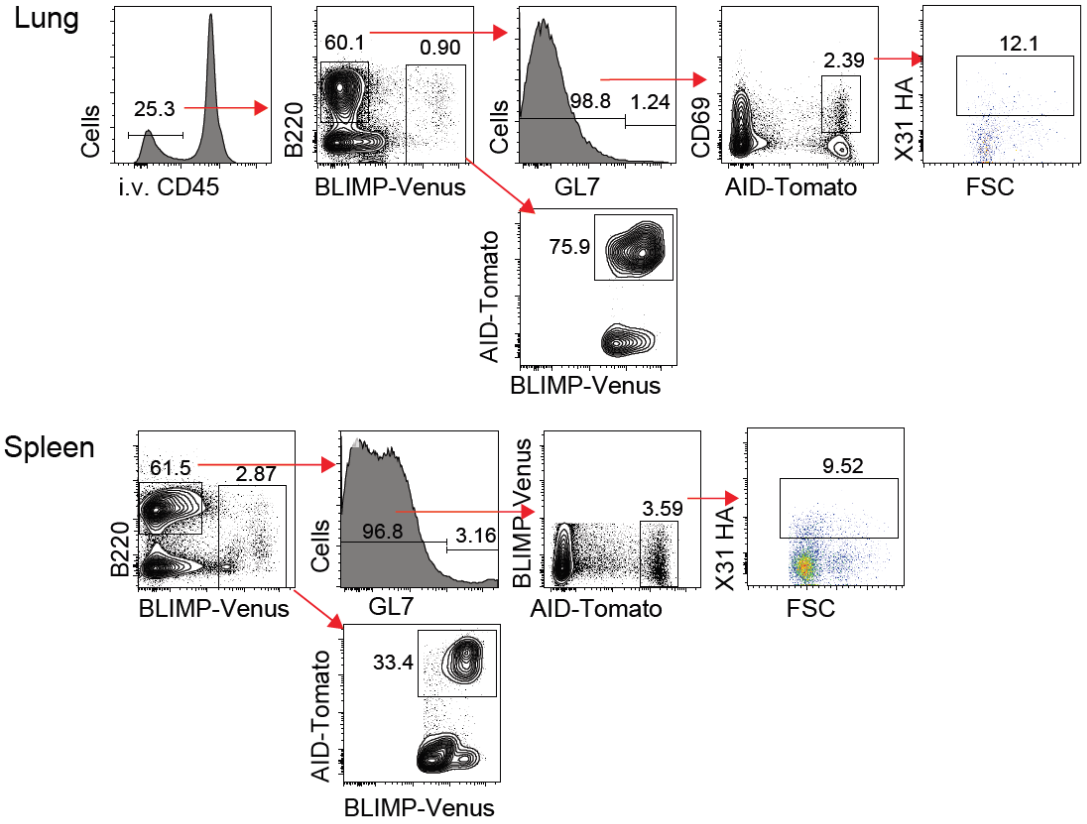


Figure 3. 2. 2. Gating strategy to define lung-resident and SLO Bmem following infection with X31 influenza. Representative plots from lung (top) and spleen (bottom) depicting Bmem and LLPC populations. Data shown are from one mouse 80d postinfection. Data are representative of two experiments performed at day 80 post-infection, each with n=4-6.

defined as large, live IV label^{-} B220$^{int/low}$ BLIMP-Venus^{+} Tomato^{+} cells (Fig.3.2.2). In the spleen and mLN, Bmem were defined without CD69 or in vivo labelling (B220^{+} BLIMP-Venus^{-} GL7^{-} AID-dTomato^{+} HA^{+}) (Fig.3.2.2, lower panel).

Tracking these influenza-specific memory B cells in the lung and secondary lymphoid organs after influenza virus infection revealed that both of these populations were fairly long lived, although we did notice a gradual decline of Bmem over time (~150-200d, Fig3.2.3). This decline was found to continue, and no Bmem were identified in any tissue in a small number of experiments analysing mice >320d p.i. (data not shown). Plasma cells numbers peaked slightly later than Bmem, as has been previously described (160), remaining relatively stable in both SLO and lung tissues over time.

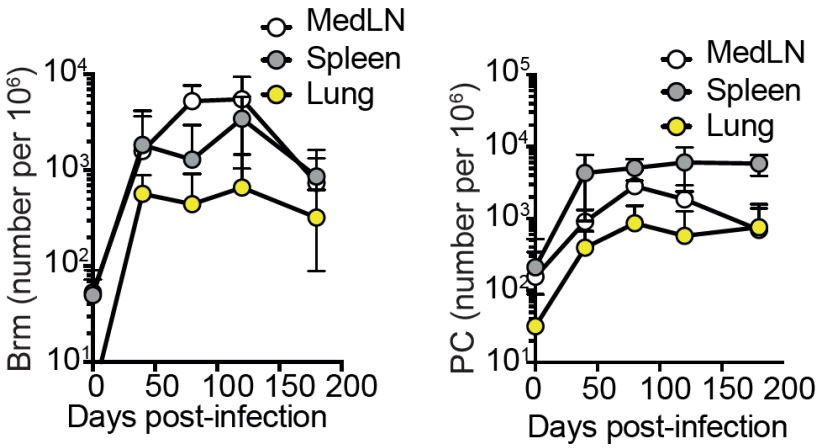


Figure 3. 2. 3. Quantitation of humoral memory populations post-infection. Memory B cell (left) and plasma cell (right) frequencies within lung-draining LN, spleen and lung parenchyma using gating strategies outlined in Fig.3.2.2. are shown. Data is displayed as mean±standard deviation. Data are pooled from 6 independent experiments with 4-6 mice per group.

3.3 Transcriptional characterisation of lung-resident memory B cells

After optimising a means to selectively and stringently track memory B cells in lymphoid organs and lung, this analysis strategy was used to isolate these cells by FACS, and small-bulk populations (~100 cells) were subsequently subjected to RNA sequencing.

Analysis of the resulting expression profiles showed that lung-resident memory B cells represent a distinct population from both splenic naïve B cells, and splenic memory B cells (Fig.3.3A,B). Lung Bmem signatures displayed significant upregulation of molecules known to be expressed by tissue-resident memory T cells

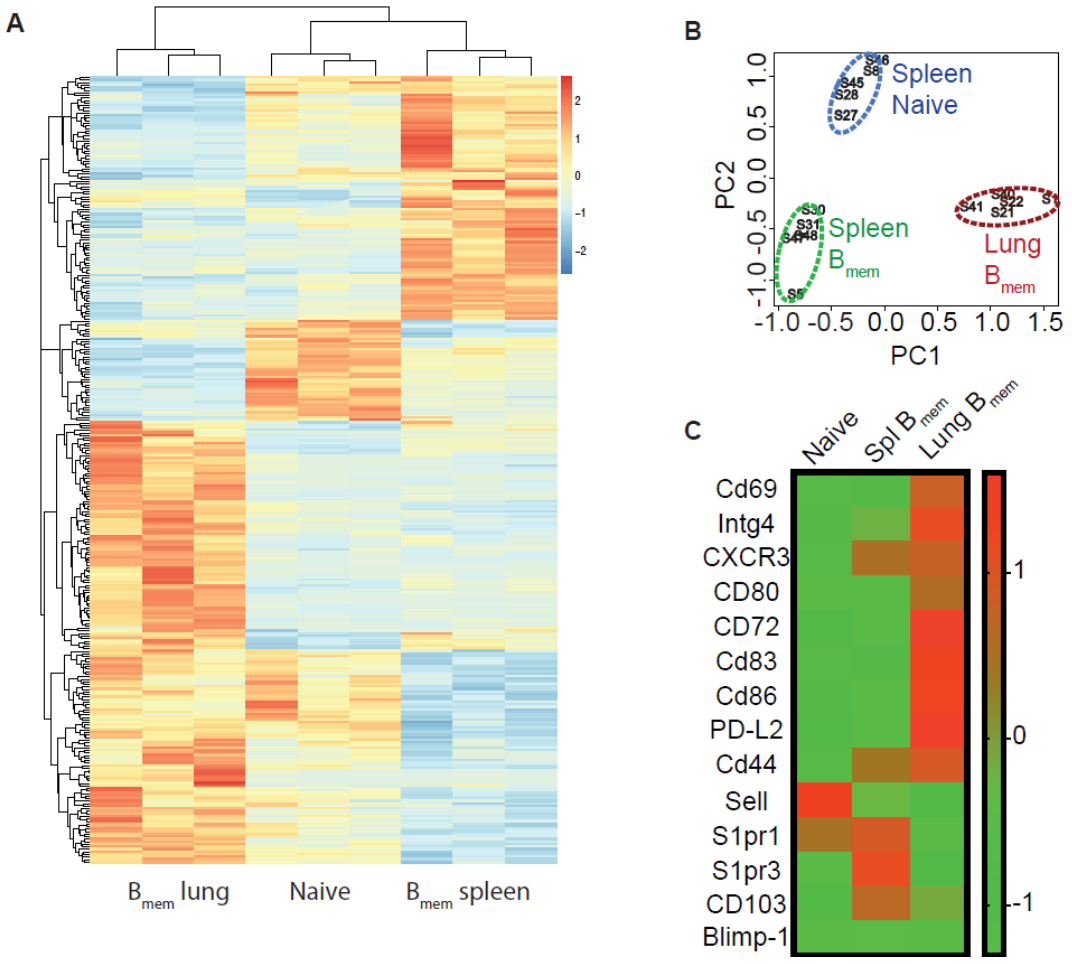


Figure 3. 3 RNA sequencing analysis of lung-resident memory, splenic circulatory memory and splenic naïve B cells. Naïve and memory B cell populations were isolated from lungs and spleens of mice 42-45d postinfection and subjected to bulk RNAseq analysis A. Heatmap displaying gene expression profile of lung Bmem, splenic Bmem and splenic naïve B cell populations. B. Principal component analysis plot of the three populations. C. Heatmap highlighting relative expression levels of selected genes of interest. All data are from 3 independent sorts, sequenced and analysed in parallel.

such as *Cd69*, *Cd44*, although, unlike some resident memory T cells, no enrichment of *Cd103* expression was identified. Likewise, we found molecules involved in the lymphocyte recirculation process such as *Sell* (CD62L) and *S1pr1* to be downregulated, a finding consistent with this population remaining resident within the lung tissue. The costimulatory molecules CD80 and CD86 are known to be constitutively expressed by a proportion of memory lymphocytes (68) and were also found to be highly expressed by lung Bmem, along with CD83. Interestingly, we found CD86 and PD-L2 to be highly expressed, as well as CXCR3 (Fig.3.3C). Deeper analysis of this transcriptional profile is in progress.

3.4 Chapter 3: Summary and discussion

Here, I have described the initial assessment of lung-resident memory B cells performed in this project. These initial stages included optimisation of methods to isolate and analyse humoral populations in the lungs of infected animals, determination of humoral response kinetics in the lung after influenza infection and transcriptional profiling of humoral memory populations in the lung and spleen.

By using recombinant antigen labelling, it was observed that 5-15% of lung Bmem bound recombinant HA at detectable levels. These findings are in agreement with previous publications showing a similar frequency of antigen-specific Bmem induced by experimental X31 infection (127). Whilst this may initially seem a low frequency of memory cells, it is important to note that soluble trimerized HA is likely to only bind surface BCRs of high-affinity Bmem. It may be of interest to test whether attaching variable densities of rHA molecules to a substrate (eg/ virus-like particles (VLP) or microbead) may reveal a population of lower affinity Bmem. Another factor that may cause variable levels of HA-binding is variation in surface BCR expression

levels, which are known to vary with B cell activation state (161). Furthermore, the influenza virus particle itself has many more antigens than HA alone. Although typically less dominant and protective than anti-HA, plasmablasts and persistent antibodies reactive to NA have been described in both animal models and human infection, and may contribute to protection (162, 163). Antibodies to NP, M1 and M2 have also been described, but little is known about the protective mechanisms of these antibodies, although there are reports indicating innate populations such as NK cells may be involved (129, 164). Bmem responsive to these alternative antigens may represent a large fraction of the non-HA-binding fraction. Lastly, there may be a population of 'natural' Bmem induced in response to the respiratory microbiota (165-167), inhaled aeroallergens or food antigens encountered in the laboratory mouse environment contributing to the HA^- lung Bmem pool.

In performing this FACS analysis, we noted that whilst ~35% of the lung AID-Tomato$^+$ GL7$^-$ B cells express CD69, there is a distinct population which remains CD69$^-$. This is consistent with the initial phenotypic definition of lung Bmem (127). Ongoing work is investigating mRNA expression and positioning of these two populations by qPCR and confocal microscopy. Potential differences in microanatomical positioning or phenotype could provide insight into the mechanism by which CD69 is regulated in peripheral tissues, and may allude to distinct functional capacities of these Bmem subsets. It is known that, whilst CD69 is a molecule associated with tissue residence, not all resident memory lymphocytes are CD69$^+$ (168). Also, CD69 is regulated by antigen stimulation in mature B and T lymphocytes (169, 170) and, in this instance, its expression may be downstream of stimulation by low levels of viral antigens found in the lung – perhaps retained by FDC or FDC-like cells. Of note, transcriptional analysis revealed no differential expression levels of *Prdm1*,

Bcl6, *S1pr2* or *Aicda* in either lung or SLO Bmem populations in comparison to naïve B cells, indicating negligible contamination from PC, GC or memory precursor populations (171).

We observed that whilst resident Bmem in the lung are long-lived, they do decline in numbers over time. Interestingly, a similar pattern of prolonged decline over ~200d has been described for influenza-induced lung Trm, perhaps indicating that the physiological functions of the lung take precedence over the retention of lymphocytes within the airways or lung interstitium (172). Even circulatory Bmem induced by systemically administered antigens peak in numbers by d30 and undergo a gradual decline to very low numbers by d300 (55). Perhaps, due to memory lymphocytes bearing more active, effector-like transcriptional profiles, these cells become somewhat dependent upon inflammatory cues for survival. Indeed, inducible deletion of PLC-γ2 caused depletion of memory B cells, suggesting that at least tonic BCR signalling events are required for Bmem survival (61). However, to date the signalling thresholds for survival of Bmem in comparison to naïve B cells remain unknown.

Interestingly, many signalling pathways downstream of the BCR, including Nr4a1(Nur77), NF-kB (Rel), MAPK, Jun and Fos kinase pathways, were enriched in resident memory B cells. Whilst circulating Bmem are maintained independently of persisting antigen (60), this data may indicate a role for greater levels of 'tonic' signalling in resident Bmem. Indeed, whilst we did not identify any live virus past day 30, there are reports of influenza virus antigens persisting for up to 2 months postinfecton (173, 174). Alternatively, the enhanced expression of these signalling pathways may represent one means by which local memory cells are primed for responsiveness. Indeed, elegant nuclear transfer experiments have shown that Bmem have BCR-independent adaptations that enhance secondary responsiveness and PC

formation (76). Relatively greater sensitivity of resident Bmem to antigen stimulation may allow these cells to respond particularly rapidly, or may skew subsequent fate decisions such as the poorly understood developmental bifurcation point directing GC B cell versus plasma cell differentiation.

Analysis of transcriptional profiles of lung Bmem revealed a signature highly consistent with previous reports of resident memory lymphocytes such as; downregulation of recirculation-associated molecules, upregulation of retention molecules and inflammatory chemokine receptors. In contrast, we show that splenic Bmem retain expression of S1PR1, and CD62L (albeit at levels lower than naïve B cells, as previously observed (68, 77)). Further investigation of this dataset is underway in the lab, with a focus on transcription factors of interest.

We also identified costimulatory molecules CD80, CD83 and CD86 to be significantly upregulated on lung Bmem. CD80 has been proposed to highlight Bmem with a greater mutation load, and fewer germline sequences in the BCR V regions (67). Indeed, lung Bmem have been directly compared to splenic Bmem and have been shown to display enhanced mutation load (123), suggesting that these populations may have been generated at distinct sites, perhaps splenic GC vs iBALT, or that these populations may have been generated at different timepoints in the anti-influenza response.

These initial observations gave a firm basis upon which to further explore the potentially unique biology of humoral immunity in peripheral sites. Analysis of this data as well as the growing literature began to indicate an underappreciated aspect of these cells; their microanatomical localisation.

Chapter 4

4. Microanatomical positioning and migratory behaviour of humoral memory populations in the lung in steady state and after rechallenge

Chapter 4: Background

Humoral immune activation is exquisitely dependent upon crucially-timed molecular and cellular interactions that occur in highly organised microanatomical niches. Despite significant insights into naive B cell activation, the spatiotemporal regulation of memory B cell responses represents a very poorly understood area of research. Even the site of memory B cell maintenance in SLO is not firmly known, with sites such as waning germinal centers, the marginal zone and the outer B cell follicle being proposed (67, 70, 71). One insight into the molecular regulation of memory B cell positioning is the proposal that CCR6 appears to be required for secondary PC formation and antibody secretion, in a manner associated with the positioning of Bmem in the spleen (70). Recently, dedicated intravital imaging studies have been performed that reveal how memory B cells become reactivated in the tissue-draining lymph nodes following rechallenge (82). This study revealed that Bmem reactivation occurs in a unique area within the draining LN, the subcapsular sinus, showing that Bmem encounter with antigen can occur in unique locations.

The observation that we can isolate *bona fide* memory B cells from the peripheral tissue – a potential site of infection – brings a number of immediate points worth investigation. Firstly, to date no information is known about the site of

maintenance of lung Bmem. This gap in understanding is striking, given that naïve B cells are known to receive survival signals from mediators such as CXCL13 and BAFF in organised lymph node follicles and that the structural orchestration in these sites is crucial for B cell survival (175, 176). Secondly, the effector responses of lung Bmem may provide an area of research with novel cellular behaviours. Uniquely, mucosal Bmem will be in direct contact with antigens in their native conformation, a crucial factor for BCR-mediated antigen recognition. Thus, for these resident Bmem, the primary site of BCR-antigen interaction is likely to be a peripheral tissue, an organ which lacks the organised lymphoid structures that support B cell activation. How these resident memory cells persist in the lung and become activated locally is likely to be fundamentally linked to how they respond to pathogens and provide functional, protective immunity.

Analysis of dynamic cellular responses by live two-photon microscopy has provided insight into the fundamental behaviour and function of the primary humoral immune response. We opted to use live imaging in a lung explant setup to visualise local Bmem responses (177). One issue that arises when studying the lung tissue is the scattering of light as it transitions through the tissue-air interface, reducing image quality and maximum imaging depths. To overcome light diffraction, lung airways were inflated with warmed agarose. This maintains airway structure and allows imaging depths of up to ~150μm on lung tissue. Another issue that arises is that immunologically relevant landmark sites in the lung, such as airway branch points, are not accessible for imaging from the outer aspect of the lung. To combat this, lung tissue is vibratome-sectioned to allow access to these deeper tissue areas. This explant imaging technique has been shown to accurately convey information about lymphocyte migration and positioning, in close agreement with other methods of intravital imaging (178). Thus,

this system represents an effective method to assess the dynamic behaviours of memory lymphocytes in the lung.

Aims:

1. Describe the microanatomical distribution and dynamic behaviour of lung Bmem and PC in the steady state
2. Assess any modifications to this behaviour that happen during recall responses

4.1 Microanatomical localisation of humoral memory populations in the lung

To provide insight to the distribution of humoral immune populations in the lung, we utilised the capabilities of two-photon laser-scanning microscopy (TPLSM) to be able to collect large 3D imaging volumes and assess cellular positioning at a microanatomical level. This approach was combined with the AID-dTomato BLIMP1-Venus reporter system introduced in Chapter 1 to visualise the microanatomical localisation of humoral memory populations in the lung.

TPLSM of lung sections revealed anatomical segregation of humoral memory components within the immune lung. dTomato$^+$ Venus$^-$ cells were identified to be distributed throughout the lung parenchyma, potentially in or around alveoli (Fig.4.1A). In contrast, dTomato$^+$ Venus$^+$ plasma cells were found in dense clusters, predominantly associated with airway branch points and bronchovascular bundles. Occasionally when imaging these sections, structures resembling classical inducible-bronchiolar lymphoid tissue (iBALT) were observed. These structures are known to form in high-level or chronic inflammatory conditions, and are thought to provide a microenvironment bearing some similarities to SLO. Variable levels of organisation and presence of antigen-presenting FDC are thought to provide a site to launch local adaptive immune responses (118, 179). As has been described, confocal analysis revealed that B cells within these iBALT stained positively for GL7 (Fig.4.1B), indicating B cells with GC phenotype reside within these areas of the lung, and that the dTomato$^+$ Venus$^-$ cells dispersed through the alveoli are likely memory B cells (121). Live imaging of AID-tomato-labelled B cells contained within iBALT structures revealed a rapid, highly-confined migratory phenotype, as expected from GC B cells (data not shown). Unfortunately, due to the high density of labelled cells in these areas these cells were unable to be tracked for quantification and statistical analysis.

To compare the visible population of dTomato^{+} Bmem (which contains both CD69^{+} and CD69^{-} subsets) to the transcriptional signature of influenza-specific Bmem, and test whether the signature is applicable to this broad population seen by imaging, we performed quantitative PCR analysis of the key residence factors identified in

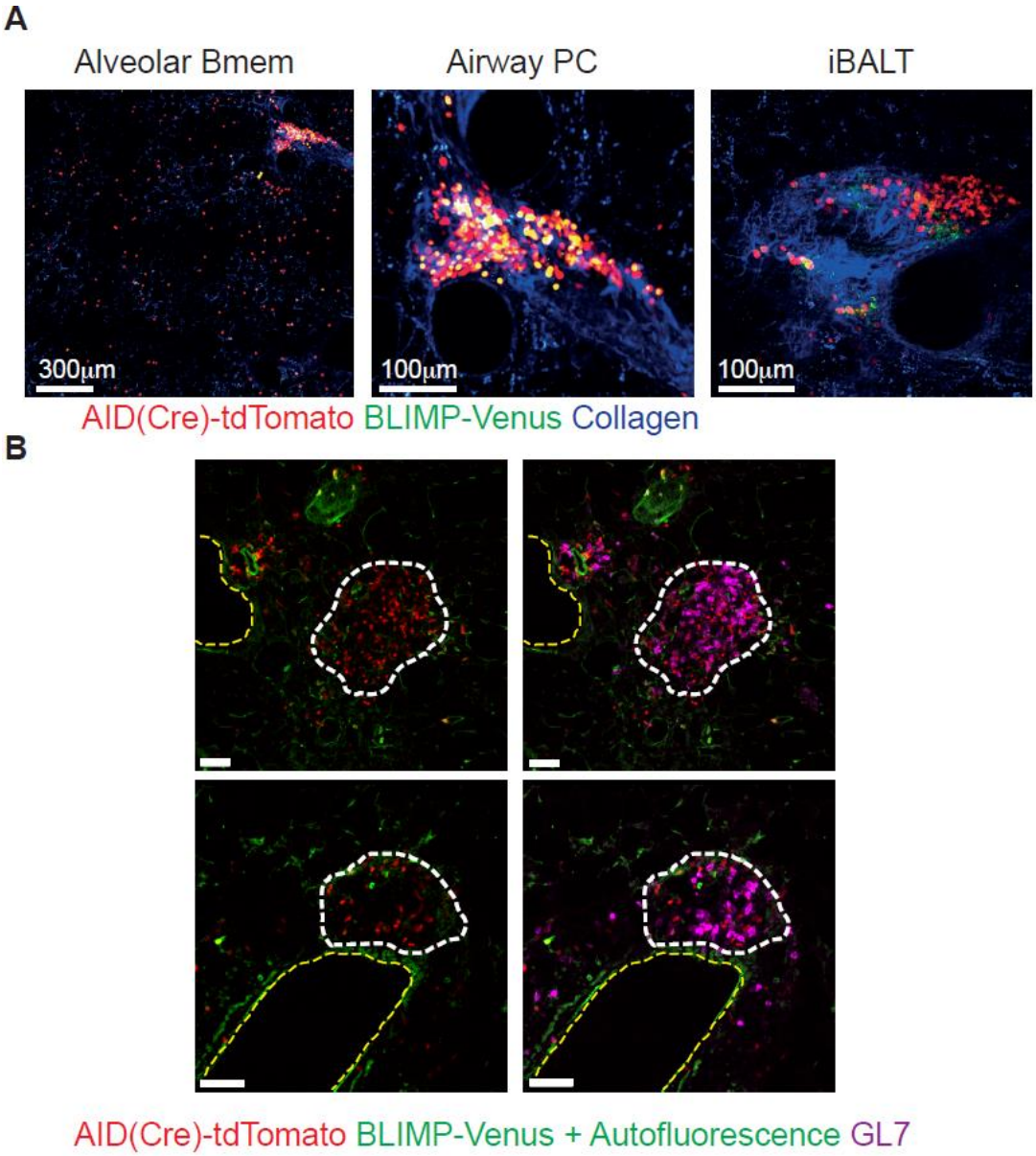


Figure 4. 1. 1 Microanatomical localisation of humoral memory populations in the lung. A. TPLSM of lung d42-64 p.i. Left, large tile of lung tissue displaying Bmem distribution throughout alveoli. Middle, zoomed region of plasma cell cluster around a collagen-rich airway branch point. Right, a representative image of an iBALT-like structure adjacent to an airway. B. Confocal microscopy of lung sections stained with GL7 antibody to highlight GC structures. Red, AID-Tomato; Green, BLIMP-Venus and autofluorescence (as collagen second harmonic signal is not captured in this image, autofluorescence (FITC channel) was used to highlight alveoli and airway structure). Dotted yellow lines indicate airways, dotted white areas indicate approximate position of iBALT borders. Scale bar represents 50µm.

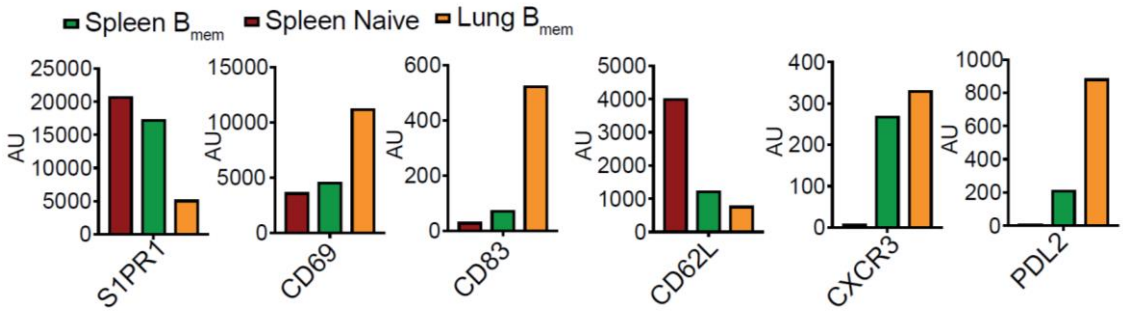


Figure 4. 1. 2 Quantitative PCR analysis of total AID-Tomato$^+$ lung Bmem. 200 naïve B cells or Bmem from lung or spleen of infected mice (d45-50) were isolated by FACS and subjected to an adapted single-cell qPCR protocol. Bmem were sorted as live i.v. label$^-$ AID-dTomato$^+$ GL7$^-$ cells, and splenic naïve B cells were isolated as B220$^+$ GL7$^-$ AID-tomato$^-$. Shown are GAPDH-normalised arbitrary units (AU) of gene expression from one experiment, representative of 3 independent experiments.

Chapter 1, using a sorting strategy that corresponded to the cells visualised. When imaging the lung, we can distinguish resident memory B cells by AID-tomato expression, and can exclude GC B cells as GL7 staining highlights a distinct anatomical compartment where GC B cells reside – iBALT (Fig.4.1.1). With this in mind, live, IV label$^-$ dTomato$^+$ GL7$^-$ cells were isolated and subjected to qPCR of key genes in the 'resident memory' signature to determine if the transcriptional profile we identified would be broadly representative of the population assessed by imaging analyses. Quantitative PCR analysis of this population showed enhanced expression levels of the central lung Bmem profile CD69, CD83, CXCR3, PD-L2 and conserved downregulation of *S1pr1* and *Sell* (Fig.4.1.2). The expression of these key genes in this broad population matched the expression profile of the influenza-specific Bmem (Fig.3.3), indicating that the population visualised by live imaging faithfully represents the core characteristics of the population of influenza-induced memory B cells.

4.2 Mobilisation of memory B cells following influenza rechallenge

To assess the steady-state migratory properties of lung-resident memory B cells we utilised TPLSM in combination with live imaging in an explant setup. Live imaging of Bmem in lungs of mice 42-64d p.i. revealed very low motility of alveolar lung Bmem (mean speed 1.99±1.68μm/min, Fig.4.2.1). Bmem were occasionally observed entering alveoli within their immediate area, potentially scanning the air-space or local cells for cognate antigen or inflammatory stimuli (Fig.4.2.1A). Consistent with their terminally-differentiated phenotype, plasma cells within the lung were immobile (mean speed 1.12±0.46μm/min) and displayed no migratory tendency (data not shown). These findings were surprising and contrasted with the highly migratory behaviour reported for resident memory T cells in mucosal sites (180), as well as follicular and GC B cell populations in secondary lymphoid organs (181-184), where extensive scanning behaviour has been described.

To assess the initial dynamic responses of lung Bmem, we performed live imaging of lungs 18-24h post-rechallenge with high dose X31 at d42-64 post-infection. Quantification of the migratory properties of these cells highlighted a significant increase in motility of a proportion of dTomato^{+} Bmem after viral reinfection. After reactivation, mean population migration velocities increased from the steady-state 1.99μm/min to 4.46±3.80μm/min (Fig.4.2.1C, Fig.4.4). Additionally, lung Bmem were observed to displace significantly greater distances through the lung parenchyma (Fig.4.2.1B; mean 30min displacement: No rechallenge, 6.2μm; X31 Day 1

Rechallenge ,13.0μm). This increase in motility was met with cells exhibiting reduced circularity and obtaining a more elongated, migratory phenotype (Fig.4.2.1D).

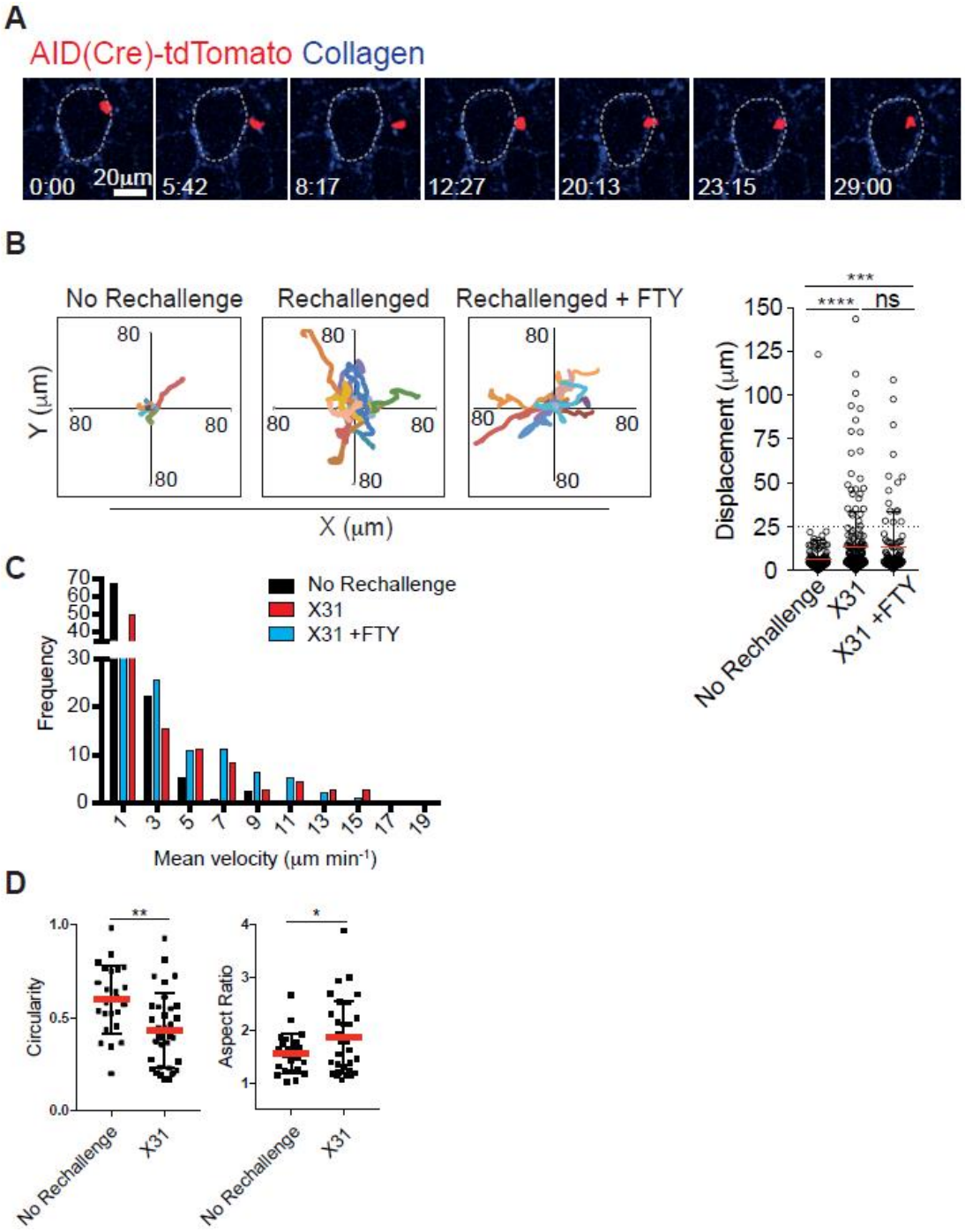


Figure 4. 2. 1 Mobilisation of memory B cells following influenza rechallenge. A. Example of alveolar probing behaviour of Bmem. Bottom left, time (min:s). B. Mice were infected with X31 influenza and on d42-70 challenged with high-dose X31, with or without FTY720-treatment 2d previously. Left, randomly selected tracks of Bmem migration in 30min have been displayed from a common point of origin to highlight displacement. Right, quantification of 30min displacement values of Bmem from the above conditions. Kruskal-Wallis test. *** p=0.0003; **** p<0.0001. Bars represent mean±SD. C. Frequency distributions of cell migration speeds from above conditions. D. Cell shape analysis. Left, circularity. Right, cell aspect ratio. Student's unpaired t test. ** p=0.002; * p=0.047. Data are pooled from 3-6 independent experiments, with 1-2 mice per experiment.

To determine whether the migratory Bmem observed were from a local source, or whether they were dependent upon rapid entry of recirculating Bmem, we asked whether circulating memory B cells can be sequestered from the blood by utilising the lymphocyte-sequestering S1P analogue FTY720. FTY720 is known to bind and internalise the receptor S1PR1, desensitizing naive T and B lymphocytes to SLO-egress signals (185-190). As circulating memory B cells express S1PR1 (Fig.3.3), we hypothesised that FTY720 will affect their ability to egress into the blood compartments similarly to naïve cells. Post-immune mice were treated with FTY720 2d prior to rechallenge, and imaged by TPLSM 24h later. FTY treatment effectively sequestered not only naïve B cells, but also Bmem from the blood. In contrast the treatment had no significant effect on lung Bmem populations, as expected from the low level of S1PR1 expression in these cells (Fig.4.2.2, Fig.3.3). We therefore used this approach to test a

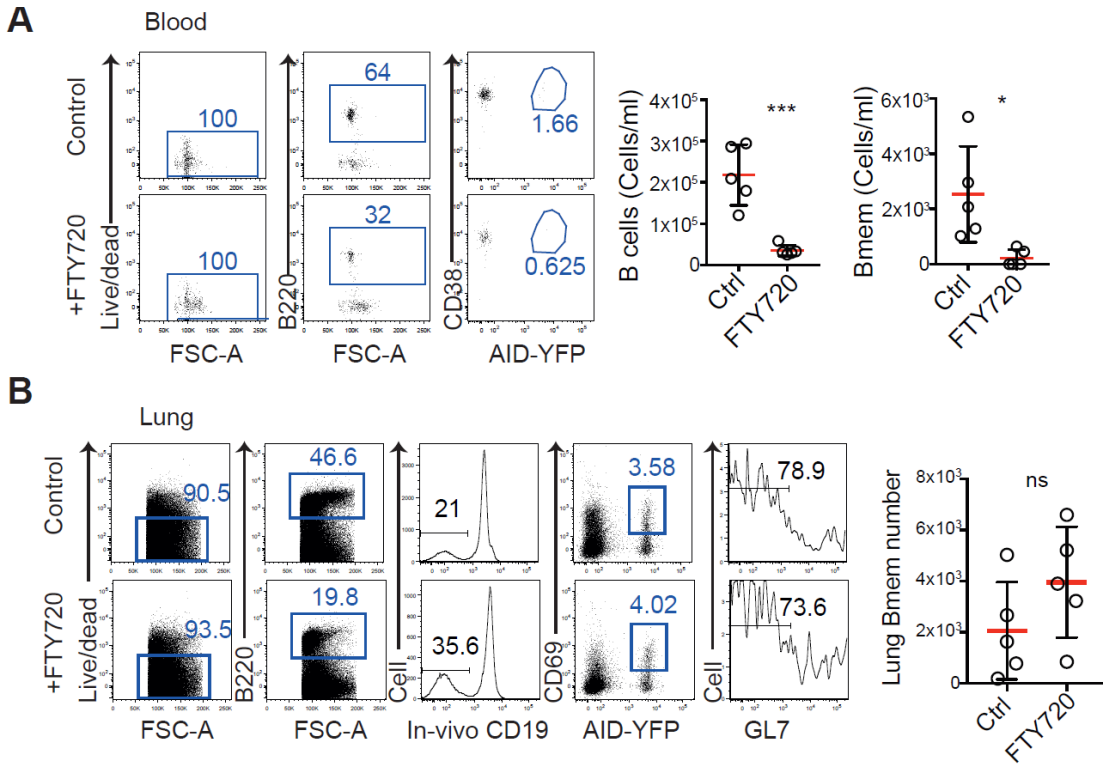


Figure 4. 2. 2. Validation of Bmem sequestration in SLO following treatment with FTY720. Mice were treated i.v. with FTY720 on d43p.i. and analysed by flow cytometry 48h later. A. Representative plots (left) and quantification (right) of circulating B cells and Bmem numbers in FTY-treated or in control mice. Student's unpaired t test *** p=0.0006; ** p=0.0166. B. Lung B cell populations in FTY-treated or control mice. Data are representative of 2 independent experiments, n=5 per group.

potential role for newly-recruited Bmem in the increased migration characteristics observed after influenza rechallenge. BLIMP1-Venus AID-Cre dTomato mice were infected with X31 and 40-54d later treated with FTY720 two days prior to X31 rechallenge. Importantly, we find that both treated and untreated mice showed similar increases in migration speeds and displacements, indicating a change in migratory behaviour of local rather than newly recruited cells (Fig.4.2.1).

4.3 Transitional behaviour in migratory Bmem following influenza rechallenge

Whilst imaging the lungs of mice 18-24h after rechallenge, a rare subset of dTomato-labelled cells were observed to undergo spontaneous transitioning between immobile and migratory phases. This behaviour was observed in approximately 3% of all cells observed over multiple ~30min imaging periods. Migratory bursts were met with reduced sphericity and temporarily increased velocity (>3µm/min; Fig.4.3). Transient periods of arrest may be indicative of interactions with other cell types, and have previously been visualised in GC B cells undergoing cognate interactions with Tfh cells, and also naïve B cells acquiring antigens from the surface of SCS macrophage in the LN (191).

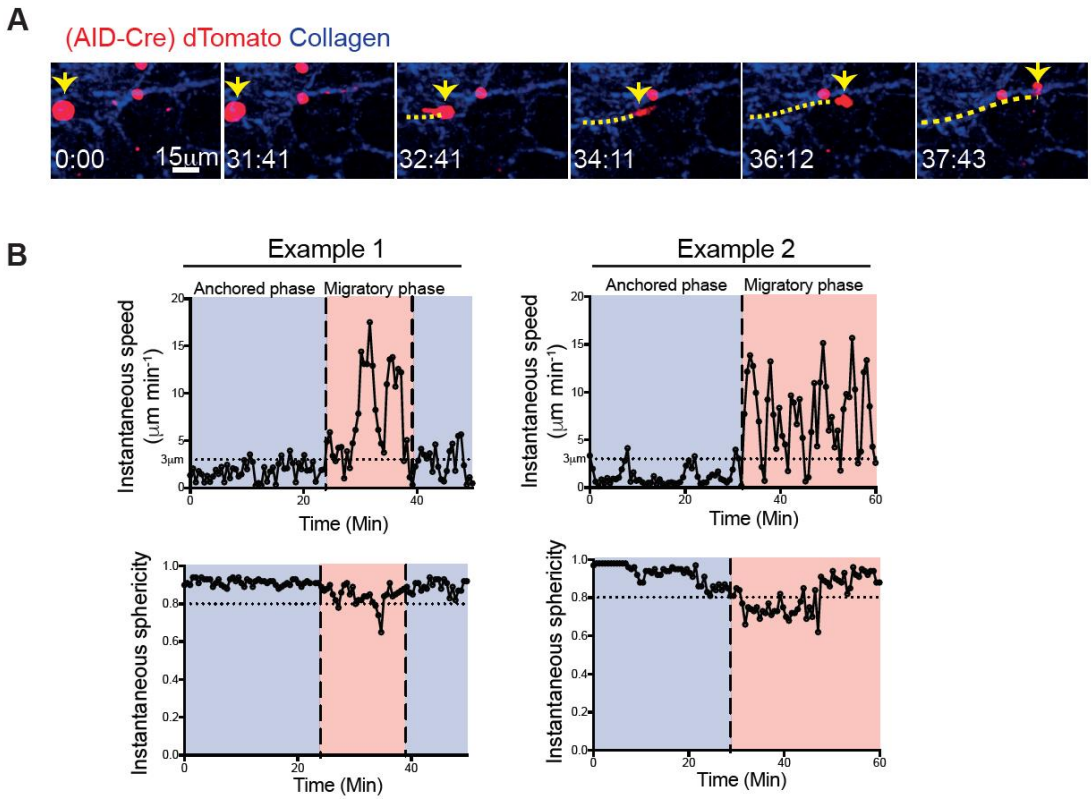


Figure 4. 3. Transitional behaviour in migratory Bmem following influenza rechallenge. Influenza-immune mice were rechallenged with high-dose X31 on d35-42 postinfection and analysed 24h later. A. Example image series of transitioning behaviour in Bmem. 24h after rechallenge with X31, a memory B cell (yellow arrow) can be observed to remain stationary for ~30min imaging, whereupon it assumes a motile phenotype for >7min. B. Plots from two example cells undergoing dynamic transition from anchored to migratory phase. Top, instantaneous cell speed. Bottom, instantaneous cell shape (sphericity). Data are representative of individual rare transitioning events, a behaviour identified in 4 different mice, and representing ~3% of cells imaged.

4.4 Molecular mechanisms underlying memory B cell reactivation in the lung

Memory B cells are known to become reactivated in response to a variety of stimuli in addition to antigen recognition through the BCR, including CpG and CD40 ligation (192-196). Given the kinetics of this response, we hypothesised that the inducing agent would be an innate signal.

To investigate whether memory B cell reactivation in the lung occurs in an antigen-dependent or independent manner, we utilised Qβ-VLPs. Qβ-VLPs, derived from the bacteriophage Qβ, are molecularly similar to virus particles; they have a self-assembling, highly repetitive protein structure and readily induce innate and adaptive immune activation (197). Interestingly, influenza-induced Bmem were found to

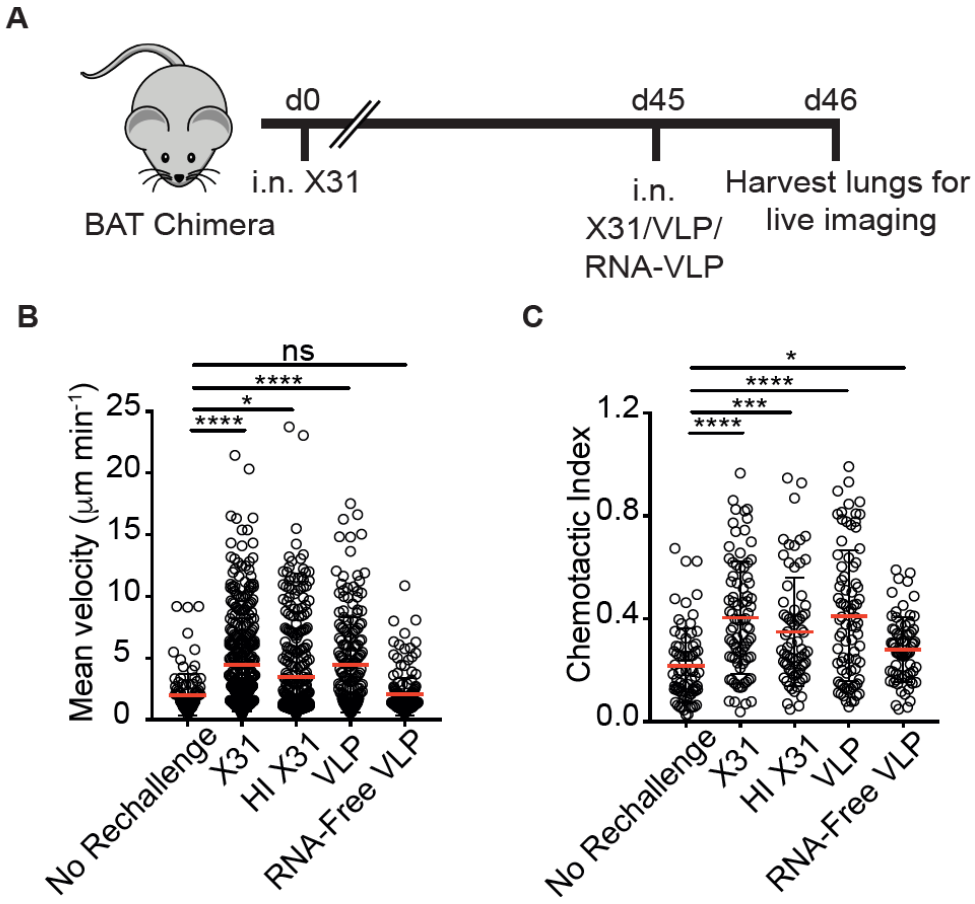


Figure 4. 4. Memory B cell mobilisation is induced by an antigen-independent RNAse-sensitive element. A. Experiment schematic displaying timecourse of rechallenge. B. Plots displaying mean cell velocities after rechallenge of immune mice with $1x10^6$ PFU X31, the same dose of inactivated virus, or 50μg of VLP or RNAse-treated VLP. C. Chemotactic indices of cells from mice treated as in B. Statistical comparisons represent results of One-way ANOVA with Dunn's multiple comparison test. ****p<0.0001; ***p=0.0002; *p<0.05. Data are representative of 3-6 independent experiments and a total of 3-6 mice per group.

increase migration speeds after intranasal administration of VLP alone, indicating an antigen-independent signal drives this early response. To test which innate signals could be involved, heat-inactivation of X31 was used to assess the relevance of infection-induced cell death. Treatment with HI X31 had a similar effect to untreated virus on reactivation-associated motility, suggesting that enhanced motility is not dependent upon live infection, specific antigen or virus-induced cell death. We thus developed a more refined approach, looking specifically at RNA as a stimulus. Qβ-VLPs are known to express a number of TLR ligands on their surface, and also are packaged with RNA. These packaged nucleic acids are known to contribute to the ability of Qβ-VLP to stimulate dendritic cells and B cells (197). It is possible to remove the RNA component from these structures by standard protocols. RNase treatment followed by diafiltration yielded VLPs with greatly reduced RNA content. We then used these RNA- VLPs to intranasally treat influenza-infected mice 45-64d postinfection to test the role of RNA in modifying Bmem motility. Interestingly, we find that intranasal-instillation of RNA- VLP failed to induce Bmem mobilisation, indicating an RNAse-sensitive element is the inducing agent of Bmem reactivation (Fig.4.4B,C).

4.5 Mononuclear phagocytes are involved in early Bmem mobilisation following rechallenge

The above results support the possibility that innate, rather than antigen-dependent mechanisms mediate local Bmem mobilisation in rechallenged mice.

Specialised macrophage subsets are known to interact with activated B cells at crucial points during the induction of the GC response in secondary lymphoid tissues (198). Macrophage and dendritic cells possess unique and exquisitely sensitive tissue surveillance machinery, allowing them to sense not only extracellular pathogens, but also – through the detection of molecular mediators - cell death, cellular metabolic stress and non-cytopathic infection. These features of pulmonary mononuclear phagocytes highlight the potential for these cells to be involved in early processes during infection, such as Bmem reactivation. Thus, we hypothesised that pulmonary mononuclear phagocytes may be involved in early antigen-independent Bmem responses to viral infection.

To test this possibility, intranasal treatment with clodronated liposomes (CLL) was used to deplete alveolar macrophages. As previously reported, CLL treatment led to rapid loss of alveolar macrophages ($F4/80^{+}$ $CD11c^{hi}$ $CD11b^{-}$), but had little effect on interstitial macrophages ($F4/80^{+}$ $CD11c^{hi}$ $CD11b^{+}$, Fig.4.5A). To test whether loss of alveolar macrophages affects Bmem mobilisation, we treated infected mice with CLL 3 and 6 days prior to rechallenge with live virus (Fig.4.5B-C). Treatment was performed twice to reduce the extent of cell-death-induced inflammation. One day later, live sections were imaged using two-photon microscopy to determine B cell motility. We found that under these conditions, lung Bmem failed to mobilise as previously observed and migratory parameters remained similar to unchallenged mice (Fig.4.5D, Fig4.2.1).

These experiments highlight a role for mononuclear phagocytes supporting early Bmem mobilisation in the rechallenged lung.

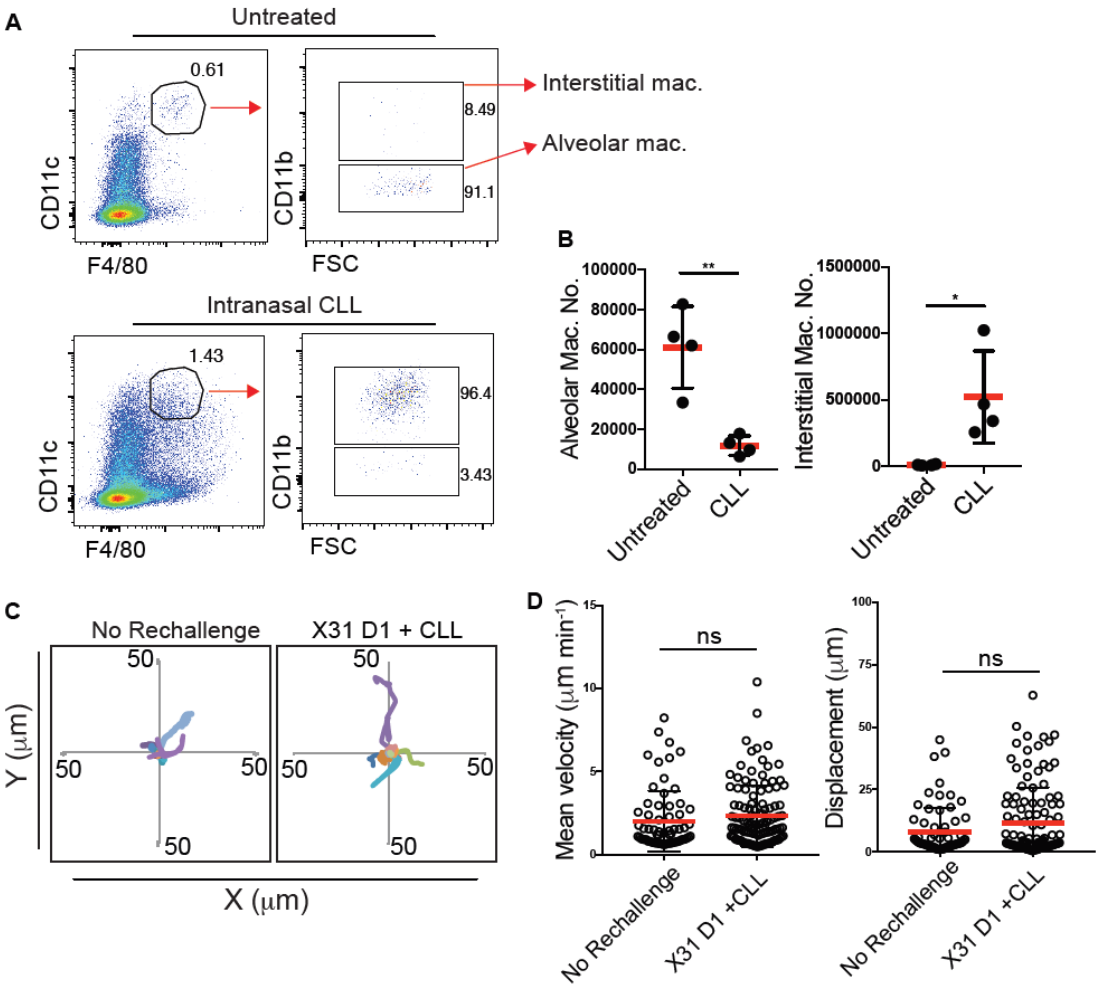


Figure 4. 5. Depletion of mononuclear phagocytes disrupts early Bmem mobilisation following rechallenge. A. Flow cytometry plots of alveolar macrophage and interstitial macrophage in the lungs of mice following PBS or CLL administration 3d and 6d before analysis. B. Quantification of macrophage numbers in the lungs of mice treated as in A. Data are representative of one experiment, n=4. C. Influenza-immune reporter mice were treated intranasally with CLL on d40 and d43 before rechallenge with X31 on day 46 postinfection. Lungs were harvested for live imaging 24h later, and Bmem motility tracked. Plots displaying randomly selected cell migration tracks from a common origin are displayed. D. Individual cell velocities and total displacements from influenza-immune mice, or mice 24h after rechallenge and CLL treatment. Data are pooled from 3 independent experiments, n=1-2 mice per experiment.

4.6 Microanatomical distribution of Bmem is altered following reinfection

In secondary lymphoid organs B cell mobilisation early during activation typically promotes entry into specialised niches where unique signals can be encountered (10, 11). We hypothesised that RNA-induced enhanced motility of Bmem may promote entry to unique areas of the lung that become immunologically relevant after encounter with potential pathogens. Notably, after influenza reinfection, Bmem in the alveoli appeared less distributed and instead clustered into smaller areas (Fig.4.6.2A-B). To quantitatively assess this in an unbiased way, we developed a means to assess Bmem distribution.

One method to track population distribution is to use the Ripley's K statistic (199, 200). This statistic defines clustering of points in a given area, and has been used to describe the clustering of data across a range of scales, for example ecological data

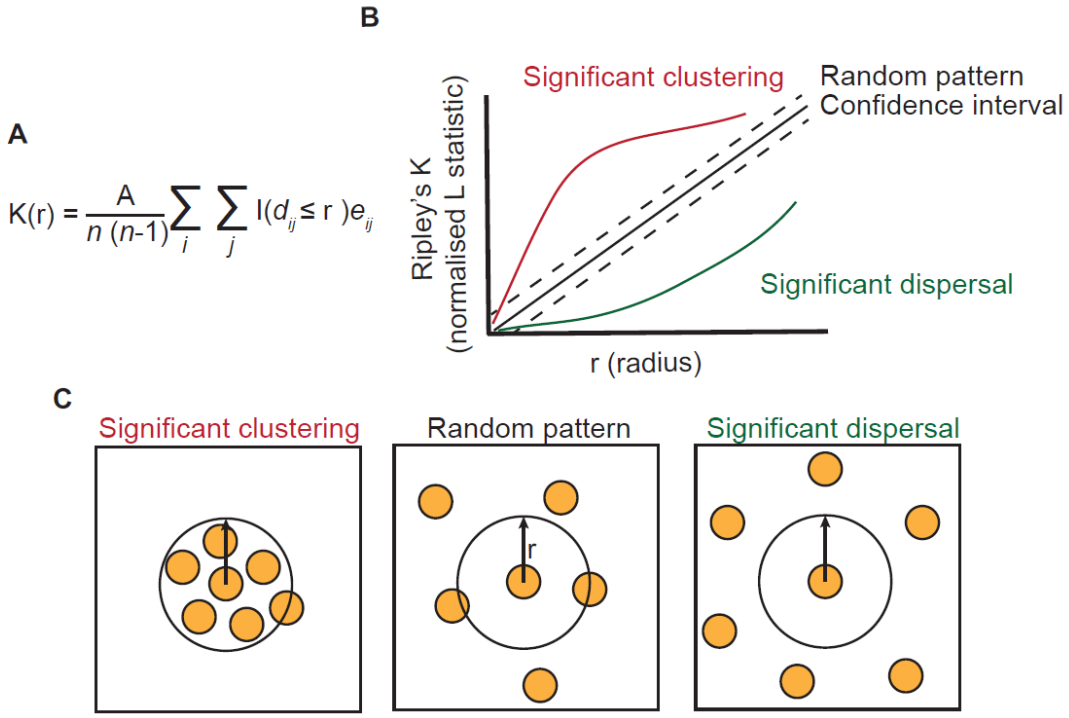


Figure 4. 6. 1 Using Ripley's K statistic to track spatial patterning. A. Ripley's K calculation, where A is plot area, n=number of data points, the sum over all pairs of points i and j. d_{ij} is the distance between two points, used in $I(d_{ij} \leq r)$ to indicate if distance between points is less than or equal to r. e_{ij} is the edge correction weight effect (without which may otherwise bias K at larger radii). B. Plots showing Ripley's K values (normalised so random distribution is linear, L value) over a range of radii. C. Example cellular distributions and graphical example of a single radius (r), for which Ripley's K would be calculated.

and disease cases as well as neuronal and membrane protein distribution (201-205). Briefly, Ripley's K calculates the mean number of cells (or 'events') within a given radius (r) from each individual cell. This value is normalised to the total number of cells in the imaging area (total density), and is compared to a set of points generated in the same area, under a random, homogenous event distribution (Fig.4.6.1). If the K value of observed data is greater than this estimated value, this indicates event clustering and if lower, event dispersal. For this form of analysis, to avoid biases >3 large tiles each covering at least $1x10^6\mu m^2$ (in XY) of each lung were collected from each of 4-6 mice.

In Figure 4.6.2A, plots displaying Ripley's K value over distances are shown in a normalised form, known as the L value. This analysis revealed that Bmem are evenly (or 'randomly') distributed throughout the lung parenchyma in the steady-state post-

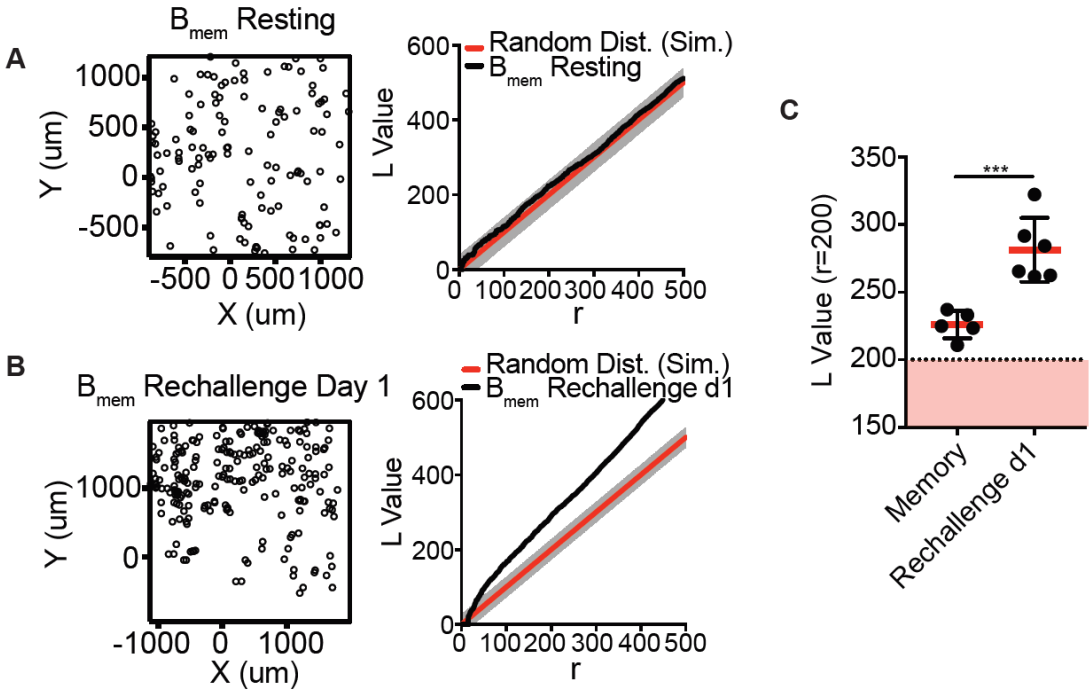


Figure 4. 6. 2. Microanatomical distribution of lung Bmem becomes altered following reinfection. A, B Data depicting Bmem distribution through lung during resting memory (A) and 24h after rechallenge wth X31 (B). Left, Spatial point patterns. Each point represents one Bmem cell in the imaging field. Right, Red line indicates simulated data with random distribution. Grey bars indicate simulation envelopes, generated by the upper and lower limits of 1000 simulations of random point processes. Black line represents experimental data from one tiled image. C. Summary data, each point represents one mouse, representative of mean values pooled from >3 tiled images per mouse from 5 or 6 independent experiments. Normalised L statistic at r=200 is shown, such that a value of ≤200 represents random distribution of cells, and larger values indicate spatial clustering. Student's unpaired t test, ***p=0.0006. Error bars represent mean±SD.

infection lung. In contrast, 24 after rechallenge a shift was observed, indicating a significant level of clustering. This is quantified in Fig.4.6.2B, where the L value from individual animals is displayed. The L value (here L=200) is a normalised form of Ripley's K, such that a value of 200 corresponds to a random distribution of cells, with greater values indicating clustering. Thus, Bmem appeared to cluster at a large scale in the alveoli shortly after rechallenge.

4.7 Bmem colocalise with infected cells early after reinfection

Influenza virus selectively infects alveolar epithelial cells and, depending on the virus strain, possibly alveolar macrophage. As we identified inhomogeneous distribution of Bmem 24h after rechallenge, we hypothesised that Bmem redistribution into alveoli may allow enhanced access to virus-derived innate inflammatory signals and antigens. To test Bmem redistribution relative to sites of infection, we generated a single-cycle virus that induces expression of eCFP in host cells upon infection (143). These viral particles are packaged from a cell line expressing H3, and so initially have a functional HA, but do not carry any gene encoding it and so fail to perform subsequent infection cycles.

To define infected areas within the lung parenchyma, we utilised a quadrat-sampling approach (Fig.4.7.1). Large image tiles of lung tissue were acquired and stitched to make a single image. These images were subjected to processing with Imaris software to generate 'Spots' features, based on CFP-channel intensity relative to background, spot size and surface quality. These 'Spots' surfaces were then verified manually and any artefacts removed (after identification by fluorescence in other channels, irregular shape, fluorescence characteristics). Using the coordinates of these spots, spatial point patterns were generated, tracked and then used to define infected

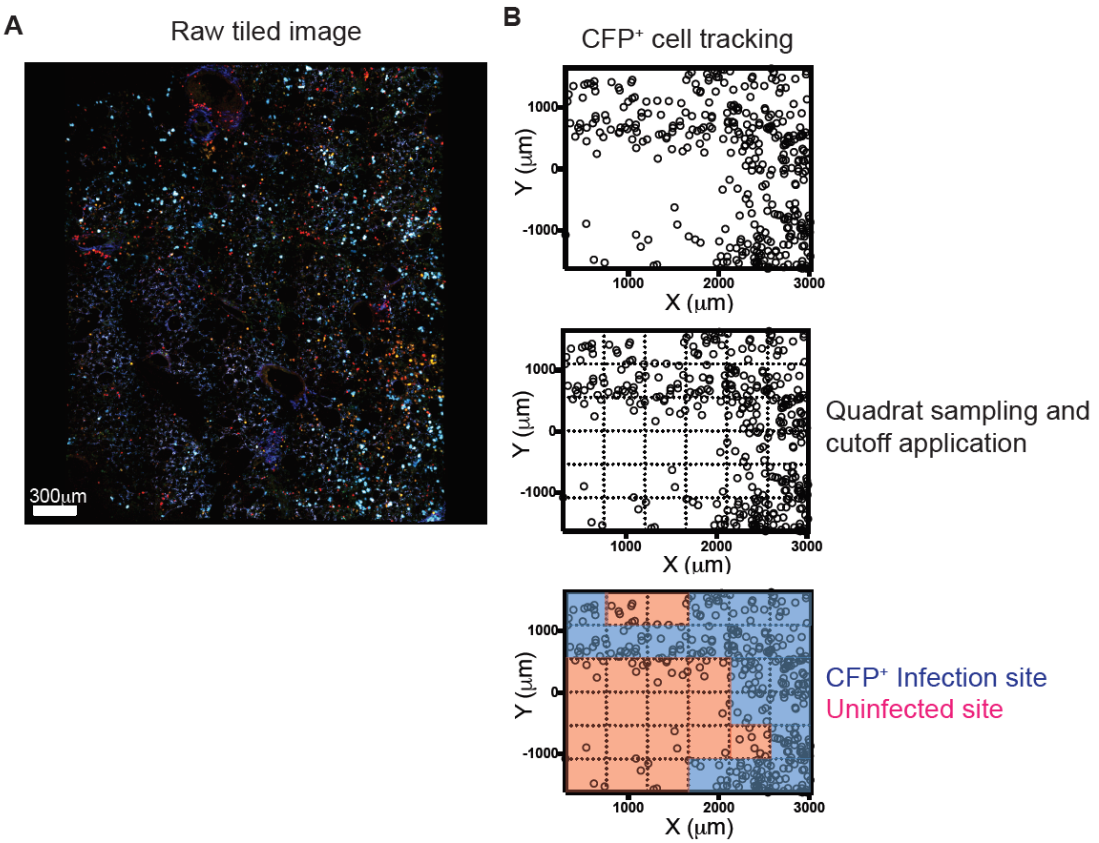


Figure 4. 7. 1. Description of infected and uninfected sites in the lungs of mice rechallenged with X31-CFP-s-flu. A. Tiled image of lung parenchyma following infection with X31 CFP-S-Flu. Red, AID-Tomato. Blue, collagen SHG. Green, BLIMP1-Venus. Cyan-CFP. Scale bar=300µm. B. Strategy for definition of infected/uninfected areas. CFP^+ cells were tracked, coordinates subjected to quadrat sampling and density thresholding, and areas were subsequently used to calculate Bmem density in the defined regions.

areas, in which Bmem densities were calculated. Areas in which infected cells were observed at a threshold density of >225cells/mm^3, corresponding to approximately 9 cells per quadrat grid, were classified as infected sites (Fig.4.7.1, bottom right).

Tracking lung Bmem in mice infected with X31 and rechallenged with CFP-s-Flu, revealed preferential positioning of Bmem in sites of infection 24h after rechallenge (Fig.4.7.2A). Notably, at this early timepoint plasma cells were still observed to reside selectively in clusters adjacent to collagen-rich airways and were largely absent from the alveoli (Fig.4.7.2A, Right).

Gαi-coupled protein receptors (GPCRs) play a key role in regulating lymphocyte migration in response to gradients of chemoattractants. Pertussis toxin (PTx) is a potent inhibitor of GPCRs which targets signalling events downstream of these receptors (206). *In vivo* treatment with PTx has been shown to significantly reduce

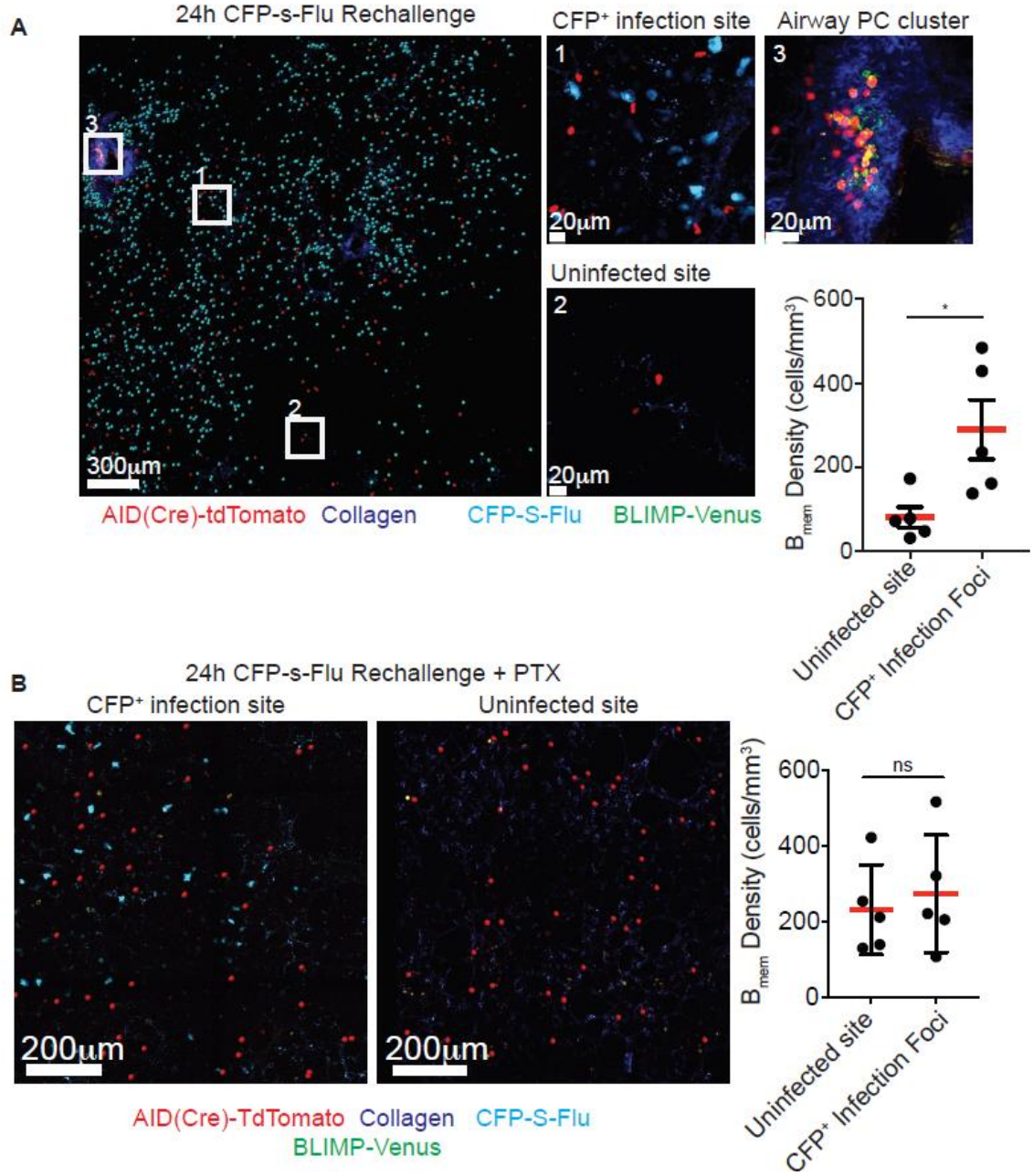


Figure 4. 7. 2. Bmem colocalise with infected cells at early timepoints after reinfection. A. Mice were infected with X31 influenza. On d48-54 mice were rechallenged with CFP-S-flu and lungs were harvested for confocal imaging 24h later. Left, tiled image displaying infected cell foci and adjacent border region. Top right, zoomed regions from tile. Bottom right, quantification of Bmem densities in infected or uninfected areas. B. X31-immunised mice were rechallenged with CFP-S-flu and 3h later treated with PTx on d36 p.i. before tissue collection 24h later. Data in A and B are analysed by paired statistical tests, as infected/uninfected areas from the same animal were used. Paired t test, *p=0.024, ns, not significant. Each point represents one mouse, as a mean of >3 tiled sections per animal, captured in 4-5 independent experiments.

migration velocities of lymph node B cells (142). To test if GPCRs are involved in Bmem clustering following rechallenge, mice were administered PTx 3h after rechallenge with CFP-S-Flu. 24h later, lungs were sectioned and imaged. It was found that, following PTx treatment, memory B cells failed to cluster in infected areas (Fig.4.7.2B). This indicates that migration of Bmem towards infected niches is likely mediated via active engagement of a GPCR and that this distribution is not the result of gross alteration of the tissue architecture following infection.

4.8 Chapter 4: Summary and discussion

Here, I describe the spatial compartmentalisation of humoral memory populations in the lung and how this changes after reactivation of lung Bmem upon viral re-encounter. Under steady state conditions, plasma cells cluster around airways, likely secreting antibody into the mucus that coats the upper airspace, whereas Bmem are distributed randomly through the lung parenchyma.

It is worth noting that when performing microscopic analysis, there appeared to be a greater number of Bmem within the lung than would be estimated by FACS. This phenomenon has been previously described, as yields of resident memory lymphocytes are up to 70-fold lower by manual tissue dissociation than by preparation for in situ imaging (89). This loss in yield has been proposed to be caused by inefficient extraction from collagen-rich tissues. Indeed, we identified two humoral populations in the post-infection lung that preferentially localise into collagen-rich airway structures. This feature may contribute to the difficulty of isolating these rare populations.

The common occurrence of iBALT adjacent to blood vessels poses an interesting possibility that proximity to blood vessels may facilitate naïve B cell entry to the GC shortly after entering the tissue. Indeed, iBALT stromal populations have

recently been shown to upregulate CXCL13, which is essential for B cell recruitment to these sites (117). This would suggest that the microanatomical distribution of these inducible SLO-like structures may promote their function, and that perhaps after rounds of selection, a proportion of mutated B cells are maintained locally as Bmem or LLPC. However, these iBALT are not the main focus of this present study, and the regulation, function and mechanisms of these structures are active areas of investigation in the field.

Stimulation by viral RNA upon reinfection leads to Bmem mobilisation and accumulation within infected sites. Interestingly, these results contrast with previous studies showing that Trm decrease migration speeds shortly after activation (180). This disparity between humoral and cellular immune systems may reflect the important differences that exist between the effector functions and cellular mechanisms used by these two cell types. B cells can detect antigen in an unprocessed form to become activated – antigen and other signals will be freely available in native states throughout the lung. In contrast, T cells must detect antigen in the context of peptide-MHC complexes on the cell surface of an antigen-presenting cell after establishing stable contacts to receive activation signals. Thus, tailored responses by Bmem and Tmem may enhance their respective stimulation pathways, differentiation and subsequent effector function.

Importantly, increased migration speed was not a uniform feature of all Bmem, and instead the appearance of an activated subset with unique migratory potential better explains the observed phenomenon. B cell activation *in vivo* is likely asynchronous, and the presence of Bmem at different activation stages may explain this observation. Indeed, in the experimental system utilised here the cells observed are undergoing a highly polyclonal response, rather than the transgenic models typically used when

exploring the migratory behaviour of activated B cells. Single-cell RNA-seq performed before and after rechallenge will provide insight into the heterogeneity of the Bmem population, and may indicate if such a developmental bifurcation occurs. Experiments in which photoactivatable-GFP is used to distinguish the local environments around these cells could provide insight into any stromal populations that may be unique to regions of activated/motile Bmem (207). Combination of this technique with FACS, qPCR or RNA sequencing may allow substantial insight into the induced or constitutive specialisations of different microanatomical regions within the lung tissue.

Whilst we have not yet determined if the detection of viral RNA was B cell intrinsic or extrinsic, the role for mononuclear phagocytes would suggest that viral RNA sensing may be handled by other cell types. Alveolar macrophage and respiratory DC populations are known to be primary responders to influenza infection. Sensing machinery including TLRs, RLRs and other nucleic acid sensing elements allow these mononuclear phagocytes to respond to viral infection rapidly (208). In addition, although we find that Bmem are broadly distributed in the tissue, they are still a rare population relative to these innate cells, a feature which would likely limit their capacity as sentinel cells. Finally, the role of stromal populations should not be ignored. It is very likely that the primary cell infected would be an alveolar epithelial cell. These cells bear nucleic acid sensing machinery of their own, and are able to initiate antiviral responses through early cytokine production (209-211). The sensitivity of Bmem to epithelial-derived stress signals may facilitate early antiviral responses with the enhanced kinetics characteristic of memory.

We do not exclude the possibility that CLL treatment may be structurally damaging or have off-target effects. Notably, Bmem were not lost following CLL treatment, which indicates that their steady-state niche is not critically dependent on

macrophage, or sensitive to inflammation-induced cell death (data not shown). Experiments using refined models that allow targeted, genetic deletion of macrophage subsets are in progress. Further work will investigate changes in alveolar macrophage expression profiles by sorting populations from naïve, resting memory and 24h post-rechallenge timepoints. Indeed, alveolar macrophage have an established protective role during influenza infection, and limit disease pathology and lung damage (208).

Periods of arrest are often indicative of interactions with other cell types, and have previously been visualised in GC B cells undergoing cognate interactions with Tfh cells, naïve B cells acquiring immune complexes from the surface of SCS macrophage in the LN (12, 191, 212) as well as other cell types. Arrest times of >30min that permit acquisition of antigen from LN FDC have also been observed (213). The finding that a number of Bmem were identified to undergo transitions between motile and stationary phases may indicate such cell-cell interactions can occur in infected peripheral tissues. Potential interaction partners include dendritic cells, alveolar macrophage and perhaps Tmem that are found in the lung tissue. Experiments are in progress to study potential crosstalk with these populations using confocal microscopy to assess the localisation of these populations relative to lung-resident Bmem. Subsequent work could expand on the depth of these findings by crossing fluorescent reporter mice to the AID-tomato line to visualise the timing, duration and dynamics of such cell interactions in real time.

After rechallenge, Bmem accumulate in infected niches, however directional migration of Bmem was not observed at any timepoint. This may be due to the architecture of the lung, requiring cells to follow highly convoluted paths along alveolar walls or interstitial spaces to sites of infection, or via the nature of the chemotactic signal that directs Bmem. This factor remains unknown, but experiments with PTx

suggest that GPCRs are involved. Further analysis of the RNA-seq dataset may offer some insight into the nature of relevant GPCRs, and a number of candidate GPCRs have been identified. Migration into sites of infection may permit Bmem to detect viral antigens in their native state via their BCR, and may allow access to unique cytokine microenvironments that could direct a number of antiviral adaptations or developmental responses of Bmem.

Of note, we did not directly observe Bmem re-entering iBALT GC structures in the lung at these timepoints. This may indicate that the frequency of Bmem that undergo this pathway after activation is low, or that it occurs predominantly at timepoints before or after the 18-24h observation window used here. Additionally, secondary germinal center B cells have been proposed to preferentially derive from IgM^+ Bmem subsets and not IgG^+ Bmem (55). One caveat of the system used here to track Bmem is that AID fate-mapping likely overlooks unmutated IgM^+ populations, and may partially explain the lack of visualisation of GC entry events.

Chapter 5

5. Distribution and activation of plasma cells in the lung during recall responses

Chapter 5: Background

The finding that upon rechallenge locally activated Bmem redistribute into microanatomical sites of infection was a striking phenomenon which has not been previously observed in nonlymphoid tissues. Whilst this primary reaction may provide essential activation signals to responding Bmem, such as acquisition of soluble signals or interaction with cells necessary for the promotion of humoral immunity, Bmem are not the central effector population of humoral immunity. Mature plasma cells have the singular capacity to secrete high quantities of protective antibodies into their immediate surroundings. Additionally, antibody-independent effector functions, for example secretion of cytokines such as GM-CSF, IL-10 and IL-35 have been proposed to be a function of plasma cells and not naïve B cells (214-216). Thus, assessing the dynamics of the plasma cell response has the potential to reveal novel information on the functional capacity of secondary humoral responses in the respiratory tract.

Plasma cells are primarily thought to enter protective niches in the bone marrow for long-term survival and antibody secretion. The bone marrow niche provides LLPC a site with access to various essential survival and retention factors (217-221). This suggests that antibodies would primarily reach peripheral tissues through the serum, after significant dilution. A number of pathogens such as influenza selectively infect peripheral tissues and do not disseminate, suggesting that induction of a localised response may be more beneficial. Indeed, plasma cells can be found lodged in mucosal

tissues such as the small intestine (222). Whilst initially thought to be a transient population, both antibody responses and plasma cell survival in these sites are now understood to be long-lived (223-225). The data presented above and in Chapter 1 show that plasma cells reside in flu-infected lungs, consistent with previous findings (127, 128), and that their positioning in steady state is consistent with an ongoing local protection of the main entry site to the lung – the branching points of the airway. However, whether this changes during reinfection is unknown.

Development into plasma cells is associated with drastic modifications to cellular structure, transcriptional profiles and induction of the unfolded protein response. These adaptations occur in a stepwise process, with activated B cells undergoing a developmental process that leads to gradual BLIMP1 upregulation (226). Thus, later timepoints must be assessed to identify mature BLIMP1^{+} plasma cell generation in peripheral tissues postinfection.

Aims:

1. Describe the kinetics and microanatomical distribution of plasma cells during secondary responses induced by influenza infection
2. Determine whether newly generated plasma cells depend on local Bmem and germinal center responses

5.1 Plasma cell establishment in the alveoli following reinfection

Secondary plasma cell responses have been proposed to develop over 3-8 days, in contrast to the primary antibody response, in which local plasma cells take up to 14d to arrive in the lung (127, 128, 227, 228). In the lung, reinfection has been shown to lead to much faster expansion of this population (128). Therefore, to test plasma cell response dynamics in the lung following rechallenge, we performed live imaging of lung sections 4d after rechallenge with X31 influenza. TPLSM of lung sections at this timepoint revealed a striking redistribution of plasma cells into the alveoli following infection (Fig.5.1). Quantification of cellular positioning using Ripley's K (initially

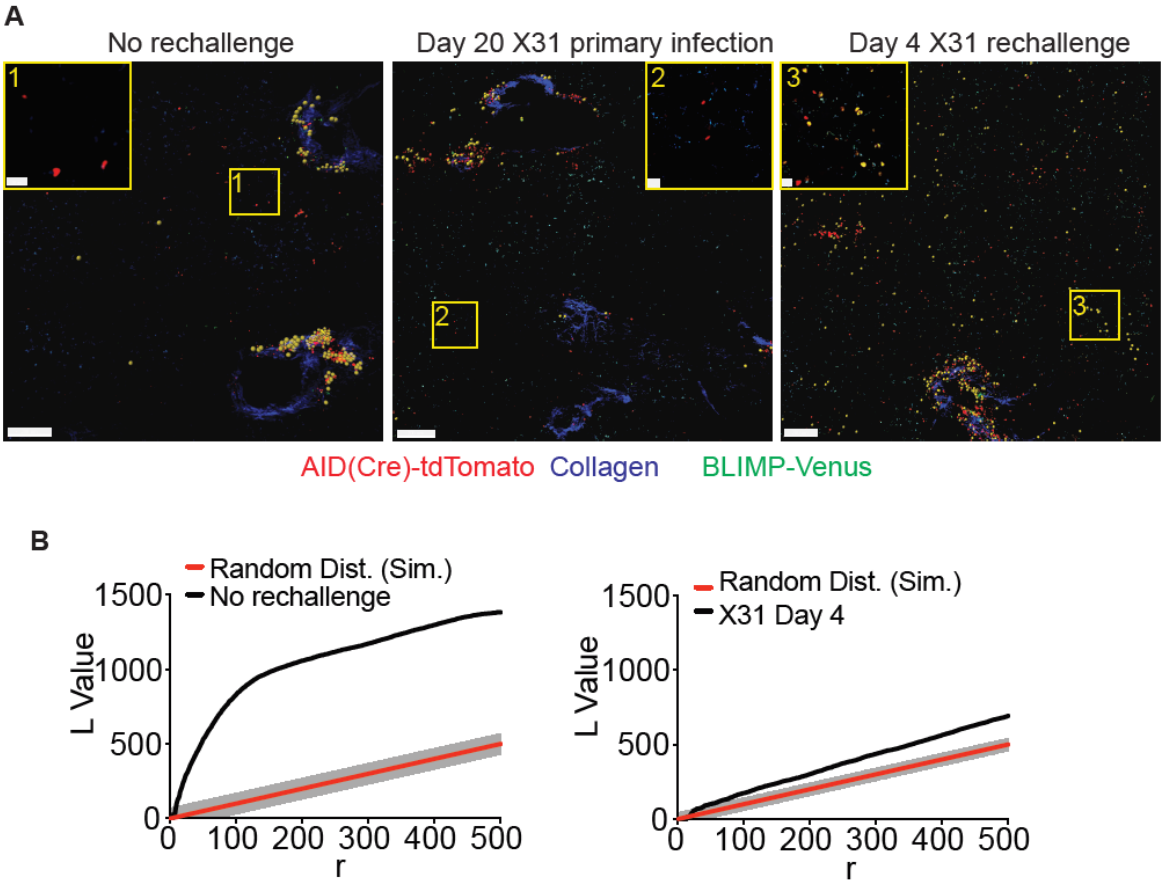


Figure 5. 1. Plasma cells redistribute into the alveoli following reinfection. A. TPLSM images displaying plasma cell and memory B cell distribution throughout lung airways and alveoli in the resting memory state (left), 20d after primary X31 infection (middle) and 4d following X31 rechallenge (right). Scale bar = 300µm. B. Plots displaying L Values (normalised Ripley's K). Red line indicates simulated data with random distribution. Grey bars indicate simulation envelopes, generated by the minimum and maximum limits of 1000 simulations of random point processes. Black line represents experimental data from one representative image per condition.

described in Chapter 4) confirmed the significance of this effect, indicating a high degree of 'declustering' of plasma cells as they entered the alveolar microenvironment (Fig.5.1B).

5.2 Plasma cell development within alveoli is antigen-independent

The plasma cell differentiation cascade is known to be induced by a range of stimuli, including CD40 signalling, BCR triggering or innate signals such as CpG ODN (192-196). As earlier stages of humoral memory reactivation were found to be antigen-independent, the signals essential for secondary PC formation and redistribution through the lung were assessed.

Reinfection of immune mice with high-dose X31 influenza caused significant repositioning of plasma cells into the alveoli 4d after rechallenge, as quantified by the L value ('clustering' index; Fig.5.1, Fig.5.2). To test whether antigen was involved in the plasma cell response, influenza-immunised mice were restimulated with intranasal treatment of VLP. Imaging of these animals 4d later revealed that plasma cell redistribution in VLP-treated mice was significant and similar to that observed in mice reinfected with live X31. In contrast, and consistent with Bmem redistribution,

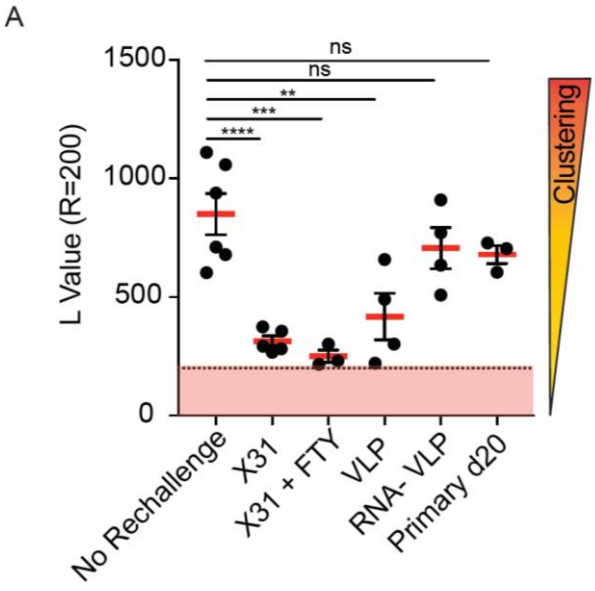


Figure 5. 2. Plasma cell appearance within alveoli is antigen-independent and induced by viral RNA. A. Plasma cell redistribution into alveoli . Each point represents one mouse, representative of mean values of >3 tiled images. Normalised L statistic at r=200 is shown, such that a value of <200 represents random distribution of cells (indicated in red shading), and larger values indicate spatial clustering. Ordinary one-way ANOVA with Bonferroni's multiple comparisons test. ****p<0.0001; ***p=0.0001; **p=0.0018. Error bars represent mean±SEM.

treatment with RNA-depleted VLP failed to induce PC entry to the alveoli. Importantly, FTY-treated mice infected with X31 also demonstrated significant levels of de-clustering, confirming that local rather than systemic B cells contributed to this effect (Fig.5.2).

This striking phenomenon of plasma cell entry into a new microanatomical site may suggest a powerful mechanism for antibodies to provide rapid, highly concentrated protective effects very early after reinfection. To discern whether this response is downstream of memory lymphocyte activation and unique to the memory response, we assessed plasma cell positioning during the primary response to influenza infection. No plasma cells were identified in the lungs of mice at d4 after primary infection (data not shown), and by the time PCs are present in this tissue at d20 they are located primarily in airway clusters as seen in the resting memory state (Fig.5.1, Fig.5.2). Thus, plasma cell redistribution into the alveoli is associated with the presence of memory B cells in the tissue, does not depend on input from circulating populations and appears to be mechanistically linked to the early process of Bmem mobilisation.

5.3 Plasma cells redistribute into infected alveoli after rechallenge

The appearance of plasma cells in alveoli in a pathway that shared dependencies with Bmem reactivation raised the possibility that these plasma cells were being generated in the infected sites where Bmem accumulated early after infection. To test the positioning of secondary plasma cells, we infected mice with CFP-s-Flu and assessed plasma cell positioning relative to infection foci at day 4. Image analysis and definitions of infected areas were performed as previously described (Chapter 4). Measurement of plasma cell densities in infected and uninfected areas highlighted preferential positioning in infected alveoli (Fig.5.3). It is noteworthy that densities in uninfected alveoli were also higher than in resting state, indicating that PC were also

situated within uninfected alveoli, or that CFP expression does not fully report on every infected cell (data not shown).

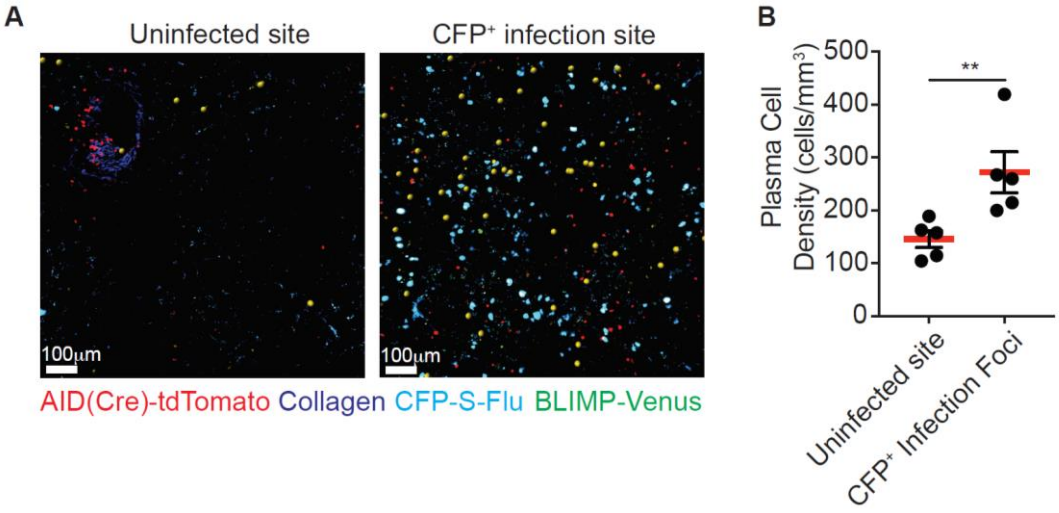


Figure 5. 3. Plasma cells redistribute out of airway niches into infected alveoli. A. Mice were infected with X31 influenza and at d40-52 rechallenged with CFP-S-Flu. Lungs were harvested for confocal microscopy 4d later. Zoomed regions from tiled images showing typical cell distributions in uninfected areas (left) or infection foci (right). B. Densities calculated using criteria outlined in Figure 4.7.1. Each point represents the mean value for one mouse, generated from >3 tiled images. Data were analysed by paired t test, as CFP-positive and -negative regions were analysed from each animal. Data are pooled from 3-4 independent experiments with 1-2 mice per experiment.

5.4 Plasma cell redistribution is independent of recruitment of systemic memory or newly activated naïve B cells

One potential caveat of our reporter system is that during secondary infections we cannot distinguish memory-derived plasma cells from plasma cells generated from naïve B cells. Whilst the generation of mature BLIMP^{+} PC from naïve B cells is unlikely to occur in a 4d timeframe, we could not fully exclude rapid passage through pre-existing lung GC or local recruitment offering accelerated developmental pathways to newly responding B cells.

To address this potential input from naïve B cells, and validate these results in another system, we used an alternative approach. For this we utilised the observation that CD19$^{-/-}$ B cells are outcompeted and fail to form mature GC responses to antigen

stimulation *in vivo* in the presence of $CD19^{wt/wt}$ B cells. To allow detection of memory B lymphocytes, $CD19^{-/-}$ mice were reconstituted with AID-dTomato B cells and infected with X31 influenza 1d later. To first assess whether any naïve B cells were remaining in this system mice were challenged 49 days later distally (subcutaneously) with an antigenically irrelevant stimulation (sheep red blood cells (SRBC)) and the GC response in local lymph nodes was analysed 8d later (Fig.5.4.1A, green). GCs in these mice were very small, and contained very few $dTomato^{+}$ reporter B cells, indicating that $CD19^{wt/wt}$ dTomato B cells that were transferred 49 days earlier were no longer present at this timepoint. In contrast, control $CD19^{-/-}$ mice which had received AID-tomato B cells 5d prior to SRBC immunisation (Fig.5.4.1A, blue) had a prominent GC response, and the majority of those were $dTomato^{+}$ (Fig.5.4.1D-E). Failure of reporter B cells to respond supports the notion that in this setup only memory B cells responsive to influenza survive and are able to participate in secondary responses.

Lungs were also harvested to assess the population of lung Bmem in these mice. Memory B cells in the lung could be identified at these timepoints, albeit in ~10-fold

lower numbers than control 'endogenous' AID-tomato reporter mice (Fig.5.4.1A, red, Fig.5.4.1B). Thus, transfer of BLIMP-AID-dTomato B cells into CD19$^{-/-}$ mice and

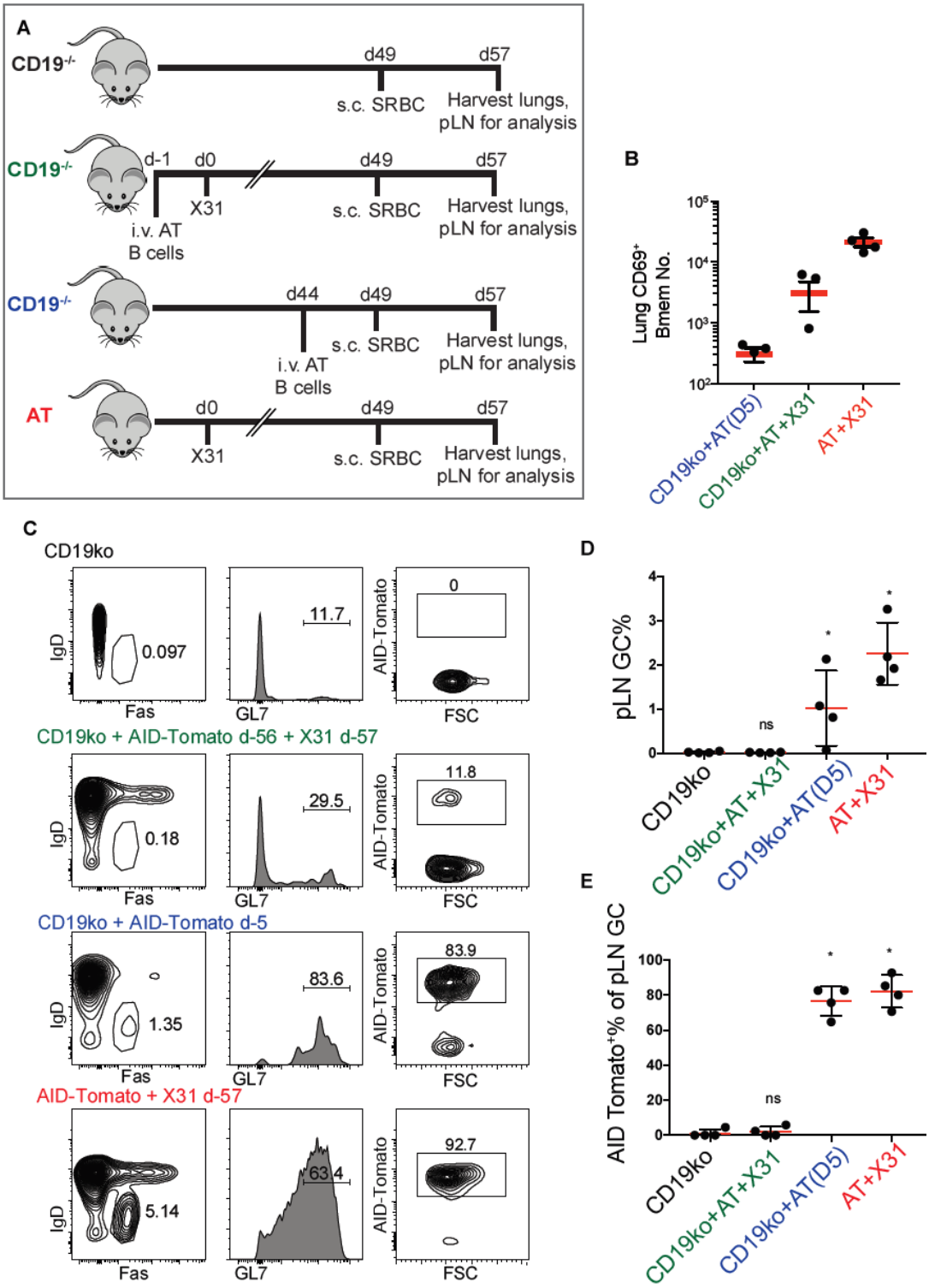


Figure 5. 4. 1. Establishment of a system to isolate input from naive B cells during secondary responses. A. Schematic showing treatment schemes for experimental groups. B. Memory B cell numbers in the lungs at d57 p.i. C. Flow cytometry plots from pLN after SRBC challenge showing GC gating and AID-Tomato^{+} frequencies. D. Total GC as a frequency of B cells. E. AID-Tomato-derived GC frequencies. Statistics in D and E represent comparison to CD19ko. *, $p<0.05$; ns, not significant. Each point represents summary data from each mouse. Data are representative of two independent experiments.

rechallenge at 45d postinfection will reveal the responses of Bmem and PC whilst avoiding any potential input from naïve B cells.

We therefore used this approach to test whether PC redistribution occurs independently of naïve B cell input. CD19$^{-/-}$ mice were reconstituted with BLIMP1-Venus AID-Cre Rosa-Stop-dTomato B cells and infected the following day. 45d later, mice were rechallenged and plasma cell positioning was analysed 4 days later. Analysis of plasma cell distribution revealed that, similarly to our previous observations using BLIMP1-Venus AID-Cre dTomato mice (Fig.5.2), large numbers of plasma cells appeared distributed throughout the alveoli 4 days postinfection. Together, these observations support the notion that alveoli-associated plasma cells developed locally from memory B cells, and that their rapid appearance in the site of infection depends on previous exposure to infection (Fig.5.4.2),

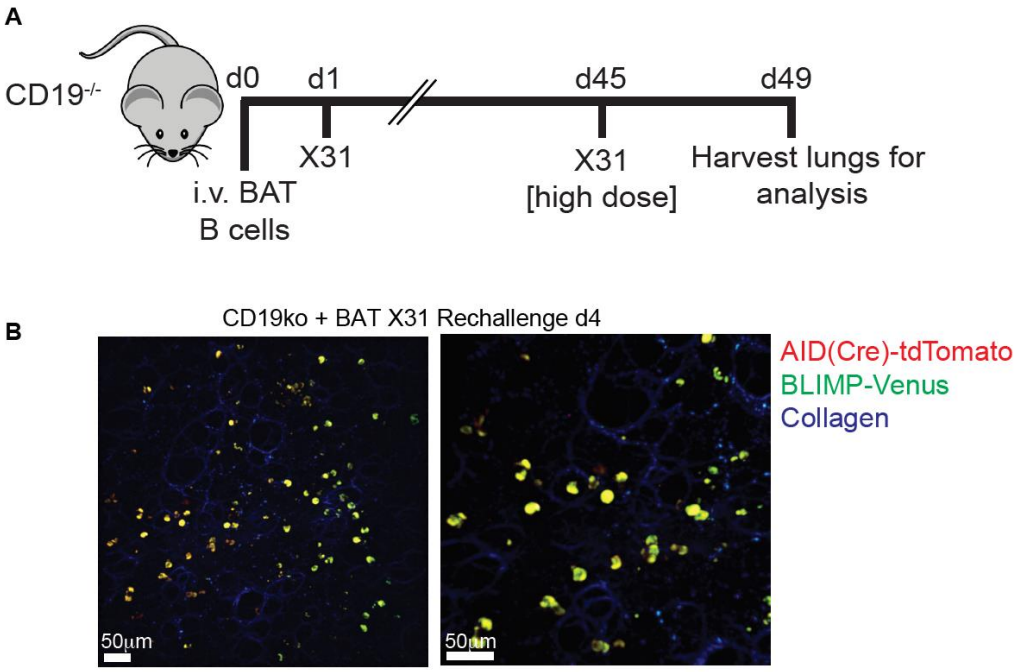


Figure 5. 4. 2. Plasma cell redistribution occurs independently of input from the naïve B cell pool. A. Experiment setup. CD19$^{-/-}$ mice were adoptively transferred enriched BLIMP-Venus AID-dTomato B cells 1d before X31 infection. 45d later mice were rechallenged with X31 influenza at high dose and lungs were collected for imaging on d49. B. Representative images showing plasma cell distribution through alveoli within lungs of infected mice. Images are representative of 3 mice from 3 independent experiments.

5.5 Plasma cell entry into the alveoli occurs independently of the GC

Previous studies suggest that Bmem could develop into secondary PC by two pathways – direct differentiation from Bmem after proliferation, or via entry to the GC and optionally undergoing BCR diversification, followed by differentiation (55). To distinguish whether Bmem were directly developing into PC in the alveoli or entering accelerated GC responses, we utilised established protocols to collapse GC in pLN, spleen and lung (128). Repeated intravenous administration of a blocking anti-CD40L antibody (MR1) successfully depleted iBALT GC in the lung, as well as SLO GC(Figure 5.5A-B and data not shown). Importantly, in agreement with a recent report (128) we find that this treatment did not affect memory B cell frequencies in the lung (data not shown). Rechallenge of influenza-immune mice after GC depletion revealed successful entry of plasma cells to the alveolar niche, displaying the independence of this phenomenon on passage through the GC response.

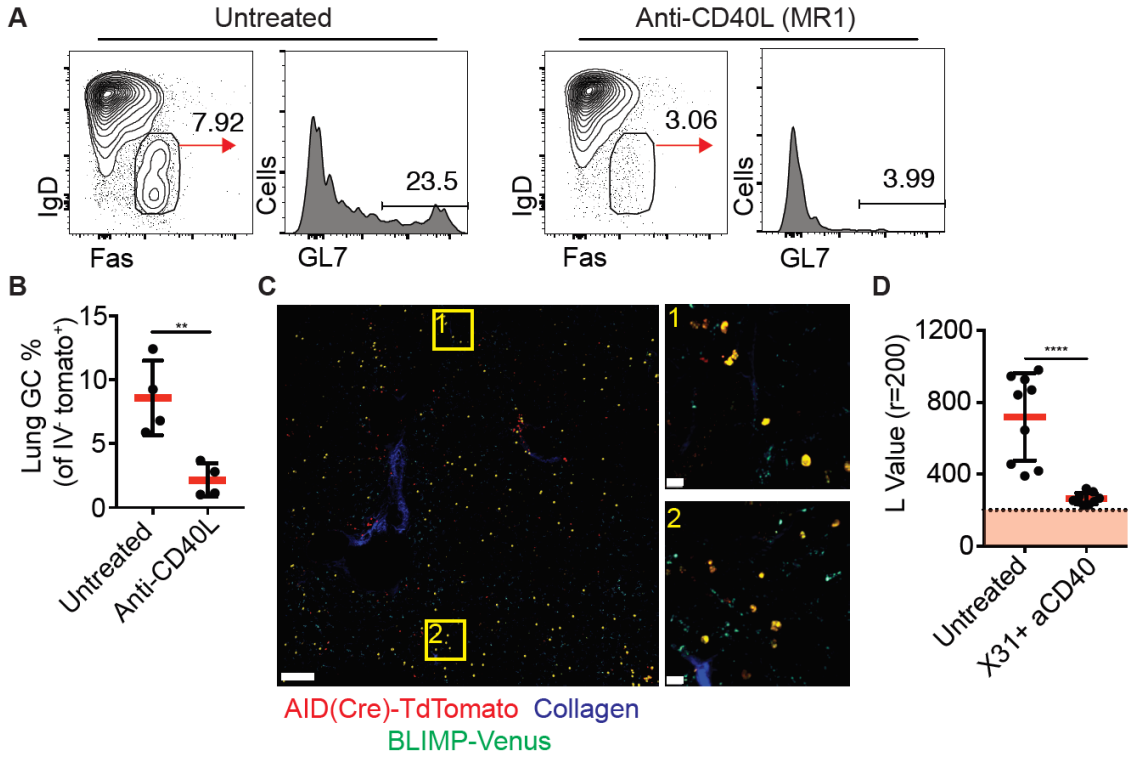


Figure 5. 5. Plasma cell entry into the alveoli occurs independently of the GC. A. Mice were treated i.v. with blocking anti-CD40L (MR1) every 2d for 10d, starting on d20p.i. and lung GC were assessed. Shown are representative flow cytometry plots from 1 independent experiment, n=4. B. Quantification of lung GC numbers from A. Each point represents one mouse. C. Left, tiled image of PC distribution d4 after X31 rechallenge. Scale bar=200μm. Right, zoomed regions of interest, highlighting alveolar plasma cells. Scale bar=20μm. D. Quantification of PC redistribution, displaying data from resting memory phase mice, and animals rechallenged with X31 for 4d after anti-CD40L-treatment.

5.6 Memory B cells and plasma cells are generated locally during secondary responses

The data presented above indicates that local development of effector plasma cells capable of secreting antibody occurs shortly after viral rechallenge. This would predict some level of local proliferation to occur, an essential step in plasma cell formation.

To assess the extent of local proliferation of Bmem and plasma cells within the lungs of rechallenged mice, we monitored incorporation of the nucleoside analogue EdU using histology-based analysis. After recovery from primary influenza infection, mice were intraperitoneally administered EdU 2d prior to virus rechallenge to synchronise labelling periods, and maintained on EdU in drinking water. To discriminate any role for circulating Bmem in local humoral proliferative responses, mice were also treated with FTY720 (as described in Chapter 4). Large tiles of lung sections were acquired, and subjected to colocalization analysis (based on dTomato and EdU fluorescence; Imaris software (Figure 5.4A)). Subsequently, Bmem and PC were manually segregated based on BLIMP1-venus expression.

In-situ analysis of cell proliferation revealed that in the steady state memory phase, approximately 17% (16.73±8.1%) of Bmem were found to undergo proliferation over the 6d labelling period. Unexpectedly, we also identified a similar frequency of PC undergoing a similar basal level of proliferation. After rechallenge, a larger fraction

of 'reactivated' Bmem and PC were observed to proliferate (Bmem 47.6±6.0%; PC

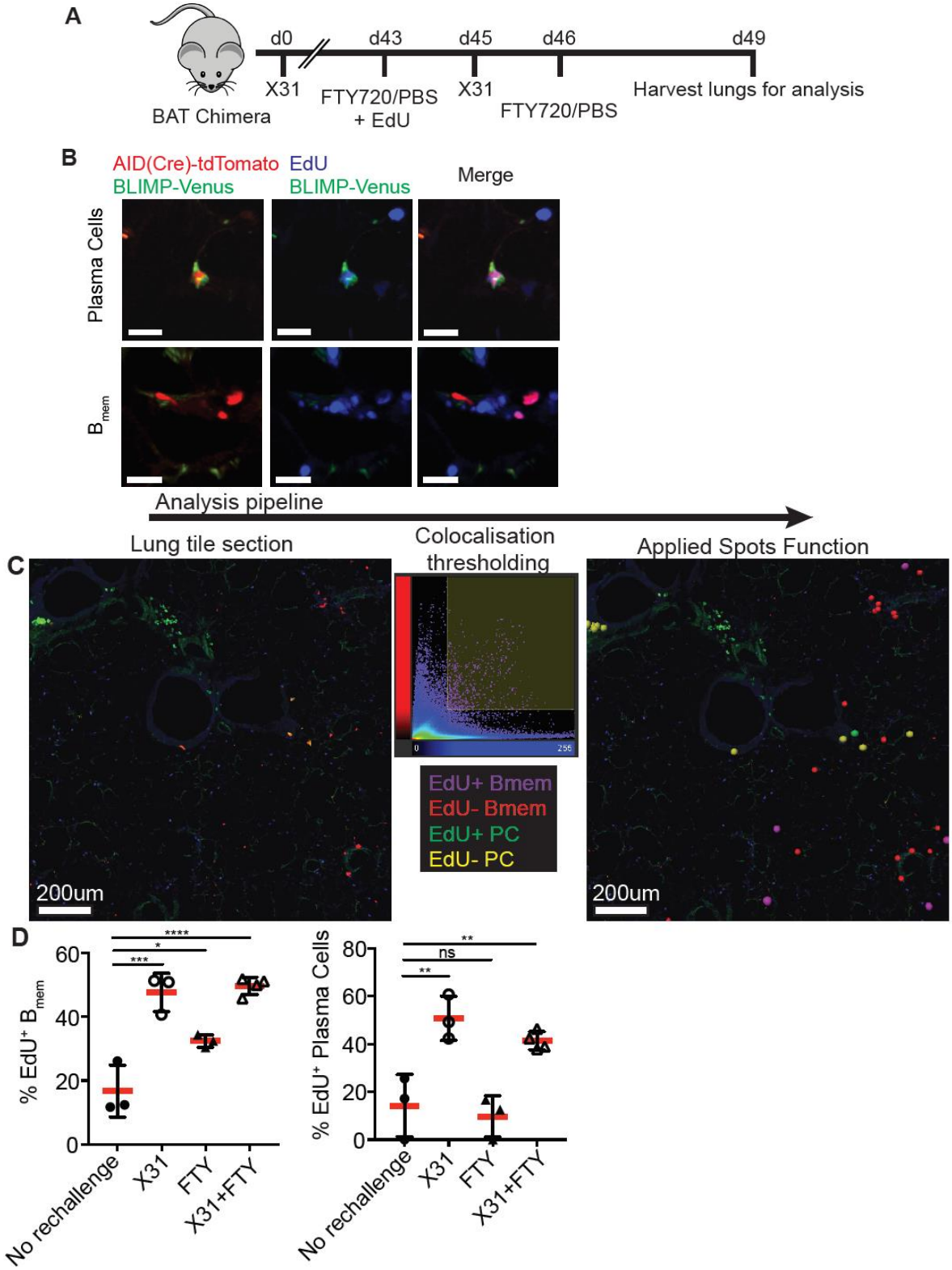


Figure 5. 6. Memory B cells and plasma cells are newly generated locally during secondary responses. A. Experimental design. B. Zoomed examples of plasma cells (top) and Bmem(bottom) after EdU labelling and fluorescence detection. C. Analysis pipeline, where large lung tiles (left) were subjected to colocalization analysis using Imaris, and EdU-labelling of PC and Bmem was determined (right). D. Quantification of Bmem (left) and PC (right) proliferation. Shown are frequencies of EdU^+ of total Bmem (left) or plasma cell (right) populations. Each individual point represents the total pooled values from >4 tiled sections from one mouse. Statistical tests represent results of one way ANOVA with Dunnet's multiple comparisons test. ****P<0.0001; ***p=0.0001; **p<0.01; *p=0.016. Data displayed is from one representative of 3 experiments, each with n=3-4 per group.

50.72±9.3%). This new generation of plasma cells was independent of cellular input from the blood, as treatment with FTY720 had no significant impact on EdU^+ cell frequencies (No rechallenge: 9.72±8.6%, Rechallenge d4: 41.32±3.8%). Interestingly, Bmem in the presence of FTY720 alone with no influenza rechallenge exhibited a significant increase in EdU^+ frequencies, suggesting some underlying phenomenon caused by treatment with FTY720.

5.7 Chapter 5: Summary and discussion

In this chapter, I characterise the secondary humoral response to influenza infection, focusing on later effector phases such as plasma cell development and dynamics. Mature PC were found to appear in infected alveoli 4d after rechallenge in a manner dependent on stimulation with viral RNA but not on cognate antigenic stimulation. These plasma cells were found to be newly generated, uniquely in the secondary response and independently of naïve B cells, strongly indicating local Bmem as a likely precursor of this population.

Plasma cells are particularly difficult to isolate from tissues, due to their large size and the requirement for tissue digestion for their isolation and potential cleavage of surface markers used to distinguish plasma cells. The use of a fluorescent reporter to identify plasma cells removes surface marker digestion as a potential point of confusion. However, using BLIMP1 as a plasma cell reporter, it is possible that during assessment of the tissue localisation of humoral immune populations, subsets such as plasmablasts, early activated B cells and naïve B cells were excluded from detection. Whilst naïve B or early activated B are unlikely to contribute to effector function, early plasmablast responses may well provide early levels of antibody that could have protective function (229-231).

Plasma cell positioning in peripheral mucosal tissues has been described previously. However, to the best of our knowledge, inducible re-localisation of PC into microanatomical niches of infection described here represents a novel phenomenon. This response may allow plasma cells to secrete antibody in the exact cellular niche in which it is required to function, or may allow highly localised concentrations of protective antibody to form. Whilst such concentrations of antibody molecules have not been reported, localised gradients of chemokines and growth factors have been proposed to be crucial for a variety of immunological and developmental processes in both peripheral tissues and SLO (232-236).

Plasma cells residing in the bone marrow or secondary lymphoid organs constitutively secrete antibody into the serum at a rate of 50-340pg/cell/day, corresponding to 12,500-85,000 IgG molecules per cell per minute (237). The concentrations of these antibodies are greatly reduced by dilution through the serum, and in infections like influenza where systemic dissemination is rare, distributing influenza-specific antibodies to distal sites other than the lungs is likely non-beneficial. Local plasma cell generation and liberation of antibodies to reach high concentrations in the immediate environment they are required may represent a more efficient immune protection strategy for infected mucosal tissues. In recent years it has become evident that broadly-neutralising antibodies can be induced, suggesting that the development of efficient vaccines targeting multiple strains may be possible. However, a major additional challenge that remains is the production of these antibodies in sufficient levels to efficiently neutralise virus. Indeed, individuals carrying neutralising antibodies to flu have been described, but these antibody titers remain very low and often ineffective in providing sufficient protection.

A recent report suggests that in the mucosa of the female reproductive tract systemic Bmem recruitment is essential for local mucosal antibody secretion after viral reinfection (124). This report noted that no Bmem were found in the mucosa in the resting state, concluding that under these conditions local antibody responses were dependent on recruitment of circulating memory cells. The mucosa of the reproductive tract may differ fundamentally from that of the lung, or alternatively, more sensitive methods of detection such as fluorescent fate-mapping may assist in the detection of a rare resident lymphocyte subset that may contribute to the effect.

Assessing the proliferation of local PC revealed a basal level of cell turnover in the steady state. Whether this represents homeostatic proliferation or constant seeding of the PC pool from the GC remains unknown, but could be assessed through the use of the AID-Cre ERT2 strain, which allows inducible activation of the AID-Cre reporter. Newly-generated plasma cells were found to expand in the lung following rechallenge, with ~40% of cells being labelled with EdU. As this technique is known to under-represent cell-cycling, it is likely that the extent of local proliferation is greater than this.

Interestingly FTY720 treatment was found to increase the frequency of Bmem taking up EdU in the absence of infection. There are a number of possible explanations for this phenomenon. Perhaps this suggests that Bmem are constantly leaving the lung after local proliferation, and FTY blockade promotes their accumulation. This would seem to be consistent with the upwards trend in Bmem numbers following 2d FTY treatment (Fig.4.2.2), however in experiments in which mice were treated with FTY for 6d (data not shown), we noted no further increase in this trend. Alternatively, local Bmem may enhance levels of homeostatic proliferation in response to FTY treatment.

Data presented here demonstrate that plasma cell formation from lung Bmem can occur in an antigen-independent manner. The mechanisms underlying antigen-independent PC formation are poorly described but, as mentioned, are commonly utilised to study plasma cell differentiation in vitro. The high levels of RNA coating the surface of VLP may act as a strong BCR-crosslinking agent, enhancing the PC differentiation programme. Alternatively, indirect or direct RNA stimulation may greatly lower the activation threshold of Bmem, to such an extent that low levels of persisting antigens may stimulate PC differentiation. A recent publication by the Pierce lab demonstrates that activation thresholds of naïve B cells can be lowered by innate inflammatory signals such as CpG (238), and it is possible Bmem are more sensitive to these effects. Interestingly this study found that CpG stimulation promoted PC differentiation at the cost of antigen processing and presentation. This may suggest that Bmem in the lung exposed to viral RNA and downstream inflammatory signalling cascades may preferentially generate short-lived plasma cells after activation.

In support of this, plasma cell entry to the alveoli after rechallenge was found to occur independently of passage through the GC. In support of this direct PC differentiation pathway, Benson et al provided evidence that reactivated Bmem do not assume GC phenotype before proliferation and differentiation into plasma cells (239). However, these data do not exclude the potential for Bmem-derived GC to contribute to secondary plasma cell responses. If present, such secondary GC-derived PC would be hypothesised to appear later in the response and perhaps bear increased mutational load than first-wave Bmem-derived PC. Inducible activation of the AID reporter system during the secondary response with AID-Cre-ERT2 would allow selective highlighting of PC generated in a secondary wave from GC.

Thus, we highlight the capability of a secondary wave of memory B cell-derived plasma cells to enter a microanatomical niche where infected cells and virus are found in abundance. Whilst the functional relevance of PC positioning in these sites is yet to be distinguished, the appearance of effector humoral populations at a site of viral infection suggests a protective role for these cells.

Chapter 6

6. Conclusions

6.1 Conclusion

Studying memory B cells is made problematic by the lack of consistency in cell descriptions. Throughout the literature, 'Bmem' have been identified by expression of $CD38^+$ (in mouse), $CD27^+$ (in human) and class-switched and/or antigen-binding BCRs. Here, we employed a fate-mapping system that defines memory B cells by activation history and not arbitrary surface marker expression. Use of this reporter system along with further reporters and surface molecule stains that allowed exclusion of plasma cells, GC B cells and blood-borne lymphocytes allowed us to stringently define a population of memory B cells. One caveat of this strict Bmem definition is that Bmem that may be generated independently of the GC response may be overlooked, as they are likely to include a significant portion of memory cells that are not labelled by the AID-dTomato reporter.

With the additional selection criteria of antigen-specificity, we identified a transcriptional profile unique to the resident memory B cell population in the lung, and RT-PCR validated that this profile is conserved in the broad population that would subsequently be analysed by microscopical techniques. This core resident memory B cell transcriptional profile was marked by increased expression of retention factors, costimulatory molecules and BCR-signalling elements. This signature shared a loss of recirculation elements with previously published transcriptional profiles of Trm in other tissues (240), and may be associated with rapid responsiveness to restimulation.

Live imaging has provided significant insight into the dynamic events that occur during primary B cell activation, however only recently has it been used to characterise secondary humoral responses. Here, TPLSM and confocal microscopy was used to

identify humoral memory populations in the post-immune lung. We identified plasma cells within dense clusters adjacent to airways and Bmem distributed evenly throughout the lung parenchyma. iBALT was also occasionally identified as dense clusters of AID-dTomato^{+} BLIMP1-Venus^{-} cells exhibiting highly constrained motility that were found to express the GL7 antigen.

Using live lung imaging in an explant setup to visualise Bmem dynamics in the steady state and after pathogen re-encounter we further characterised the motility parameters of this population. Low-grade alveolar surveillance behaviour was observed in the memory phase, with cells observed undergoing a low rate of diffusion through the tissue. After reactivation, Bmem were found to mobilise and displace significant distances through the lung before accumulating in infected sites. This effect was independent of live infection or antigen specificity, but required viral RNA, suggesting a role for innate signals.

Studies assessing resident memory T cell migration in peripheral tissues show that lymphocyte migration through tissue is defined by the local microenvironment. Trm in the female reproductive tract migrate at 6µm/min, whilst imaging of CD8^{+} Trm in the skin epidermis reveals low migration speeds (2µm/min)(180, 241). Physical barriers such as basement membranes, collagen-rich barrier tissues, blood and lymphatic vessels in nonlymphoid organs may limit the migration pathways and maximum speeds of cells in their local vicinity. However, as PTx treatment was found to abrogate activation-induced Bmem mobilisation, the favoured hypothesis is that this process, in the lung, is an active receptor-mediated process, rather than an indirect modification of physical properties of the tissue.

Secondary plasma cell formation was identified after influenza challenge. These plasma cells were found to be derived from local Bmem, and to localise in the alveoli

with a bias towards infected sites. Appearance of plasma cells within the alveoli resulted in a more dispersed positioning, and was induced in an antigen-independent manner. Polyclonal activation of Bmem and subsequent differentiation into plasma cells has been proposed as a means of long-term maintenance of serum antibody levels (194, 242, 243). Proposed by the Lanzavecchia group, these reports suggest that continual generation of plasma cells by innately-stimulated Bmem contributes to the maintenance of serum antibody titres. The observation of lung plasma cells undergoing recent proliferation in the memory phase may suggest a similar process in the lung in response to innate environmental stressors. This raises the possibility that after infection or vaccination with RNA-rich agents, polyclonal activation of lung Bmem may be responsible for boosting pulmonary plasma cell populations.

Model for humoral memory in the lung

The data presented in this thesis leads us to propose a model for protective humoral immunity in the lung (Fig.6.1). In the resting memory state after the resolution of the primary immune response, long-lived plasma cells maintained in airway-associated clusters constitutively provide a first level of protection through the secretion of antibodies into the airways, possibly helping to neutralise incoming virus. Memory B cells are seeded through the alveoli, where they appear to sample their immediate environment without displacing large distances. Shortly (within 24h) after reinfection these Bmem are induced (directly or indirectly) by innate signals to mobilise into

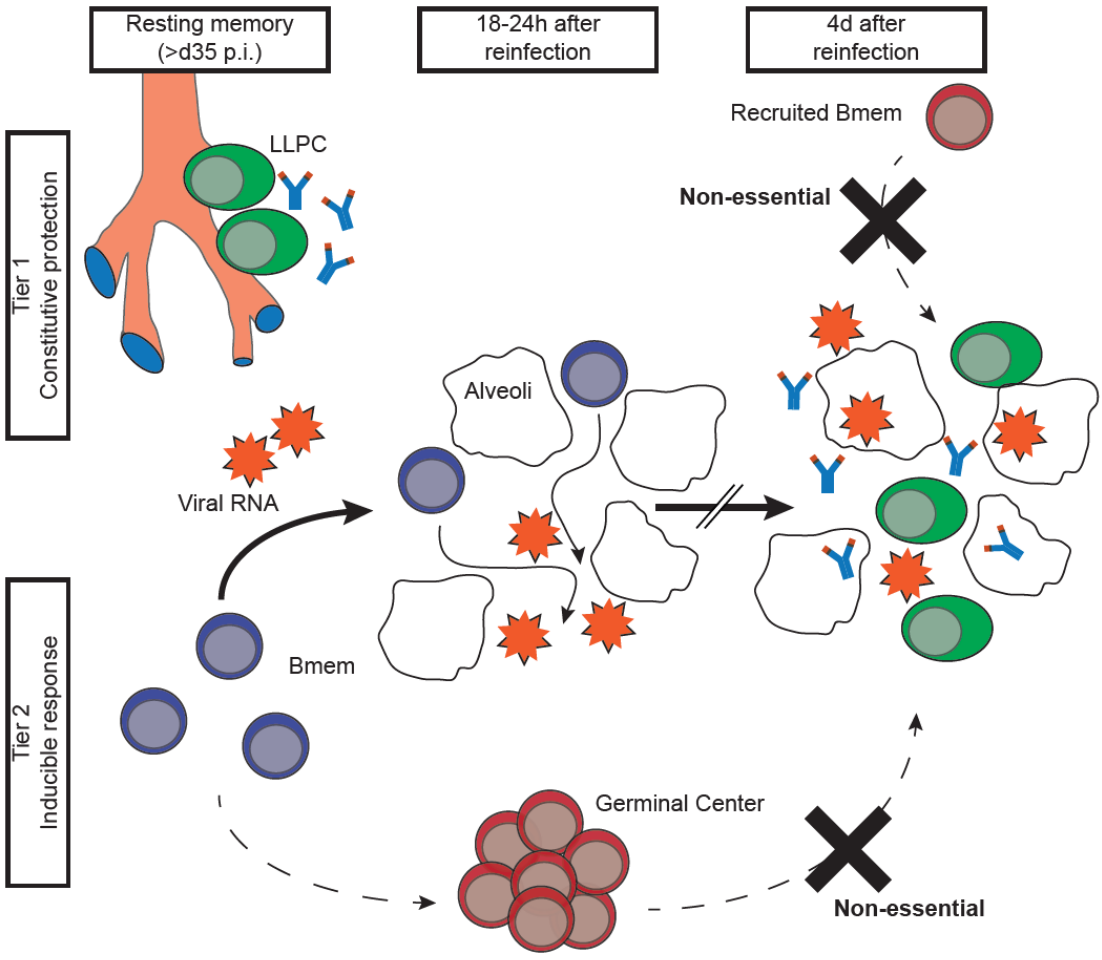


Figure 6. 1 Proposed model for humoral immunological memory in the lung. In the post-resolution influenza infected lung, long-lived plasma cells mediate a first level of protective immunity through liberation of antibody into the airway-lining mucus. If pathogens should evade or bypass this tier of immunity, Bmem resident in the lung tissue become activated in an innate manner, mobilise into infected niches and locally develop into plasma cells, in a manner that is not dependent on the GC response or B cell recruitment from the blood. Locally induced plasma cells are thought to secrete antibody locally to reach high functional concentrations capable of antiviral effector function.

infected alveoli. Over the next few days, Bmem may initiate the developmental processes necessary to differentiate locally into plasma cells, resulting in the establishment of a plasma cell population in infected alveoli. We hypothesise that these plasma cells supply high affinity antibody into the local environment, possibly reaching high functional concentrations across a very small tissue volume. Whilst Bmem may enter secondary GCs, or be recruited from the periphery to support this process in natural rechallenge, no dependence on either the GC or Bmem recruitment from blood was identified here. As such, these processes may contribute to secondary plasma cell or Bmem populations that arise later after secondary challenge.

Implications for vaccination

Currently, very few vaccines are designed to utilise the enhanced protective capabilities of tissue-resident lymphocytes. This is likely due to the requirement of local stimulation for their induction and associated technical difficulties. Efforts to overcome these technical difficulties are underway, and aerosol delivery of virus-based vaccines has been proposed to provide enhanced protection of the respiratory tract, and is associated with induction of local immunity (244-246). Indeed S-flu-based influenza vaccination experiments have shown that for protective efficacy, the vaccine has to be administered to the lungs of animals (143, 247), and aerosol administration of a mycoplasma vaccine induced local antibody responses in the respiratory tract of pigs (248). Interestingly, the attenuated childhood intranasal influenza vaccine is known to have greater efficacy than the tri-/tetra-valent inactivated vaccine administered intramuscularly (249).

Broadly neutralising antibodies have the potential to protect from a wide range of influenza virus strains, and prevent viral escape from vaccine-induced protection. While such antibodies can be induced in human blood by vaccination, broadly-

protective immunity is not routinely achieved (137). One potential explanation of this observation is that these antibodies fail to reach effective titres in the tissues where they are needed to provide protection. Many viruses do not disseminate through the body, and pathogens such as influenza have a highly restricted tissue tropism. As such, antibody responses in peripheral sites are much more relevant to the outcome of tissue-restricted infection, a situation where the advantage of systemic dissemination of antibodies is largely redundant.

The findings presented here indicate that lung-resident humoral immune populations undergo dynamic responses to influenza reinfection including positioning in infected sites and spatially-regulated development into effector plasma cells. In addition, this population displays unique transcriptional adaptations to the lung tissue including the expression of a number of GPCRs. Whilst much fundamental research remains to be performed, it is feasible that vaccine formulation using adjuvants that induce robust expression of ligands for such receptors in the lung tissue may enhance the induction or longevity of these protective lymphocyte populations. Future studies into the effect of these candidate GPCRs on lung Bmem maintenance and induction may reveal such potential for enhancing vaccine efficacy.

The induction of local adaptive immunity will activate both humoral and cellular branches of the immune system with highly protective effector responses. Together, broadly-reactive antibodies and T cell clones targeting conserved influenza epitopes may provide broader protection than previously achieved via standard vaccination strategies. To bypass the need for seasonal vaccination, the signals mediating long-term maintenance of these cells will need to be mechanistically understood and manipulated through vaccine formulation with innate stimulatory components through existing or novel adjuvants.

Lastly, the persistence (and potential manipulation) of a highly-reactive lymphocyte population in the lungs has to be viewed with caution. Immunological conditions of the respiratory tract such as asthma, chronic obstructive pulmonary disease (COPD) or Goodpasture's syndrome have persistent qualities, and induction of memory lymphocytes with effector-skewed profiles may not always be protective, and may contribute to pathology in some circumstances (250).

The first step in harnessing the potential therapeutic effect of these resident populations will be to establish safe and effective methods of local vaccine delivery to the lungs. Once this has been accomplished, formulation of vaccines with agents that promote memory lymphocyte retention, but limit overt inflammation, has the potential to provide great benefits to vaccine-induced pathogen resistance.

6.2 Future work

Bmem heterogeneity

Lung Bmem are composed of at least two subsets that can be differentiated based on CD69 expression, and after reactivation a proportion of cells exhibit enhanced migration characteristics. These features hint at underlying heterogeneity of this already poorly-defined population. Single cell RNA sequencing of B cell populations in the lung will reveal the extent of the heterogeneity within this specialised cell subset. Application of data interpretation techniques such as pseudotime analysis, where single cell RNAseq datasets are used to approximately linearize cell transcriptional profiles, potentially revealing differentiation pathways, may reveal further insight into the dynamic shifts in transcription profiles that occur early after Bmem stimulation (82, 251, 252).

Another related point of further research is the potential clonal relationships of lung Bmem, LLPC and splenic circulating Bmem. Single-cell sequencing analysis may be combined with BCR sequencing of lung and splenic Bmem populations in the memory phase and after rechallenge to simultaneously assess clonality and expression profiles (253-255). This has the potential to highlight clonal relationships between systemic Bmem, local Bmem and plasma cell populations. Previous work provides indications that Bmem in systemic or local lymphoid tissues exhibit little clonal relationships to gut or bone marrow PC (256). It would be of interest to assess whether a similar phenomenon occurs in the lung, and whether this becomes altered upon viral reinfection. These studies will provide insight into the clonal relationships, potential inter-migration, and origins of the systemic and resident memory pools.

Bmem mobilisation

Ongoing and future experiments will focus on trying to gain understanding of the mechanisms regulating Bmem reactivation in the lung following virus exposure. One remaining question was whether RNA-sensing occurred directly by the Bmem, or via other populations such as epithelial cells or local macrophage. Due to the rarity of antigen-specific Bmem, we hypothesise that epithelial cells or macrophage are more likely to be the initial responders to infection. In support of this hypothesis, CLL treatment was found to deplete alveolar macrophage and prevent Bmem mobilisation, implicating a role for alveolar macrophage in this process.

To directly address this possibility, we plan to use more refined targeted genetic deletion of the prime candidate population, alveolar macrophage, and assess the potential impact on Bmem mobilisation in the rechallenged lung. Better definitions of this supporting cell type in terms of phenotype and response kinetics to influenza infection will be performed by flow cytometric analyses, and qPCR or RNA-

sequencing may be performed to characterise expression profile changes and assist in the identification of potential chemotactic factors involved in Bmem mobilisation.

Subsequent studies will assess the viral sensing mechanism in the relevant populations. Mitochondrial antiviral-signalling protein (MAVS) has been shown to be involved in the detection of viral RNA through the RIG-I-like receptor pathway, which is upstream of antiviral cytokine secretion in most cell types, and specifically in alveolar macrophage, dendritic cells and alveolar epithelial cells (208, 257, 258). To assess a potential role for epithelial MAVS signalling in Bmem reactivation, mice deficient for MAVS will be irradiated and reconstituted with BLIMP1-venus AID-dTomato bone marrow. Resultant chimeras will lack select RNA signalling elements in the non-haematopoietic compartment alone. Rechallenge of these animals followed by live imaging 24h later will provide insight into the stromal input to this secondary response. These experiments may be performed with lung shielding during irradiation, to restrict MAVS deficiency to alveolar macrophage as well as the non-haematopoietic lineage.

In these ways, ongoing work performed by myself and other members of the lab will continue to build upon the initial observations described here, with the aim to provide a greater understanding of the dynamics of humoral immunity at mucosal barrier sites such as the lung.

6.3 Acknowledgements

I would like to thank Dr Tal Arnon for supervision and guidance throughout this project, as well as training in two-photon microscopy, image analysis techniques, data interpretation and experimental design, and also Dr Oliver Bannard for assisting in experimental design, helpful discussion and in particular guidance and assistance in the performance and analysis of RNA-sequencing experiments.

I would also like to express my gratitude to Professor Alain Townsend for insightful discussion about influenza viral infection, and technical guidance in the production of S-flu strains, recombinant haemagglutinin and in viral preparation protocols. Special thanks to Professor Martin Bachmann and Dr Ariane Cruz-Gomes for kindly synthesising and providing Qβ virus-like particles for use in rechallenge experiments.

I would also like to thank Dr Emily Thornton for the introduction to explant imaging, Dr Bin Xie for training in cloning and other molecular techniques along with Dr Anne Chauveau, Gabriela Pirgova and Niamh Richmond for insightful discussion and feedback.

Lastly, final thanks go to my family; my parents Elizabeth and Andrew MacLean and my brother Calum, for putting up with discussions of antibodies, cells and viruses, and to my fiancée Rebecca Brown, for whom these conversations are a daily occurrence.

For my dad,

I have not failed, I've just found 10,000 ways that won't work.

Thomas A. Edison

6.4 References

1. Zinkernagel RM, Hengartner H. 2006. Protective 'immunity' by pre-existent neutralizing antibody titers and preactivated T cells but not by so-called 'immunological memory'. *Immunol Rev* 211: 310-9
2. Letvin NL. 2007. Correlates of immune protection and the development of a human immunodeficiency virus vaccine. *Immunity* 27: 366-9
3. Lu LL, Suscovich TJ, Fortune SM, Alter G. 2018. Beyond binding: antibody effector functions in infectious diseases. *Nat Rev Immunol* 18: 46-61
4. Xu R, Johnson AJ, Liggitt D, Bevan MJ. 2004. Cellular and humoral immunity against vaccinia virus infection of mice. *J Immunol* 172: 6265-71
5. Belyakov IM, Earl P, Dzutsev A, Kuznetsov VA, Lemon M, Wyatt LS, Snyder JT, Ahlers JD, Franchini G, Moss B, Berzofsky JA. 2003. Shared modes of protection against poxvirus infection by attenuated and conventional smallpox vaccine viruses. *Proc Natl Acad Sci U S A* 100: 9458-63
6. Edghill-Smith Y, Golding H, Manischewitz J, King LR, Scott D, Bray M, Nalca A, Hooper JW, Whitehouse CA, Schmitz JE, Reimann KA, Franchini G. 2005. Smallpox vaccine-induced antibodies are necessary and sufficient for protection against monkeypox virus. *Nat Med* 11: 740-7
7. McLain L, Dimmock NJ. 1989. Protection of mice from lethal influenza by adoptive transfer of non-neutralizing haemagglutination-inhibiting IgG obtained from the lungs of infected animals treated with defective interfering virus. *J Gen Virol* 70 (Pt 10): 2615-24
8. Victora GD, Nussenzweig MC. 2012. Germinal centers. *Annu Rev Immunol* 30: 429-57
9. Song S, Matthias PD. 2018. The Transcriptional Regulation of Germinal Center Formation. *Front Immunol* 9: 2026
10. Pereira JP, Kelly LM, Cyster JG. 2010. Finding the right niche: B-cell migration in the early phases of T-dependent antibody responses. *Int Immunol* 22: 413-9
11. Cyster JG. 2010. B cell follicles and antigen encounters of the third kind. *Nat Immunol* 11: 989-96
12. Phan TG, Grigorova I, Okada T, Cyster JG. 2007. Subcapsular encounter and complement-dependent transport of immune complexes by lymph node B cells. *Nat Immunol* 8: 992-1000
13. Roozendaal R, Mempel TR, Pitcher LA, Gonzalez SF, Verschoor A, Mebius RE, von Andrian UH, Carroll MC. 2009. Conduits mediate transport of low-molecular-weight antigen to lymph node follicles. *Immunity* 30: 264-76
14. Gretz JE, Norbury CC, Anderson AO, Proudfoot AE, Shaw S. 2000. Lymph-borne chemokines and other low molecular weight molecules reach high endothelial venules via specialized conduits while a functional barrier limits access to the lymphocyte microenvironments in lymph node cortex. *J Exp Med* 192: 1425-40
15. Sixt M, Kanazawa N, Selg M, Samson T, Roos G, Reinhardt DP, Pabst R, Lutz MB, Sorokin L. 2005. The conduit system transports soluble antigens from the afferent lymph to resident dendritic cells in the T cell area of the lymph node. *Immunity* 22: 19-29

16. Nolte MA, Belien JA, Schadee-Eestermans I, Jansen W, Unger WW, van Rooijen N, Kraal G, Mebius RE. 2003. A conduit system distributes chemokines and small blood-borne molecules through the splenic white pulp. *J Exp Med* 198: 505-12
17. Reynoso GV, Weisberg AS, Shannon JP, McManus DT, Shores L, Americo JL, Stan RV, Yewdell JW, Hickman HD. 2019. Lymph node conduits transport virions for rapid T cell activation. *Nat Immunol* 20: 602-12
18. Cyster JG, Dang EV, Reboldi A, Yi T. 2014. 25-Hydroxycholesterols in innate and adaptive immunity. *Nat Rev Immunol* 14: 731-43
19. Gatto D, Wood K, Caminschi I, Murphy-Durland D, Schofield P, Christ D, Karupiah G, Brink R. 2013. The chemotactic receptor EBI2 regulates the homeostasis, localization and immunological function of splenic dendritic cells. *Nat Immunol* 14: 446-53
20. Kelly LM, Pereira JP, Yi T, Xu Y, Cyster JG. 2011. EBI2 guides serial movements of activated B cells and ligand activity is detectable in lymphoid and nonlymphoid tissues. *J Immunol* 187: 3026-32
21. Okada T, Miller MJ, Parker I, Krummel MF, Neighbors M, Hartley SB, O'Garra A, Cahalan MD, Cyster JG. 2005. Antigen-engaged B cells undergo chemotaxis toward the T zone and form motile conjugates with helper T cells. *PLoS Biol* 3: e150
22. Qi H, Kastenmuller W, Germain RN. 2014. Spatiotemporal basis of innate and adaptive immunity in secondary lymphoid tissue. *Annu Rev Cell Dev Biol* 30: 141-67
23. Reif K, Ekland EH, Ohl L, Nakano H, Lipp M, Förster R, Cyster JG. 2002. Balanced responsiveness to chemoattractants from adjacent zones determines B-cell position. *Nature* 416: 94-9
24. Crotty S. 2014. T follicular helper cell differentiation, function, and roles in disease. *Immunity* 41: 529-42
25. De Silva NS, Klein U. 2015. Dynamics of B cells in germinal centres. *Nat Rev Immunol* 15: 137-48
26. Crotty S. 2015. A brief history of T cell help to B cells. *Nat Rev Immunol* 15: 185-9
27. Chan TD, Gatto D, Wood K, Camidge T, Basten A, Brink R. 2009. Antigen affinity controls rapid T-dependent antibody production by driving the expansion rather than the differentiation or extrafollicular migration of early plasmablasts. *J Immunol* 183: 3139-49
28. Paus D, Phan TG, Chan TD, Gardam S, Basten A, Brink R. 2006. Antigen recognition strength regulates the choice between extrafollicular plasma cell and germinal center B cell differentiation. *J Exp Med* 203: 1081-91
29. MacLennan IC, Toellner KM, Cunningham AF, Serre K, Sze DM, Zuniga E, Cook MC, Vinuesa CG. 2003. Extrafollicular antibody responses. *Immunol Rev* 194: 8-18
30. Stavnezer J, Guikema JE, Schrader CE. 2008. Mechanism and regulation of class switch recombination. *Annu Rev Immunol* 26: 261-92
31. Kurosaki T, Kometani K, Ise W. 2015. Memory B cells. *Nat Rev Immunol* 15: 149-59
32. Radbruch A, Muehlinghaus G, Luger EO, Inamine A, Smith KG, Dorner T, Hiepe F. 2006. Competence and competition: the challenge of becoming a long-lived plasma cell. *Nat Rev Immunol* 6: 741-50

33. Smith KG, Light A, Nossal GJ, Tarlinton DM. 1997. The extent of affinity maturation differs between the memory and antibody-forming cell compartments in the primary immune response. *EMBO J* 16: 2996-3006
34. Odendahl M, Mei H, Hoyer BF, Jacobi AM, Hansen A, Muehlinghaus G, Berek C, Hiepe F, Manz R, Radbruch A, Dorner T. 2005. Generation of migratory antigen-specific plasma blasts and mobilization of resident plasma cells in a secondary immune response. *Blood* 105: 1614-21
35. Weisel FJ, Zuccarino-Catania GV, Chikina M, Shlomchik MJ. 2016. A Temporal Switch in the Germinal Center Determines Differential Output of Memory B and Plasma Cells. *Immunity* 44: 116-30
36. Manz RA, Löhning M, Cassese G, Thiel A, Radbruch A. 1998. Survival of long-lived plasma cells is independent of antigen. *Int Immunol* 10: 1703-11
37. Manz RA, Thiel A, Radbruch A. 1997. Lifetime of plasma cells in the bone marrow. *Nature* 388: 133-4
38. Hammarlund E, Lewis MW, Hansen SG, Strelow LI, Nelson JA, Sexton GJ, Hanifin JM, Slifka MK. 2003. Duration of antiviral immunity after smallpox vaccination. *Nat Med* 9: 1131-7
39. Nutt SL, Hodgkin PD, Tarlinton DM, Corcoran LM. 2015. The generation of antibody-secreting plasma cells. *Nat Rev Immunol* 15: 160-71
40. Minges Wols HA, Underhill GH, Kansas GS, Witte PL. 2002. The role of bone marrow-derived stromal cells in the maintenance of plasma cell longevity. *J Immunol* 169: 4213-21
41. Cassese G, Arce S, Hauser AE, Lehnert K, Moewes B, Mostarac M, Muehlinghaus G, Szyska M, Radbruch A, Manz RA. 2003. Plasma cell survival is mediated by synergistic effects of cytokines and adhesion-dependent signals. *J Immunol* 171: 1684-90
42. Weisel F, Shlomchik M. 2017. Memory B Cells of Mice and Humans. *Annu Rev Immunol* 35: 255-84
43. McHeyzer-Williams M, Okitsu S, Wang N, McHeyzer-Williams L. 2011. Molecular programming of B cell memory. *Nat Rev Immunol* 12: 24-34
44. Tangye SG, Liu YJ, Aversa G, Phillips JH, de Vries JE. 1998. Identification of functional human splenic memory B cells by expression of CD148 and CD27. *J Exp Med* 188: 1691-703
45. Klein U, Kuppers R, Rajewsky K. 1997. Evidence for a large compartment of IgM-expressing memory B cells in humans. *Blood* 89: 1288-98
46. Wu YC, Kipling D, Dunn-Walters DK. 2011. The relationship between CD27 negative and positive B cell populations in human peripheral blood. *Front Immunol* 2: 81
47. Blink EJ, Light A, Kallies A, Nutt SL, Hodgkin PD, Tarlinton DM. 2005. Early appearance of germinal center-derived memory B cells and plasma cells in blood after primary immunization. *J Exp Med* 201: 545-54
48. Smith KG, Light A, O'Reilly LA, Ang SM, Strasser A, Tarlinton D. 2000. bcl-2 transgene expression inhibits apoptosis in the germinal center and reveals differences in the selection of memory B cells and bone marrow antibody-forming cells. *J Exp Med* 191: 475-84
49. Toyama H, Okada S, Hatano M, Takahashi Y, Takeda N, Ichii H, Takemori T, Kuroda Y, Tokuhisa T. 2002. Memory B cells without somatic

hypermutation are generated from Bcl6-deficient B cells. *Immunity* 17: 329-39
50. Berkowska MA, Driessen GJ, Bikos V, Grosserichter-Wagener C, Stamatopoulos K, Cerutti A, He B, Biermann K, Lange JF, van der Burg M, van Dongen JJ, van Zelm MC. 2011. Human memory B cells originate from three distinct germinal center-dependent and -independent maturation pathways. *Blood* 118: 2150-8
51. Inamine A, Takahashi Y, Baba N, Miyake K, Tokuhisa T, Takemori T, Abe R. 2005. Two waves of memory B-cell generation in the primary immune response. *Int Immunol* 17: 581-9
52. Tangye SG, Good KL. 2007. Human IgM+CD27+ B cells: memory B cells or "memory" B cells? *J Immunol* 179: 13-9
53. Obukhanych TV, Nussenzweig MC. 2006. T-independent type II immune responses generate memory B cells. *J Exp Med* 203: 305-10
54. Dogan I, Bertocci B, Vilmont V, Delbos F, Mégret J, Storck S, Reynaud CA, Weill JC. 2009. Multiple layers of B cell memory with different effector functions. *Nat Immunol* 10: 1292-9
55. Pape KA, Taylor JJ, Maul RW, Gearhart PJ, Jenkins MK. 2011. Different B cell populations mediate early and late memory during an endogenous immune response. *Science* 331: 1203-7
56. Crotty S, Felgner P, Davies H, Glidewell J, Villarreal L, Ahmed R. 2003. Cutting edge: long-term B cell memory in humans after smallpox vaccination. *J Immunol* 171: 4969-73
57. Yu X, Tsibane T, McGraw PA, House FS, Keefer CJ, Hicar MD, Tumpey TM, Pappas C, Perrone LA, Martinez O, Stevens J, Wilson IA, Aguilar PV, Altschuler EL, Basler CF, Crowe JE, Jr. 2008. Neutralizing antibodies derived from the B cells of 1918 influenza pandemic survivors. *Nature* 455: 532-6
58. Taylor JJ, Pape KA, Jenkins MK. 2012. A germinal center-independent pathway generates unswitched memory B cells early in the primary response. *J Exp Med* 209: 597-606
59. Gray D, Skarvall H. 1988. B-cell memory is short-lived in the absence of antigen. *Nature* 336: 70-3
60. Maruyama M, Lam KP, Rajewsky K. 2000. Memory B-cell persistence is independent of persisting immunizing antigen. *Nature* 407: 636-42
61. Hikida M, Casola S, Takahashi N, Kaji T, Takemori T, Rajewsky K, Kurosaki T. 2009. PLC-gamma2 is essential for formation and maintenance of memory B cells. *J Exp Med* 206: 681-9
62. Vieira P, Rajewsky K. 1990. Persistence of memory B cells in mice deprived of T cell help. *Int Immunol* 2: 487-94
63. Coulie PG, Van Snick J. 1985. Rheumatoid factor (RF) production during anamnestic immune responses in the mouse. III. Activation of RF precursor cells is induced by their interaction with immune complexes and carrier-specific helper T cells. *J Exp Med* 161: 88-97
64. Hebeis BJ, Klenovsek K, Rohwer P, Ritter U, Schneider A, Mach M, Winkler TH. 2004. Activation of virus-specific memory B cells in the absence of T cell help. *J Exp Med* 199: 593-602
65. Dorner T, Radbruch A. 2007. Antibodies and B cell memory in viral immunity. *Immunity* 27: 384-92

66. Crotty S, Ahmed R. 2004. Immunological memory in humans. *Semin Immunol* 16: 197-203
67. Anderson SM, Tomayko MM, Ahuja A, Haberman AM, Shlomchik MJ. 2007. New markers for murine memory B cells that define mutated and unmutated subsets. *J Exp Med* 204: 2103-14
68. Bhattacharya D, Cheah MT, Franco CB, Hosen N, Pin CL, Sha WC, Weissman IL. 2007. Transcriptional profiling of antigen-dependent murine B cell differentiation and memory formation. *J Immunol* 179: 6808-19
69. Liu YJ, Oldfield S, MacLennan IC. 1988. Memory B cells in T cell-dependent antibody responses colonize the splenic marginal zones. *Eur J Immunol* 18: 355-62
70. Elgueta R, Marks E, Nowak E, Menezes S, Benson M, Raman VS, Ortiz C, O'Connell S, Hess H, Lord GM, Noelle R. 2015. CCR6-dependent positioning of memory B cells is essential for their ability to mount a recall response to antigen. *J Immunol* 194: 505-13
71. Aiba Y, Kometani K, Hamadate M, Moriyama S, Sakaue-Sawano A, Tomura M, Luche H, Fehling HJ, Casellas R, Kanagawa O, Miyawaki A, Kurosaki T. 2010. Preferential localization of IgG memory B cells adjacent to contracted germinal centers. *Proc Natl Acad Sci U S A* 107: 12192-7
72. Purtha WE, Tedder TF, Johnson S, Bhattacharya D, Diamond MS. 2011. Memory B cells, but not long-lived plasma cells, possess antigen specificities for viral escape mutants. *J Exp Med* 208: 2599-606
73. Zuccarino-Catania GV, Sadanand S, Weisel FJ, Tomayko MM, Meng H, Kleinstein SH, Good-Jacobson KL, Shlomchik MJ. 2014. CD80 and PD-L2 define functionally distinct memory B cell subsets that are independent of antibody isotype. *Nat Immunol* 15: 631-7
74. Jones DD, Wilmore JR, Allman D. 2015. Cellular Dynamics of Memory B Cell Populations: IgM+ and IgG+ Memory B Cells Persist Indefinitely as Quiescent Cells. *J Immunol* 195: 4753-9
75. Engels N, Konig LM, Heemann C, Lutz J, Tsubata T, Griep S, Schrader V, Wienands J. 2009. Recruitment of the cytoplasmic adaptor Grb2 to surface IgG and IgE provides antigen receptor-intrinsic costimulation to class-switched B cells. *Nat Immunol* 10: 1018-25
76. Kometani K, Nakagawa R, Shinnakasu R, Kaji T, Rybouchkin A, Moriyama S, Furukawa K, Koseki H, Takemori T, Kurosaki T. 2013. Repression of the transcription factor Bach2 contributes to predisposition of IgG1 memory B cells toward plasma cell differentiation. *Immunity* 39: 136-47
77. Tomayko MM, Anderson SM, Brayton CE, Sadanand S, Steinel NC, Behrens TW, Shlomchik MJ. 2008. Systematic comparison of gene expression between murine memory and naive B cells demonstrates that memory B cells have unique signaling capabilities. *J Immunol* 181: 27-38
78. Good KL, Avery DT, Tangye SG. 2009. Resting human memory B cells are intrinsically programmed for enhanced survival and responsiveness to diverse stimuli compared to naive B cells. *J Immunol* 182: 890-901
79. Good KL, Tangye SG. 2007. Decreased expression of Kruppel-like factors in memory B cells induces the rapid response typical of secondary antibody responses. *Proc Natl Acad Sci U S A* 104: 13420-5

80. Ehrhardt GR, Hijikata A, Kitamura H, Ohara O, Wang JY, Cooper MD. 2008. Discriminating gene expression profiles of memory B cell subpopulations. *J Exp Med* 205: 1807-17
81. Klein U, Tu Y, Stolovitzky GA, Keller JL, Haddad J, Jr., Miljkovic V, Cattoretti G, Califano A, Dalla-Favera R. 2003. Transcriptional analysis of the B cell germinal center reaction. *Proc Natl Acad Sci U S A* 100: 2639-44
82. Moran I, Nguyen A, Khoo WH, Butt D, Bourne K, Young C, Hermes JR, Biro M, Gracie G, Ma CS, Munier CML, Luciani F, Zaunders J, Parker A, Kelleher AD, Tangye SG, Croucher PI, Brink R, Read MN, Phan TG. 2018. Memory B cells are reactivated in subcapsular proliferative foci of lymph nodes. *Nat Commun* 9: 3372
83. Grigorova IL, Schwab SR, Phan TG, Pham TH, Okada T, Cyster JG. 2009. Cortical sinus probing, S1P1-dependent entry and flow-based capture of egressing T cells. *Nat Immunol* 10: 58-65
84. Grigorova IL, Panteleev M, Cyster JG. 2010. Lymph node cortical sinus organization and relationship to lymphocyte egress dynamics and antigen exposure. *Proc Natl Acad Sci U S A* 107: 20447-52
85. Sinha RK, Park C, Hwang IY, Davis MD, Kehrl JH. 2009. B lymphocytes exit lymph nodes through cortical lymphatic sinusoids by a mechanism independent of sphingosine-1-phosphate-mediated chemotaxis. *Immunity* 30: 434-46
86. Pham TH, Okada T, Matloubian M, Lo CG, Cyster JG. 2008. S1P1 receptor signaling overrides retention mediated by G alpha i-coupled receptors to promote T cell egress. *Immunity* 28: 122-33
87. Arnon TI, Xu Y, Lo C, Pham T, An J, Coughlin S, Dorn GW, Cyster JG. 2011. GRK2-dependent S1PR1 desensitization is required for lymphocytes to overcome their attraction to blood. *Science* 333: 1898-903
88. Girard JP, Moussion C, Forster R. 2012. HEVs, lymphatics and homeostatic immune cell trafficking in lymph nodes. *Nat Rev Immunol* 12: 762-73
89. Masopust D, Soerens AG. 2019. Tissue-Resident T Cells and Other Resident Leukocytes. *Annu Rev Immunol* 37: 521-46
90. Masopust D, Vezys V, Marzo AL, Lefrancois L. 2001. Preferential localization of effector memory cells in nonlymphoid tissue. *Science* 291: 2413-7
91. Bankovich AJ, Shiow LR, Cyster JG. 2010. CD69 suppresses sphingosine 1-phosophate receptor-1 (S1P1) function through interaction with membrane helix 4. *J Biol Chem* 285: 22328-37
92. Shiow LR, Rosen DB, Brdickova N, Xu Y, An J, Lanier LL, Cyster JG, Matloubian M. 2006. CD69 acts downstream of interferon-alpha/beta to inhibit S1P1 and lymphocyte egress from lymphoid organs. *Nature* 440: 540-4
93. Skon CN, Lee JY, Anderson KG, Masopust D, Hogquist KA, Jameson SC. 2013. Transcriptional downregulation of S1pr1 is required for the establishment of resident memory CD8+ T cells. *Nat Immunol* 14: 1285-93
94. Arnon TI, Cyster JG. 2014. Blood, sphingosine-1-phosphate and lymphocyte migration dynamics in the spleen. *Curr Top Microbiol Immunol* 378: 107-28

95. Liang B, Hyland L, Hou S. 2001. Nasal-associated lymphoid tissue is a site of long-term virus-specific antibody production following respiratory virus infection of mice. *J Virol* 75: 5416-20
96. Etchart N, Baaten B, Andersen SR, Hyland L, Wong SY, Hou S. 2006. Intranasal immunisation with inactivated RSV and bacterial adjuvants induces mucosal protection and abrogates eosinophilia upon challenge. *Eur J Immunol* 36: 1136-44
97. Szyszko EA, Brokstad KA, Oijordsbakken G, Jonsson MV, Jonsson R, Skarstein K. 2011. Salivary glands of primary Sjogren's syndrome patients express factors vital for plasma cell survival. *Arthritis Res Ther* 13: R2
98. Szyszko EA, Aqrawi LA, Jonsson R, Brokstad KA, Skarstein K. 2016. Non-proliferating plasma cells detected in the salivary glands and bone marrow of autoimmune NOD.B10.H2b mice, a model for primary Sjogren's syndrome. *Autoimmunity* 49: 41-9
99. Taubenberger JK, Morens DM. 2008. The pathology of influenza virus infections. *Annu Rev Pathol* 3: 499-522
100. van Laar JM, Melchers M, Teng YK, van der Zouwen B, Mohammadi R, Fischer R, Margolis L, Fitzgerald W, Grivel JC, Breedveld FC, Lipsky PE, Grammer AC. 2007. Sustained secretion of immunoglobulin by long-lived human tonsil plasma cells. *Am J Pathol* 171: 917-27
101. Reboldi A, Cyster JG. 2016. Peyer's patches: organizing B-cell responses at the intestinal frontier. *Immunol Rev* 271: 230-45
102. Yeap LS, Hwang JK, Du Z, Meyers RM, Meng FL, Jakubauskaite A, Liu M, Mani V, Neuberg D, Kepler TB, Wang JH, Alt FW. 2015. Sequence-Intrinsic Mechanisms that Target AID Mutational Outcomes on Antibody Genes. *Cell* 163: 1124-37
103. Gutzeit C, Magri G, Cerutti A. 2014. Intestinal IgA production and its role in host-microbe interaction. *Immunol Rev* 260: 76-85
104. Johansen FE, Pekna M, Norderhaug IN, Haneberg B, Hietala MA, Krajci P, Betsholtz C, Brandtzaeg P. 1999. Absence of epithelial immunoglobulin A transport, with increased mucosal leakiness, in polymeric immunoglobulin receptor/secretory component-deficient mice. *J Exp Med* 190: 915-22
105. Strugnell RA, Wijburg OL. 2010. The role of secretory antibodies in infection immunity. *Nat Rev Microbiol* 8: 656-67
106. Fischer M, Kuppers R. 1998. Human IgA- and IgM-secreting intestinal plasma cells carry heavily mutated VH region genes. *Eur J Immunol* 28: 2971-7
107. Dunn-Walters DK, Boursier L, Spencer J. 1997. Hypermutation, diversity and dissemination of human intestinal lamina propria plasma cells. *Eur J Immunol* 27: 2959-64
108. Lindner C, Thomsen I, Wahl B, Ugur M, Sethi MK, Friedrichsen M, Smoczek A, Ott S, Baumann U, Suerbaum S, Schreiber S, Bleich A, Gaboriau-Routhiau V, Cerf-Bensussan N, Hazanov H, Mehr R, Boysen P, Rosenstiel P, Pabst O. 2015. Diversification of memory B cells drives the continuous adaptation of secretory antibodies to gut microbiota. *Nat Immunol* 16: 880-8

109. Yuvaraj S, Dijkstra G, Burgerhof JG, Dammers PM, Stoel M, Visser A, Kroese FG, Bos NA. 2009. Evidence for local expansion of IgA plasma cell precursors in human ileum. *J Immunol* 183: 4871-8
110. He B, Xu W, Santini PA, Polydorides AD, Chiu A, Estrella J, Shan M, Chadburn A, Villanacci V, Plebani A, Knowles DM, Rescigno M, Cerutti A. 2007. Intestinal bacteria trigger T cell-independent immunoglobulin A(2) class switching by inducing epithelial-cell secretion of the cytokine APRIL. *Immunity* 26: 812-26
111. Snir O, Mesin L, Gidoni M, Lundin KE, Yaari G, Sollid LM. 2015. Analysis of celiac disease autoreactive gut plasma cells and their corresponding memory compartment in peripheral blood using high-throughput sequencing. *J Immunol* 194: 5703-12
112. Sohn HW, Krueger PD, Davis RS, Pierce SK. 2011. FcRL4 acts as an adaptive to innate molecular switch dampening BCR signaling and enhancing TLR signaling. *Blood* 118: 6332-41
113. Tan HX, Esterbauer R, Vanderven HA, Juno JA, Kent SJ, Wheatley AK. 2019. Inducible Bronchus-Associated Lymphoid Tissues (iBALT) Serve as Sites of B Cell Selection and Maturation Following Influenza Infection in Mice. *Front Immunol* 10: 611
114. Foo SY, Phipps S. 2010. Regulation of inducible BALT formation and contribution to immunity and pathology. *Mucosal Immunol* 3: 537-44
115. GeurtsvanKessel CH, Willart MA, Bergen IM, van Rijt LS, Muskens F, Elewaut D, Osterhaus AD, Hendriks R, Rimmelzwaan GF, Lambrecht BN. 2009. Dendritic cells are crucial for maintenance of tertiary lymphoid structures in the lung of influenza virus-infected mice. *J Exp Med* 206: 2339-49
116. Hwang JY, Randall TD, Silva-Sanchez A. 2016. Inducible Bronchus-Associated Lymphoid Tissue: Taming Inflammation in the Lung. *Front Immunol* 7: 258
117. Denton AE, Innocentin S, Carr EJ, Bradford BM, Lafouresse F, Mabbott NA, Morbe U, Ludewig B, Groom JR, Good-Jacobson KL, Linterman MA. 2019. Type I interferon induces CXCL13 to support ectopic germinal center formation. *J Exp Med* 216: 621-37
118. Rangel-Moreno J, Moyron-Quiroz JE, Hartson L, Kusser K, Randall TD. 2007. Pulmonary expression of CXC chemokine ligand 13, CC chemokine ligand 19, and CC chemokine ligand 21 is essential for local immunity to influenza. *Proc Natl Acad Sci U S A* 104: 10577-82
119. Rangel-Moreno J, Carragher DM, de la Luz Garcia-Hernandez M, Hwang JY, Kusser K, Hartson L, Kolls JK, Khader SA, Randall TD. 2011. The development of inducible bronchus-associated lymphoid tissue depends on IL-17. *Nat Immunol* 12: 639-46
120. Xu B, Wagner N, Pham LN, Magno V, Shan Z, Butcher EC, Michie SA. 2003. Lymphocyte homing to bronchus-associated lymphoid tissue (BALT) is mediated by L-selectin/PNAd, alpha4beta1 integrin/VCAM-1, and LFA-1 adhesion pathways. *J Exp Med* 197: 1255-67
121. Moyron-Quiroz JE, Rangel-Moreno J, Kusser K, Hartson L, Sprague F, Goodrich S, Woodland DL, Lund FE, Randall TD. 2004. Role of inducible bronchus associated lymphoid tissue (iBALT) in respiratory immunity. *Nat Med* 10: 927-34

122. Moyron-Quiroz JE, Rangel-Moreno J, Hartson L, Kusser K, Tighe MP, Klonowski KD, Lefrancois L, Cauley LS, Harmsen AG, Lund FE, Randall TD. 2006. Persistence and responsiveness of immunologic memory in the absence of secondary lymphoid organs. *Immunity* 25: 643-54
123. Adachi Y, Onodera T, Yamada Y, Daio R, Tsuiji M, Inoue T, Kobayashi K, Kurosaki T, Ato M, Takahashi Y. 2015. Distinct germinal center selection at local sites shapes memory B cell response to viral escape. *J Exp Med* 212: 1709-23
124. Oh JE, Iijima N, Song E, Lu P, Klein J, Jiang R, Kleinstein SH, Iwasaki A. 2019. Migrant memory B cells secrete luminal antibody in the vagina. *Nature* 571: 122-6
125. Mahanonda R, Champaiboon C, Subbalekha K, Sa-Ard-Iam N, Rattanathammatada W, Thawanaphong S, Rerkyen P, Yoshimura F, Nagano K, Lang NP, Pichyangkul S. 2016. Human Memory B Cells in Healthy Gingiva, Gingivitis, and Periodontitis. *J Immunol* 197: 715-25
126. Ehrhardt GR, Hsu JT, Gartland L, Leu CM, Zhang S, Davis RS, Cooper MD. 2005. Expression of the immunoregulatory molecule FcRH4 defines a distinctive tissue-based population of memory B cells. *J Exp Med* 202: 783-91
127. Onodera T, Takahashi Y, Yokoi Y, Ato M, Kodama Y, Hachimura S, Kurosaki T, Kobayashi K. 2012. Memory B cells in the lung participate in protective humoral immune responses to pulmonary influenza virus reinfection. *Proc Natl Acad Sci U S A* 109: 2485-90
128. Allie SR, Bradley JE, Mudunuru U, Schultz MD, Graf BA, Lund FE, Randall TD. 2019. The establishment of resident memory B cells in the lung requires local antigen encounter. *Nat Immunol* 20: 97-108
129. Krammer F. 2019. The human antibody response to influenza A virus infection and vaccination. *Nat Rev Immunol* 19: 383-97
130. Guan Y, Vijaykrishna D, Bahl J, Zhu H, Wang J, Smith GJ. 2010. The emergence of pandemic influenza viruses. *Protein Cell* 1: 9-13
131. Lu LY, Askonas BA. 1980. Cross-reactivity for different type A influenza viruses of a cloned T-killer cell line. *Nature* 288: 164-5
132. Liang S, Mozdzanowska K, Palladino G, Gerhard W. 1994. Heterosubtypic immunity to influenza type A virus in mice. Effector mechanisms and their longevity. *J Immunol* 152: 1653-61
133. Zweerink HJ, Courtneidge SA, Skehel JJ, Crumpton MJ, Askonas BA. 1977. Cytotoxic T cells kill influenza virus infected cells but do not distinguish between serologically distinct type A viruses. *Nature* 267: 354-6
134. McHeyzer-Williams LJ, Milpied PJ, Okitsu SL, McHeyzer-Williams MG. 2015. Class-switched memory B cells remodel BCRs within secondary germinal centers. *Nat Immunol* 16: 296-305
135. Ekiert DC, Friesen RH, Bhabha G, Kwaks T, Jongeneelen M, Yu W, Ophorst C, Cox F, Korse HJ, Brandenburg B, Vogels R, Brakenhoff JP, Kompier R, Koldijk MH, Cornelissen LA, Poon LL, Peiris M, Koudstaal W, Wilson IA, Goudsmit J. 2011. A highly conserved neutralizing epitope on group 2 influenza A viruses. *Science* 333: 843-50
136. Ekiert DC, Bhabha G, Elsliger MA, Friesen RH, Jongeneelen M, Throsby M, Goudsmit J, Wilson IA. 2009. Antibody recognition of a highly conserved influenza virus epitope. *Science* 324: 246-51

137. Kallewaard NL, Corti D, Collins PJ, Neu U, McAuliffe JM, Benjamin E, Wachter-Rosati L, Palmer-Hill FJ, Yuan AQ, Walker PA, Vorlaender MK, Bianchi S, Guarino B, De Marco A, Vanzetta F, Agatic G, Foglierini M, Pinna D, Fernandez-Rodriguez B, Fruehwirth A, Silacci C, Ogrodowicz RW, Martin SR, Sallusto F, Suzich JA, Lanzavecchia A, Zhu Q, Gamblin SJ, Skehel JJ. 2016. Structure and Function Analysis of an Antibody Recognizing All Influenza A Subtypes. *Cell* 166: 596-608
138. Corti D, Voss J, Gamblin SJ, Codoni G, Macagno A, Jarrossay D, Vachieri SG, Pinna D, Minola A, Vanzetta F, Silacci C, Fernandez-Rodriguez BM, Agatic G, Bianchi S, Giacchetto-Sasselli I, Calder L, Sallusto F, Collins P, Haire LF, Temperton N, Langedijk JP, Skehel JJ, Lanzavecchia A. 2011. A neutralizing antibody selected from plasma cells that binds to group 1 and group 2 influenza A hemagglutinins. *Science* 333: 850-6
139. van der Brugge-Gamelkoorn GJ, van de Ende MB, Sminia T. 1985. Non-lymphoid cells of bronchus-associated lymphoid tissue of the rat in situ and in suspension. With special reference to interdigitating and follicular dendritic cells. *Cell Tissue Res* 239: 177-82
140. Rickert RC, Rajewsky K, Roes J. 1995. Impairment of T-cell-dependent B-cell responses and B-1 cell development in CD19-deficient mice. *Nature* 376: 352-5
141. Ohinata Y, Payer B, O'Carroll D, Ancelin K, Ono Y, Sano M, Barton SC, Obukhanych T, Nussenzweig M, Tarakhovsky A, Saitou M, Surani MA. 2005. Blimp1 is a critical determinant of the germ cell lineage in mice. *Nature* 436: 207-13
142. Fooksman DR, Schwickert TA, Victora GD, Dustin ML, Nussenzweig MC, Skokos D. 2010. Development and migration of plasma cells in the mouse lymph node. *Immunity* 33: 118-27
143. Powell TJ, Silk JD, Sharps J, Fodor E, Townsend AR. 2012. Pseudotyped influenza A virus as a vaccine for the induction of heterotypic immunity. *J Virol* 86: 13397-406
144. Powell TJ, Rijal P, McEwen-Smith RM, Byun H, Hardwick M, Schimanski LM, Huang KA, Daniels RS, Townsend ARM. 2019. A single cycle influenza virus coated in H7 haemagglutinin generates neutralizing antibody responses to haemagglutinin and neuraminidase glycoproteins and protection from heterotypic challenge. *J Gen Virol* 100: 431-45
145. Gomes AC, Flace A, Saudan P, Zabel F, Cabral-Miranda G, Turabi AE, Manolova V, Bachmann MF. 2017. Adjusted Particle Size Eliminates the Need of Linkage of Antigen and Adjuvants for Appropriated T Cell Responses in Virus-Like Particle-Based Vaccines. *Front Immunol* 8: 226
146. Gomes AC, Mohsen MO, Mueller JE, Leoratti FMS, Cabral-Miranda G, Bachmann MF. 2019. Early Transcriptional Signature in Dendritic Cells and the Induction of Protective T Cell Responses Upon Immunization With VLPs Containing TLR Ligands-A Role for CCL2. *Front Immunol* 10: 1679
147. Kozlovska TM, Cielens I, Dreilinna D, Dislers A, Baumanis V, Ose V, Pumpens P. 1993. Recombinant RNA phage Q beta capsid particles synthesized and self-assembled in Escherichia coli. *Gene* 137: 133-7

148. Picelli S, Faridani OR, Bjorklund AK, Winberg G, Sagasser S, Sandberg R. 2014. Full-length RNA-seq from single cells using Smart-seq2. *Nat Protoc* 9: 171-81
149. Radtke D, Bannard O. 2018. Expression of the Plasma Cell Transcriptional Regulator Blimp-1 by Dark Zone Germinal Center B Cells During Periods of Proliferation. *Front Immunol* 9: 3106
150. Muramatsu M, Kinoshita K, Fagarasan S, Yamada S, Shinkai Y, Honjo T. 2000. Class switch recombination and hypermutation require activation-induced cytidine deaminase (AID), a potential RNA editing enzyme. *Cell* 102: 553-63
151. Roco JA, Mesin L, Binder SC, Nefzger C, Gonzalez-Figueroa P, Canete PF, Ellyard J, Shen Q, Robert PA, Cappello J, Vohra H, Zhang Y, Nowosad CR, Schiepers A, Corcoran LM, Toellner KM, Polo JM, Meyer-Hermann M, Victora GD, Vinuesa CG. 2019. Class-Switch Recombination Occurs Infrequently in Germinal Centers. *Immunity*
152. Frank GM, Angeletti D, Ince WL, Gibbs JS, Khurana S, Wheatley AK, Max EE, McDermott AB, Golding H, Stevens J, Bennink JR, Yewdell JW. 2015. A Simple Flow-Cytometric Method Measuring B Cell Surface Immunoglobulin Avidity Enables Characterization of Affinity Maturation to Influenza A Virus. *MBio* 6: e01156
153. Whittle JR, Wheatley AK, Wu L, Lingwood D, Kanekiyo M, Ma SS, Narpala SR, Yassine HM, Frank GM, Yewdell JW, Ledgerwood JE, Wei CJ, McDermott AB, Graham BS, Koup RA, Nabel GJ. 2014. Flow cytometry reveals that H5N1 vaccination elicits cross-reactive stem-directed antibodies from multiple Ig heavy-chain lineages. *J Virol* 88: 4047-57
154. Meisner J, Szretter KJ, Bradley KC, Langley WA, Li ZN, Lee BJ, Thoennes S, Martin J, Skehel JJ, Russell RJ, Katz JM, Steinhauer DA. 2008. Infectivity studies of influenza virus hemagglutinin receptor binding site mutants in mice. *J Virol* 82: 5079-83
155. Anderson KG, Sung H, Skon CN, Lefrancois L, Deisinger A, Vezys V, Masopust D. 2012. Cutting edge: intravascular staining redefines lung CD8 T cell responses. *J Immunol* 189: 2702-6
156. Pereira JP, An J, Xu Y, Huang Y, Cyster JG. 2009. Cannabinoid receptor 2 mediates the retention of immature B cells in bone marrow sinusoids. *Nat Immunol* 10: 403-11
157. Galkina E, Thatte J, Dabak V, Williams MB, Ley K, Braciale TJ. 2005. Preferential migration of effector CD8+ T cells into the interstitium of the normal lung. *J Clin Invest* 115: 3473-83
158. Turner DL, Bickham KL, Thome JJ, Kim CY, D'Ovidio F, Wherry EJ, Farber DL. 2014. Lung niches for the generation and maintenance of tissue-resident memory T cells. *Mucosal Immunol* 7: 501-10
159. Arnon TI, Horton RM, Grigorova IL, Cyster JG. 2013. Visualization of splenic marginal zone B-cell shuttling and follicular B-cell egress. *Nature* 493: 684-8
160. Rothaeusler K, Baumgarth N. 2010. B-cell fate decisions following influenza virus infection. *Eur J Immunol* 40: 366-77
161. Stewart I, Radtke D, Phillips B, McGowan SJ, Bannard O. 2018. Germinal Center B Cells Replace Their Antigen Receptors in Dark Zones and Fail

Light Zone Entry when Immunoglobulin Gene Mutations are Damaging. *Immunity* 49: 477-89 e7
162. Chen YQ, Wohlbold TJ, Zheng NY, Huang M, Huang Y, Neu KE, Lee J, Wan H, Rojas KT, Kirkpatrick E, Henry C, Palm AE, Stamper CT, Lan LY, Topham DJ, Treanor J, Wrammert J, Ahmed R, Eichelberger MC, Georgiou G, Krammer F, Wilson PC. 2018. Influenza Infection in Humans Induces Broadly Cross-Reactive and Protective Neuraminidase-Reactive Antibodies. *Cell* 173: 417-29 e10
163. Rajendran M, Nachbagauer R, Ermler ME, Bunduc P, Amanat F, Izikson R, Cox M, Palese P, Eichelberger M, Krammer F. 2017. Analysis of Anti-Influenza Virus Neuraminidase Antibodies in Children, Adults, and the Elderly by ELISA and Enzyme Inhibition: Evidence for Original Antigenic Sin. *MBio* 8
164. Jegerlehner A, Schmitz N, Storni T, Bachmann MF. 2004. Influenza A vaccine based on the extracellular domain of M2: weak protection mediated via antibody-dependent NK cell activity. *J Immunol* 172: 5598-605
165. Marsland BJ, Gollwitzer ES. 2014. Host-microorganism interactions in lung diseases. *Nat Rev Immunol* 14: 827-35
166. Charlson ES, Bittinger K, Haas AR, Fitzgerald AS, Frank I, Yadav A, Bushman FD, Collman RG. 2011. Topographical continuity of bacterial populations in the healthy human respiratory tract. *Am J Respir Crit Care Med* 184: 957-63
167. Charlson ES, Diamond JM, Bittinger K, Fitzgerald AS, Yadav A, Haas AR, Bushman FD, Collman RG. 2012. Lung-enriched organisms and aberrant bacterial and fungal respiratory microbiota after lung transplant. *Am J Respir Crit Care Med* 186: 536-45
168. Steinert EM, Schenkel JM, Fraser KA, Beura LK, Manlove LS, Igyarto BZ, Southern PJ, Masopust D. 2015. Quantifying Memory CD8 T Cells Reveals Regionalization of Immunosurveillance. *Cell* 161: 737-49
169. Benschop RJ, Melamed D, Nemazee D, Cambier JC. 1999. Distinct signal thresholds for the unique antigen receptor-linked gene expression programs in mature and immature B cells. *J Exp Med* 190: 749-56
170. Risso A, Cosulich ME, Rubartelli A, Mazza MR, Bargellesi A. 1989. MLR3 molecule is an activation antigen shared by human B, T lymphocytes and T cell precursors. *Eur J Immunol* 19: 323-8
171. Laidlaw BJ, Schmidt TH, Green JA, Allen CD, Okada T, Cyster JG. 2017. The Eph-related tyrosine kinase ligand Ephrin-B1 marks germinal center and memory precursor B cells. *J Exp Med* 214: 639-49
172. Slutter B, Van Braeckel-Budimir N, Abboud G, Varga SM, Salek-Ardakani S, Harty JT. 2017. Dynamics of influenza-induced lung-resident memory T cells underlie waning heterosubtypic immunity. *Sci Immunol* 2
173. Zammit DJ, Turner DL, Klonowski KD, Lefrancois L, Cauley LS. 2006. Residual antigen presentation after influenza virus infection affects CD8 T cell activation and migration. *Immunity* 24: 439-49
174. Keeler SP, Agapov EV, Hinojosa ME, Letvin AN, Wu K, Holtzman MJ. 2018. Influenza A Virus Infection Causes Chronic Lung Disease Linked to Sites of Active Viral RNA Remnants. *J Immunol* 201: 2354-68

175. Cremasco V, Woodruff MC, Onder L, Cupovic J, Nieves-Bonilla JM, Schildberg FA, Chang J, Cremasco F, Harvey CJ, Wucherpfennig K, Ludewig B, Carroll MC, Turley SJ. 2014. B cell homeostasis and follicle confines are governed by fibroblastic reticular cells. *Nat Immunol* 15: 973-81
176. Schiemann B, Gommerman JL, Vora K, Cachero TG, Shulga-Morskaya S, Dobles M, Frew E, Scott ML. 2001. An essential role for BAFF in the normal development of B cells through a BCMA-independent pathway. *Science* 293: 2111-4
177. Thornton EE, Looney MR, Bose O, Sen D, Sheppard D, Locksley R, Huang X, Krummel MF. 2012. Spatiotemporally separated antigen uptake by alveolar dendritic cells and airway presentation to T cells in the lung. *J Exp Med* 209: 1183-99
178. Dzhagalov IL, Melichar HJ, Ross JO, Herzmark P, Robey EA. 2012. Two-photon imaging of the immune system. *Curr Protoc Cytom* Chapter 12: Unit12 26
179. Fleige H, Ravens S, Moschovakis GL, Bolter J, Willenzon S, Sutter G, Haussler S, Kalinke U, Prinz I, Forster R. 2014. IL-17-induced CXCL12 recruits B cells and induces follicle formation in BALT in the absence of differentiated FDCs. *J Exp Med* 211: 643-51
180. Beura LK, Mitchell JS, Thompson EA, Schenkel JM, Mohammed J, Wijeyesinghe S, Fonseca R, Burbach BJ, Hickman HD, Vezys V, Fife BT, Masopust D. 2018. Intravital mucosal imaging of CD8(+) resident memory T cells shows tissue-autonomous recall responses that amplify secondary memory. *Nat Immunol* 19: 173-82
181. Miller MJ, Wei SH, Parker I, Cahalan MD. 2002. Two-photon imaging of lymphocyte motility and antigen response in intact lymph node. *Science* 296: 1869-73
182. Schwickert TA, Lindquist RL, Shakhar G, Livshits G, Skokos D, Kosco-Vilbois MH, Dustin ML, Nussenzweig MC. 2007. In vivo imaging of germinal centres reveals a dynamic open structure. *Nature* 446: 83-7
183. Allen CD, Okada T, Cyster JG. 2007. Germinal-center organization and cellular dynamics. *Immunity* 27: 190-202
184. Hauser AE, Junt T, Mempel TR, Sneddon MW, Kleinstein SH, Henrickson SE, von Andrian UH, Shlomchik MJ, Haberman AM. 2007. Definition of germinal-center B cell migration in vivo reveals predominant intrazonal circulation patterns. *Immunity* 26: 655-67
185. Matloubian M, Lo CG, Cinamon G, Lesneski MJ, Xu Y, Brinkmann V, Allende ML, Proia RL, Cyster JG. 2004. Lymphocyte egress from thymus and peripheral lymphoid organs is dependent on S1P receptor 1. *Nature* 427: 355-60
186. Brinkmann V, Davis MD, Heise CE, Albert R, Cottens S, Hof R, Bruns C, Prieschl E, Baumruker T, Hiestand P, Foster CA, Zollinger M, Lynch KR. 2002. The immune modulator FTY720 targets sphingosine 1-phosphate receptors. *J Biol Chem* 277: 21453-7
187. Brinkmann V, Pinschewer D, Chiba K, Feng L. 2000. FTY720: a novel transplantation drug that modulates lymphocyte traffic rather than activation. *Trends Pharmacol Sci* 21: 49-52
188. Chiba K, Yanagawa Y, Masubuchi Y, Kataoka H, Kawaguchi T, Ohtsuki M, Hoshino Y. 1998. FTY720, a novel immunosuppressant, induces

sequestration of circulating mature lymphocytes by acceleration of lymphocyte homing in rats. I. FTY720 selectively decreases the number of circulating mature lymphocytes by acceleration of lymphocyte homing. *J Immunol* 160: 5037-44

189. Mandala S, Hajdu R, Bergstrom J, Quackenbush E, Xie J, Milligan J, Thornton R, Shei GJ, Card D, Keohane C, Rosenbach M, Hale J, Lynch CL, Rupprecht K, Parsons W, Rosen H. 2002. Alteration of lymphocyte trafficking by sphingosine-1-phosphate receptor agonists. *Science* 296: 346-9
190. Pinschewer DD, Ochsenbein AF, Odermatt B, Brinkmann V, Hengartner H, Zinkernagel RM. 2000. FTY720 immunosuppression impairs effector T cell peripheral homing without affecting induction, expansion, and memory. *J Immunol* 164: 5761-70
191. Liu D, Xu H, Shih C, Wan Z, Ma X, Ma W, Luo D, Qi H. 2015. T-B-cell entanglement and ICOSL-driven feed-forward regulation of germinal centre reaction. *Nature* 517: 214-8
192. Arpin C, Dechanet J, Van Kooten C, Merville P, Grouard G, Briere F, Banchereau J, Liu YJ. 1995. Generation of memory B cells and plasma cells in vitro. *Science* 268: 720-2
193. Arpin C, Banchereau J, Liu YJ. 1997. Memory B cells are biased towards terminal differentiation: a strategy that may prevent repertoire freezing. *J Exp Med* 186: 931-40
194. Bernasconi NL, Traggiai E, Lanzavecchia A. 2002. Maintenance of serological memory by polyclonal activation of human memory B cells. *Science* 298: 2199-202
195. Tarte K, De Vos J, Thykjaer T, Zhan F, Fiol G, Costes V, Reme T, Legouffe E, Rossi JF, Shaughnessy J, Jr., Orntoft TF, Klein B. 2002. Generation of polyclonal plasmablasts from peripheral blood B cells: a normal counterpart of malignant plasmablasts. *Blood* 100: 1113-22
196. Poeck H, Wagner M, Battiany J, Rothenfusser S, Wellisch D, Hornung V, Jahrsdorfer B, Giese T, Endres S, Hartmann G. 2004. Plasmacytoid dendritic cells, antigen, and CpG-C license human B cells for plasma cell differentiation and immunoglobulin production in the absence of T-cell help. *Blood* 103: 3058-64
197. Mohsen MO, Gomes AC, Vogel M, Bachmann MF. 2018. Interaction of Viral Capsid-Derived Virus-Like Particles (VLPs) with the Innate Immune System. *Vaccines (Basel)* 6
198. Moran I, Grootveld AK, Nguyen A, Phan TG. 2019. Subcapsular Sinus Macrophages: The Seat of Innate and Adaptive Memory in Murine Lymph Nodes. *Trends Immunol* 40: 35-48
199. Baddeley A, Rubak E, Turner R. 2015. Spatial point patterns : methodology and applications with R. In *Chapman & Hall/CRC interdisciplinary statistics series*, pp. 1 online resource. Boca Raton: Chapman & Hall/CRC,
200. Ripley BD. 1977. Modelling Spatial Patterns. *Journal of the Royal Statistical Society. Series B (Methodological)* 39: 172-212
201. Diggle PJ, Chetwynd AG. 1991. Second-order analysis of spatial clustering for inhomogeneous populations. *Biometrics* 47: 1155-63

202. Kiskowski MA, Hancock JF, Kenworthy AK. 2009. On the use of Ripley's K-function and its derivatives to analyze domain size. *Biophys J* 97: 1095-103
203. Jafari-Mamaghani M, Andersson M, Krieger P. 2010. Spatial Point Pattern Analysis of Neurons Using Ripley's K-Function in 3D. *Front Neuroinform* 4: 9
204. Wilson EA, Sullivan PJ, Dickinson JL. 2014. Spatial distribution of oak mistletoe as it relates to habits of oak woodland frugivores. *PLoS One* 9: e111947
205. Ruiz-Moreno D, Pascual M, Emch M, Yunus M. 2010. Spatial clustering in the spatio-temporal dynamics of endemic cholera. *BMC Infect Dis* 10: 51
206. Kaslow HR, Burns DL. 1992. Pertussis toxin and target eukaryotic cells: binding, entry, and activation. *FASEB J* 6: 2684-90
207. Victora GD, Schwickert TA, Fooksman DR, Kamphorst AO, Meyer-Hermann M, Dustin ML, Nussenzweig MC. 2010. Germinal center dynamics revealed by multiphoton microscopy with a photoactivatable fluorescent reporter. *Cell* 143: 592-605
208. Iwasaki A, Pillai PS. 2014. Innate immunity to influenza virus infection. *Nat Rev Immunol* 14: 315-28
209. Hancock AS, Stairiker CJ, Boesteanu AC, Monzon-Casanova E, Lukasiak S, Mueller YM, Stubbs AP, Garcia-Sastre A, Turner M, Katsikis PD. 2018. Transcriptome Analysis of Infected and Bystander Type 2 Alveolar Epithelial Cells during Influenza A Virus Infection Reveals In Vivo Wnt Pathway Downregulation. *J Virol* 92
210. Herold S, von Wulffen W, Steinmueller M, Pleschka S, Kuziel WA, Mack M, Srivastava M, Seeger W, Maus UA, Lohmeyer J. 2006. Alveolar epithelial cells direct monocyte transepithelial migration upon influenza virus infection: impact of chemokines and adhesion molecules. *J Immunol* 177: 1817-24
211. Le Goffic R, Pothlichet J, Vitour D, Fujita T, Meurs E, Chignard M, Si-Tahar M. 2007. Cutting Edge: Influenza A virus activates TLR3-dependent inflammatory and RIG-I-dependent antiviral responses in human lung epithelial cells. *J Immunol* 178: 3368-72
212. Phan TG, Green JA, Gray EE, Xu Y, Cyster JG. 2009. Immune complex relay by subcapsular sinus macrophages and noncognate B cells drives antibody affinity maturation. *Nat Immunol* 10: 786-93
213. Suzuki K, Grigorova I, Phan TG, Kelly LM, Cyster JG. 2009. Visualizing B cell capture of cognate antigen from follicular dendritic cells. *J Exp Med* 206: 1485-93
214. Hilgendorf I, Theurl I, Gerhardt LM, Robbins CS, Weber GF, Gonen A, Iwamoto Y, Degousee N, Holderried TA, Winter C, Zirlik A, Lin HY, Sukhova GK, Butany J, Rubin BB, Witztum JL, Libby P, Nahrendorf M, Weissleder R, Swirski FK. 2014. Innate response activator B cells aggravate atherosclerosis by stimulating T helper-1 adaptive immunity. *Circulation* 129: 1677-87
215. Shen P, Roch T, Lampropoulou V, O'Connor RA, Stervbo U, Hilgenberg E, Ries S, Dang VD, Jaimes Y, Daridon C, Li R, Jouneau L, Boudinot P, Wilantri S, Sakwa I, Miyazaki Y, Leech MD, McPherson RC, Wirtz S, Neurath M, Hoehlig K, Meinl E, Grützkau A, Grün JR, Horn K, Kühl AA, Dörner T, Bar-

Or A, Kaufmann SH, Anderton SM, Fillatreau S. 2014. IL-35-producing B cells are critical regulators of immunity during autoimmune and infectious diseases. *Nature* 507: 366-70

216. Shen P, Fillatreau S. 2015. Antibody-independent functions of B cells: a focus on cytokines. *Nat Rev Immunol* 15: 441-51
217. Belnoue E, Pihlgren M, McGaha TL, Tougne C, Rochat AF, Bossen C, Schneider P, Huard B, Lambert PH, Siegrist CA. 2008. APRIL is critical for plasmablast survival in the bone marrow and poorly expressed by early-life bone marrow stromal cells. *Blood* 111: 2755-64
218. Benson MJ, Dillon SR, Castigli E, Geha RS, Xu S, Lam KP, Noelle RJ. 2008. Cutting edge: the dependence of plasma cells and independence of memory B cells on BAFF and APRIL. *J Immunol* 180: 3655-9
219. Belnoue E, Tougne C, Rochat AF, Lambert PH, Pinschewer DD, Siegrist CA. 2012. Homing and adhesion patterns determine the cellular composition of the bone marrow plasma cell niche. *J Immunol* 188: 1283-91
220. O'Connor BP, Raman VS, Erickson LD, Cook WJ, Weaver LK, Ahonen C, Lin LL, Mantchev GT, Bram RJ, Noelle RJ. 2004. BCMA is essential for the survival of long-lived bone marrow plasma cells. *J Exp Med* 199: 91-8
221. Chu VT, Berek C. 2013. The establishment of the plasma cell survival niche in the bone marrow. *Immunol Rev* 251: 177-88
222. Mattioli CA, Tomasi TB, Jr. 1973. The life span of IgA plasma cells from the mouse intestine. *J Exp Med* 138: 452-60
223. Landsverk OJ, Snir O, Casado RB, Richter L, Mold JE, Reu P, Horneland R, Paulsen V, Yaqub S, Aandahl EM, Oyen OM, Thorarensen HS, Salehpour M, Possnert G, Frisen J, Sollid LM, Baekkevold ES, Jahnsen FL. 2017. Antibody-secreting plasma cells persist for decades in human intestine. *J Exp Med* 214: 309-17
224. Hapfelmeier S, Lawson MA, Slack E, Kirundi JK, Stoel M, Heikenwalder M, Cahenzli J, Velykoredko Y, Balmer ML, Endt K, Geuking MB, Curtiss R, 3rd, McCoy KD, Macpherson AJ. 2010. Reversible microbial colonization of germ-free mice reveals the dynamics of IgA immune responses. *Science* 328: 1705-9
225. Lemke A, Kraft M, Roth K, Riedel R, Lammerding D, Hauser AE. 2016. Long-lived plasma cells are generated in mucosal immune responses and contribute to the bone marrow plasma cell pool in mice. *Mucosal Immunol* 9: 83-97
226. Kallies A, Hasbold J, Fairfax K, Pridans C, Emslie D, McKenzie BS, Lew AM, Corcoran LM, Hodgkin PD, Tarlinton DM, Nutt SL. 2007. Initiation of plasma-cell differentiation is independent of the transcription factor Blimp-1. *Immunity* 26: 555-66
227. Frolich D, Giesecke C, Mei HE, Reiter K, Daridon C, Lipsky PE, Dorner T. 2010. Secondary immunization generates clonally related antigen-specific plasma cells and memory B cells. *J Immunol* 185: 3103-10
228. Blanchard-Rohner G, Pulickal AS, Jol-van der Zijde CM, Snape MD, Pollard AJ. 2009. Appearance of peripheral blood plasma cells and memory B cells in a primary and secondary immune response in humans. *Blood* 114: 4998-5002
229. Lee FE, Halliley JL, Walsh EE, Moscatiello AP, Kmush BL, Falsey AR, Randall TD, Kaminiski DA, Miller RK, Sanz I. 2011. Circulating human

antibody-secreting cells during vaccinations and respiratory viral infections are characterized by high specificity and lack of bystander effect. *J Immunol* 186: 5514-21

230. Wrammert J, Koutsonanos D, Li GM, Edupuganti S, Sui J, Morrissey M, McCausland M, Skountzou I, Hornig M, Lipkin WI, Mehta A, Razavi B, Del Rio C, Zheng NY, Lee JH, Huang M, Ali Z, Kaur K, Andrews S, Amara RR, Wang Y, Das SR, O'Donnell CD, Yewdell JW, Subbarao K, Marasco WA, Mulligan MJ, Compans R, Ahmed R, Wilson PC. 2011. Broadly cross-reactive antibodies dominate the human B cell response against 2009 pandemic H1N1 influenza virus infection. *J Exp Med* 208: 181-93
231. Huang KY, Li CK, Clutterbuck E, Chui C, Wilkinson T, Gilbert A, Oxford J, Lambkin-Williams R, Lin TY, McMichael AJ, Xu XN. 2014. Virus-specific antibody secreting cell, memory B-cell, and sero-antibody responses in the human influenza challenge model. *J Infect Dis* 209: 1354-61
232. Weber M, Hauschild R, Schwarz J, Moussion C, de Vries I, Legler DF, Luther SA, Bollenbach T, Sixt M. 2013. Interstitial dendritic cell guidance by haptotactic chemokine gradients. *Science* 339: 328-32
233. Ulvmar MH, Werth K, Braun A, Kelay P, Hub E, Eller K, Chan L, Lucas B, Novitzky-Basso I, Nakamura K, Rulicke T, Nibbs RJ, Worbs T, Forster R, Rot A. 2014. The atypical chemokine receptor CCRL1 shapes functional CCL21 gradients in lymph nodes. *Nat Immunol* 15: 623-30
234. McDonald B, Pittman K, Menezes GB, Hirota SA, Slaba I, Waterhouse CC, Beck PL, Muruve DA, Kubes P. 2010. Intravascular danger signals guide neutrophils to sites of sterile inflammation. *Science* 330: 362-6
235. Affolter M, Basler K. 2007. The Decapentaplegic morphogen gradient: from pattern formation to growth regulation. *Nat Rev Genet* 8: 663-74
236. Bollenbach T, Heisenberg CP. 2015. Gradients are shaping up. *Cell* 161: 431-2
237. Salmon SE, Smith BA. 1970. Immunoglobulin synthesis and total body tumor cell number in IgG multiple myeloma. *J Clin Invest* 49: 1114-21
238. Akkaya M, Akkaya B, Kim AS, Miozzo P, Sohn H, Pena M, Roesler AS, Theall BP, Henke T, Kabat J, Lu J, Dorward DW, Dahlstrom E, Skinner J, Miller LH, Pierce SK. 2018. Toll-like receptor 9 antagonizes antibody affinity maturation. *Nat Immunol* 19: 255-66
239. Benson MJ, Elgueta R, Schpero W, Molloy M, Zhang W, Usherwood E, Noelle RJ. 2009. Distinction of the memory B cell response to cognate antigen versus bystander inflammatory signals. *J Exp Med* 206: 2013-25
240. Mackay LK, Minnich M, Kragten NA, Liao Y, Nota B, Seillet C, Zaid A, Man K, Preston S, Freestone D, Braun A, Wynne-Jones E, Behr FM, Stark R, Pellicci DG, Godfrey DI, Belz GT, Pellegrini M, Gebhardt T, Busslinger M, Shi W, Carbone FR, van Lier RA, Kallies A, van Gisbergen KP. 2016. Hobit and Blimp1 instruct a universal transcriptional program of tissue residency in lymphocytes. *Science* 352: 459-63
241. Gebhardt T, Whitney PG, Zaid A, Mackay LK, Brooks AG, Heath WR, Carbone FR, Mueller SN. 2011. Different patterns of peripheral migration by memory CD4+ and CD8+ T cells. *Nature* 477: 216-9
242. Bernasconi NL, Onai N, Lanzavecchia A. 2003. A role for Toll-like receptors in acquired immunity: up-regulation of TLR9 by BCR triggering

in naive B cells and constitutive expression in memory B cells. *Blood* 101: 4500-4
243. Traggiai E, Puzone R, Lanzavecchia A. 2003. Antigen dependent and independent mechanisms that sustain serum antibody levels. *Vaccine* 21 Suppl 2: S35-7
244. Morgan SB, Hemmink JD, Porter E, Harley R, Shelton H, Aramouni M, Everett HE, Brookes SM, Bailey M, Townsend AM, Charleston B, Tchilian E. 2016. Aerosol Delivery of a Candidate Universal Influenza Vaccine Reduces Viral Load in Pigs Challenged with Pandemic H1N1 Virus. *J Immunol* 196: 5014-23
245. Jeyanathan M, Thanthrige-Don N, Afkhami S, Lai R, Damjanovic D, Zganiacz A, Feng X, Yao XD, Rosenthal KL, Medina MF, Gauldie J, Ertl HC, Xing Z. 2015. Novel chimpanzee adenovirus-vectored respiratory mucosal tuberculosis vaccine: overcoming local anti-human adenovirus immunity for potent TB protection. *Mucosal Immunol* 8: 1373-87
246. Meyer M, Garron T, Lubaki NM, Mire CE, Fenton KA, Klages C, Olinger GG, Geisbert TW, Collins PL, Bukreyev A. 2015. Aerosolized Ebola vaccine protects primates and elicits lung-resident T cell responses. *J Clin Invest* 125: 3241-55
247. Baz M, Boonnak K, Paskel M, Santos C, Powell T, Townsend A, Subbarao K. 2015. Nonreplicating influenza A virus vaccines confer broad protection against lethal challenge. *MBio* 6: e01487-15
248. Feng ZX, Wei YN, Li GL, Lu XM, Wan XF, Pharr GT, Wang ZW, Kong M, Gan Y, Bai FF, Liu MJ, Xiong QY, Wu XS, Shao GQ. 2013. Development and validation of an attenuated Mycoplasma hyopneumoniae aerosol vaccine. *Vet Microbiol* 167: 417-24
249. Carter NJ, Curran MP. 2011. Live attenuated influenza vaccine (FluMist(R); Fluenz): a review of its use in the prevention of seasonal influenza in children and adults. *Drugs* 71: 1591-622
250. Hiepe F, Dorner T, Hauser AE, Hoyer BF, Mei H, Radbruch A. 2011. Long-lived autoreactive plasma cells drive persistent autoimmune inflammation. *Nat Rev Rheumatol* 7: 170-8
251. Trapnell C, Cacchiarelli D, Grimsby J, Pokharel P, Li S, Morse M, Lennon NJ, Livak KJ, Mikkelsen TS, Rinn JL. 2014. The dynamics and regulators of cell fate decisions are revealed by pseudotemporal ordering of single cells. *Nat Biotechnol* 32: 381-6
252. Ji Z, Ji H. 2016. TSCAN: Pseudo-time reconstruction and evaluation in single-cell RNA-seq analysis. *Nucleic Acids Res* 44: e117
253. Canzar S, Neu KE, Tang Q, Wilson PC, Khan AA. 2017. BASIC: BCR assembly from single cells. *Bioinformatics* 33: 425-7
254. Upadhyay AA, Kauffman RC, Wolabaugh AN, Cho A, Patel NB, Reiss SM, Havenar-Daughton C, Dawoud RA, Tharp GK, Sanz I, Pulendran B, Crotty S, Lee FE, Wrammert J, Bosinger SE. 2018. BALDR: a computational pipeline for paired heavy and light chain immunoglobulin reconstruction in single-cell RNA-seq data. *Genome Med* 10: 20
255. Shlemov A, Bankevich S, Bzikadze A, Turchaninova MA, Safonova Y, Pevzner PA. 2017. Reconstructing Antibody Repertoires from Error-Prone Immunosequencing Reads. *J Immunol* 199: 3369-80

256. Bemark M, Hazanov H, Stromberg A, Komban R, Holmqvist J, Koster S, Mattsson J, Sikora P, Mehr R, Lycke NY. 2016. Limited clonal relatedness between gut IgA plasma cells and memory B cells after oral immunization. *Nat Commun* 7: 12698
257. Rehwinkel J, Tan CP, Goubau D, Schulz O, Pichlmair A, Bier K, Robb N, Vreede F, Barclay W, Fodor E, Reis e Sousa C. 2010. RIG-I detects viral genomic RNA during negative-strand RNA virus infection. *Cell* 140: 397-408
258. Baum A, Sachidanandam R, Garcia-Sastre A. 2010. Preference of RIG-I for short viral RNA molecules in infected cells revealed by next-generation sequencing. *Proc Natl Acad Sci U S A* 107: 16303-8